AIR FORCE INSTITUTE OF TECHNOLOGY

AIR UNIVERSITY
UNITED STATES AIR FORCE

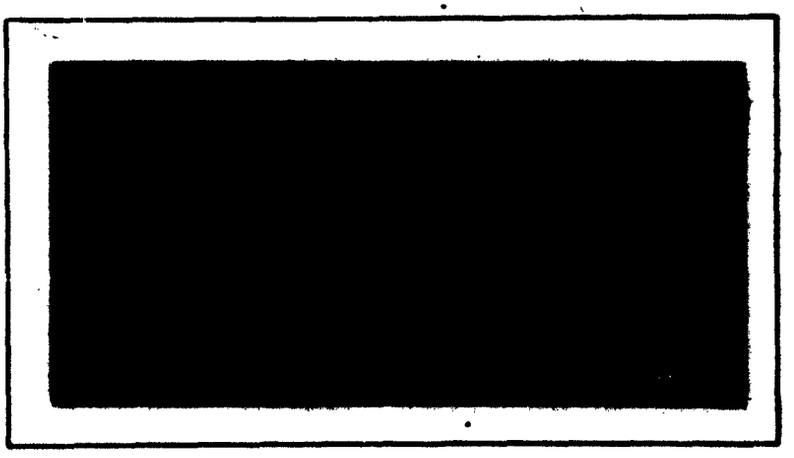

SCHOOL OF ENGINEERING

WRIGHT-PATTERSON AIR FORCE BASE, OHIO

AN EXPERIMENTAL INVESTIGATION OF NOZZLE COOLING FOR A SMALL ROCKET ENGINE

THESIS

GAE/ME/63-1

Donald J. Alser
Capt USAF

AF-WP-O-SEP 63 25

AN EXPERIMENTAL INVESTIGATION OF NOZZLE COOLING FOR A SMALL ROCKET ENGINE

THESIS

Presented to the Faculty of the School of Engineering of
The Institute of Technology
Air University
in Partial Fulfillment of the
Requirements for the Degree of
Master of Science

By
Donald J. Alser, B.S.E.
Captain USAF
Graduate Aeronautical Engineering
August 1963

Preface

In this report, I have presented a method for applying gaseous film cooling to a rocket nozzle. Also, I have shown how variations in coolant flow, velocity and angle of injection affect engine performance and cooling effectiveness. By experimentally demonstrating the advantages of a reacting coolant gas, it is hoped that future investigators will find the results and technique of value in exploring other areas of rocket propulsion.

The introduction and bibliography, I think, provide a fairly complete coverage of cooling methods thus far developed and should provide a good source of more advanced information for those interested in the cooling problem.

I would like to express my gratitude to Lt P. Meyfarth for his technical assistance in solving the calibration problems and improving the instrumentation of the test facility. I am indebted to Mr. J. Parks for his efficient maintenance of the test equipment and the many hours he willingly devoted to assist me in the experimental work. My thanks also go to my advisor, Lt Colonel W. McKenna, who provided timely support and suggestions for this project; and finally, I would like to express special thanks to my wife, Sandy, for her efforts in editing and typing the original draft and her encouragement and patience which led to the completion of this work.

Donald J. Alser

CONTENTS

CONTENTS

LIST OF FIGURES

LIST OF FIGURES
(Continued)

LIST OF FIGURES
(Continued)

LIST OF SYMBOLS

A	Area, sq. in.
C*	Characteristic velocity, ft/sec
C	Frictional discnarge coefficient
C_F	Nozzle thrust coefficient
D	Diameter, inches
F	Thrust, lb
g	Gravitational conversion factor, 32.174 (lbm-ft/lbf-sec^2)
h	Film heat transfer coefficient, Btu/ft^2-sec-$^\circ$F
Is	Optimum specific impulse ($P_e = P_a$), lbf-sec/lbm (sec)
k	Isentropic exponent (specific heat ratio, C_p/C_v)
K	Thermal conductivity, Btu/ft-sec-$^\circ$F
L*	Characteristic length (V_c/A_t), inches (V_c includes volume of the nozzle convergent section)
M	Molecular weight, lb/lb-mole
MR	Mixture ratio, $\dot{w}_o/\dot{w}_f$
P	Static pressure, psia
q	Specific rate of heat flow, Btu/ft^2-sec
r	Nozzle convergent area ratio, A_c/A_t
R	Universal gas constant, 1545.4 ft-lbf/lb-mole$^\circ$F
T	Temperature, $^\circ$F or $^\circ$R
t	Wall thickness, inches
V	Volume, cubic inches; Velocity, ft/sec
$\dot{w}$	Weight-flow rate, lb/sec
x	Nozzle axial distance from entrance, inches

LIST OF SYMBOLS
(Continued)

Y_a	Compressibility correction factor
α	Nozzle half-angle of divergence degrees
β	Diameter ratio, A/A_t
γ	Nozzle half-angle of convergence degrees
ϵ	Nozzle expansion area ratio, A_e/A_t
η	Characteristic velocity quality factor, C^*_X/C^*_T
λ	Thrust coefficient quality factor, C_{Fx}/C_{FT}
ξ	Specific impulse quality factor, I_{sx}/I_{sT}
ρ	Density, lb/cu. in.
ω	Coolant flow ratio, $\dot{w}_i/\dot{w}_h$

Subscripts:

a	Atmospheric
i	Coolant
c	Combustion chamber
e	Nozzle exit
f	Fuel
h	Hydrogen
in	Injection
o	Oxidizer (oxygen)
s	Freestream
T	Theoretical
t	Nozzle throat
w	Nozzle wall
x	Experimental

Abstract

The purpose of this investigation was to determine experimentally the effect of film-cooling a rocket engine nozzle with a reactant gas. Coolant quantities, injection velocities and angles, and axial injection location were varied to determine the conditions under which adequate film cooling could be achieved.

For various cooling schemes engine performance was evaluated to determine coolant effects on engine performance, and nozzle wall temperatures were measured to determine cooling effectiveness. The experimental data showing rocket performance efficiencies (based upon equilibrium isentropic flow) and nozzle wall temperature reductions are presented in tables and graphs.

Testing was conducted on a 100 pound thrust engine using gaseous H_2-O_2 bi-propellants and operating at a nominal chamber pressure of 300 psia. A self-impinging oxygen injection pattern was used in conjunction with radial injection of hydrogen which also served to film cool the combustion chamber.

Five basic coolant configurations consisting of three De Laval type nozzles and three coolant chamber liners provided coolant injection at the nozzle entrance and/or near the nozzle throat. Decreasing the injection velocity resulted in increased wall temperature reductions so that critical areas of the nozzle could be adequately film cooled.

For the range of mixture ratios from 1.5 to 6.5, coolant flow ratios (with respect to total hydrogen flow) were varied from .084 to .178 while hydrogen flow rates ranged from .126 lb/sec to .040 lb/sec. Thrust coefficients were near 100% of theoretical performance; and characteristic velocity and specific impulse efficiencies from 82% to 89% were obtained for the coolant configurations where adequate film cooling was realized.

At a mixture ratio of 3.0, experimental results showed average wall temperature reductions of 30% from the nozzle entrance to a point half-way through the nozzle divergent section, for tangential coolant injection at the nozzle entrance and 45° radial injection near the nozzle throat. At the same time, performance loss was less than 3%.

Engine performance loss was dependent only upon coolant flow rate while wall temperature reductions were a function of coolant flow rate and coolant injection location. For equal coolant flow rates, small angles of injection resulted in practically no change in wall temperatures from that of tangential coolant injection.

AN EXPERIMENTAL INVESTIGATION OF NOZZLE COOLING FOR A SMALL ROCKET ENGINE

I. Introduction

Advances in rocket engine development for space exploration and missile weapon systems have created new environments of extremely high temperatures. The flame temperatures in combustion chambers are on the order of 5000°F and heat transfer rates as high as 14 Btu/in^2-sec have been observed. Associated with this severe engineering environment is the containment and control of the hot combustion gases in a rocket nozzle to provide the necessary propulsive thrust. In addition to adverse temperature gradients and extremely high heat transfer rates near the throat, the nozzle is subjected to high gas pressures and convective shear forces, chemical corrosion and sometimes particle erosion. Thus, the exposure of rocket engine components to such an environment will ultimately result in their destruction unless some form of thermal protection is provided.

Cooling Techniques

Several thermal protection techniques have been designed and tested which offer possible solutions to the heating problem.

Heat Sinks. Conductive heat sinks are an absorptive type system whereby incident energy is stored in a large mass of

material by sensible temperature rise. This method is usually not practical from a weight requirement point of view.

Refractories. Materials capable of withstanding severe temperatures have been developed and employed in nozzle throats and combustion chambers. However, available refractories rapidly fail in the presence of high pressures and shear forces, and therefore provide a relatively short service life.

Regenerative Cooling. Convective regenerative cooling is another absorptive type cooling system. Heat is absorbed by the exposed surface and conducted to a regulated flowing fluid, thereby maintaining the surface at a temperature below the structural failure temperature of the material. This method is widely used in liquid propellant systems since the fuel or oxidizer can often function as the coolant prior to injection into the combustion chamber. Regenerative cooling, which increases propellant pumping requirements, is not time limited but is subject to the undesirable characteristic of bubbling due to heating prior to injection. In addition, many propellants do not have the capacity for absorbing the required heat flux (Ref 3:447-462).

Transpiration Cooling. This cooling technique uses either a regulated or passive mass transfer system. A gaseous or liquid coolant is passed through a porous wall material with the injected mass flowing in a direction opposite to the incident heat flow. Energy absorption takes place through temperature rise, and

sometimes, mass phase change. Skin friction and surface heating is reduced by the continual mixing of the coolant and hot combustive gases. Although this method has received increased emphasis as a cooling scheme for the combustion chambers of gaseous, plasma, and nuclear rocket engines, there has been only limited usage to date. The limited use of transpiration cooling is attributed to non-availability of high temperature uniformly porous materials, pore clogging by combustion products and residues, susceptibility to local hot spots, and high coolant weight and bulk requirements (Ref 14:36-40).

Ablative Cooling. (Ref 21:2-8) Ablation of a material is another means of mass transfer cooling. This method involves the sacrificial erosion of plastic materials and can be employed with both liquid and solid propellant rocket systems. Cooling of the surface is accomplished when the hot gas stream heats the exposed material, thereby forming gases within the surface layers. The released gases then create a transpiration type cooling process. At the same time, a charred insulative surface is formed which is ultimately swept away by the high shear force gas stream. Ablative cooling is desirable in that the materials utilized are light weight, have a low thermal conductivity (high thermal insulation), and have the ability to accommodate intensive heating without failure. Factors limiting the use of ablative cooling are: a susceptibility to high gas stream shear forces, high

temperature corrosion and a finite material service life under 30 seconds. Present applications of ablative cooling are found in re-entry thermal shields and rocket nozzle skirts and throats.

Film Cooling. Last of the mass transfer cooling methods being investigated is that of film cooling. It is based on forcing a coolant through a series of slots or perforations, and onto a wall surface to form a thermal insulating layer between an exposed surface and a hot gas stream. The insulating layer is formed adjacent to the injection area and is carried downstream until it evaporates and/or diffuses with the hot gas stream. In the case of liquid film cooling, heat is transferred principally by means of evaporation (Ref 8:301-302). With gaseous film cooling, heat transfer occurs by means of sensible heat exchange. In both cases, the film coolant serves to insulate and protect the hot surface from excessive heating. Liquid film cooling has a decided advantage over gaseous film cooling in that the density storage requirements are less, and the utilization of the latent heat of evaporation of a liquid significantly improves the cooling technique. Film cooling has been successfully and efficiently used in liquid propulsion systems and has good possibilities for future applications to solid propellant rockets (Ref 14:29-36).

The previously described cooling techniques have all contributed in the effort to solve the rocket heating problem and have aided the development of more advanced rocket propulsion systems. However,

it must be born in mind that no one method can always be described as the best. Thus, the rocket engineer is faced with the problem of deciding which cooling scheme, or combination of schemes, is the best to fulfill the mission requirement and, at the same time, meet economical restraints.

Cooling Method Undertaken

In considering the application of a cooling technique to a rocket nozzle, transpiration and ablative cooling appear to offer the most promising means for effective cooling and overall performance optimization. However, an extensive program to evaluate ablative nozzles has been conducted by the Aerojet-General Corporation (Ref 25), and the non-availability of acceptable porous materials to facilitate nozzle transpiration cooling dictated the use of some other cooling scheme. Eckert suggested that film cooling be used where cooling of a specific location is required, or where average rather than maximum temperatures are important (Ref 9:210). Therefore, the film cooling scheme was undertaken as a possible method for reducing average wall temperatures throughout the nozzle while decreasing the maximum-incurred temperatures at the nozzle throat.

Several experimental investigations on liquid film-cooled nozzles have been conducted by Boden, Zucrow and Graham, Morrell, Welsh, Abramson, and Ferri. Some of the more important results are summarized:

1. Film cooling can reduce wall heat transfer rates up to 85% (Ref 5:385 and Ref 26:1).

2. Heat transfer rates are greatest at nozzle throats (Ref 5:388).

3. Higher reduction in wall heat transfer rates is obtained with organic coolants than with inorganic coolants due to gaseous dissociation and wall coating characteristics (Ref 26:1).

4. Adequate nozzle cooling is obtained with coolant flow rates from 5 to 15% of total mass flow rate (Ref 17, Ref 5:390, and Ref 26:1).

5. High rocket efficiency is obtained at the low coolant mass transfer rates (Ref 17 and Ref 16:362).

6. Coolant injection near the nozzle throat requires the least coolant flow rate to obtain the maximum local and total cooling effect (Ref 5:389 and Ref 26:7).

7. Radial coolant injection is least effective at the nozzle entrance and most effective near the nozzle throat where the rate of change of mainstream velocity and heat transfer increases rapidly (Ref 23 and Ref 5:389).

8. Tangential injection is the most effective method for coolant injection at any location (Ref 26:1 and Ref 5:389).

9. Effective liquid film attachment is obtained with simple radial hole injectors so that a more complex means of injection is unnecessary (Ref 16:362).

10. Critical injection velocity, defined as velocity above which the coolant film begins to detach from the wall surface at the point of injection, is a determining factor in cooling effectiveness (Ref 16:362, Ref 29:650, and Ref 12:2).

11. Reacting coolants cause a lower decrease in rocket performance than do non-reactants since a reacting coolant may also function as an injected propellant (Ref 17, Ref 16:360, Ref 1:7 and Ref 26:7).

12. Film cooling can prevent hot gas stream deposits and chemical reaction on the nozzle surface (Ref 16:359).

13. Coolants made up of light elements are better than those containing heavier elements since their sonic velocity is higher and rocket performance is less effected (Ref 12:1).

There has been some theoretical and experimental work performed with gaseous film cooling but these investigations have been confined to flow over a flat plate. Theoretical results of Eckert and Livingood, with air as a film coolant, show that cooling effectiveness increases with the number of injection slots and that, for equal maximum surface temperature and equal coolant flow rate per slot, the slot spacing must increase in the downstream direction (Ref 10). Papell and Trout, in their experiments, used two appreciably different temperature levels of injected gaseous coolants and observed that both the low-temperature and high-temperature injections produced about the same wall temperature

distributions beyond a short distance downstream of the point of injection. They explained that the coolant gas having the higher temperature possesses higher injection velocity which tends to improve the persistance of the cooling film (Ref 19).

Due to greater mixing between the mainstream and the coolant jet, normal (radial) gaseous injection has been recognized as much inferior to tangential injection. Sevan, Chan, and Scesa observed that the reduction in wall temperature effectiveness from tangential injection to normal injection amounted to 50% (Ref 22). Thus, wall temperature reductions due to injection at an angle to the main stream flow direction should be between the effects due to normal injection and tangential injection.

Analytical investigations by Eckert and Schneider show that light-weight gases of high thermal capacity are the most promising means for gaseous film cooling. They point out that helium injection is better for ease of application and is more effective than air injection, but is less effective than hydrogen injection since it has higher density and lower thermal capacity. Hydrogen influences heat transfer by increasing the boundary layer thickness caused by injection, and providing a high thermal capacity which tends to markedly decrease the heat transfer rate. In addition, the low density at the surface with hydrogen injection over-shadows poorer conductivity effects (Ref 11:35).

In view of the lack of experimental work on <u>gaseous</u> film

cooled nozzles, further study was deemed necessary to: (a) determine the effects of gaseous film cooling on overall rocket performance, (b) correlate experimental heat transfer results to analytical film cooling theories, and (c) obtain more insight into liquid film cooling effects after vaporization. Thus, this investigation was undertaken. It involves the modification of a small gaseous H_2-O_2 rocket engine, designed originally by Ow (Ref 18), to incorporate a film cooled nozzle employing gaseous hydrogen as a reacting coolant. The design and evaluation of the film cooled nozzles is based upon the results obtained from liquid film cooled nozzles and gaseous cooling over a flat plate (See Pages 5-8).

Ow designed the basic rocket engine to investigate gaseous film cooling of the combustion chamber. He was successful in his efforts to cool the chamber walls and determined the optimum cooling configuration for the chamber. However, Ow found it necessary to cool the nozzle with exterior water flow. During the following year Pickitt applied gaseous film cooling to the nozzle by modifying the aft combustion chamber liner for hydrogen injection tangential to the nozzle entrance (Ref 20). He was unsuccessful in this attempt, as he encountered propellant surge problems which caused a high mixture ratio, low coolant mass flow, and thus resulted in nozzle failure.

For this study, in order to investigate the various possibilities

for applying the film cooling technique, three nozzles comprising five coolant configurations were used. Two coolant configurations provided coolant injection at the nozzle entrance, a third configuration introduced the film coolant near the throat, and a fourth configuration provided a combination of the first three methods. A fifth configuration, which involved an uncooled nozzle, provided a means for comparing the effects of the various coolant configurations on rocket engine performance and coolant efficiency.

Rocket engine evaluation is based upon a comparison of performance parameters (specific impulse, characteristic velocity and thrust coefficient) versus mixture ratio and the reduction of specific impulse versus coolant flow ratio. The effectiveness of gaseous film cooling is based upon a comparison of axial wall temperature profiles as a function of mixture ratio and coolant flow ratio.

The limitations imposed by using gaseous propellants and coolant in this investigation should not in itself prevent the general extrapolation of film cooling results to other liquid propellant rockets even though specific injector requirements may differ.

In spite of the fact that rocket system optimization has stressed the use of liquids for propellants and coolants, indications are that future rocket systems will continue to use

high energy fuels but in gaseous form, regardless of the cost in weight factor. This may be the case in small low-thrust rockets intended for indefinite use in stabilization and attitude control of space vehicles. Also, the use of gaseous reacting coolants would eliminate the need for an additional coolant system, thereby partially offsetting the low density disadvantage.

The following sections of this study describe the design and modifications of the basic rocket engine, instrumentation and test procedures, data reduction, and evaluation.

II. Rocket Engine Design and Modifications

The basic engine used in this investigation was designed by Ow (Ref 18) following a design example given by Sutton (Ref 24:256). It was later modified by Pickitt in an attempt to film cool the rocket nozzle (Ref 20).

Ow selected the size of the rocket engine to provide a thrust of 100 pounds and a chamber pressure of 300 psia for an ideal weight flow rate of .286 lb/sec and specific impulse of 350 seconds.

To be compatible with existing facilities, the engine was designed to use gaseous hydrogen and gaseous oxygen as the propellant combination.

In this study, all nozzle cooling tests were performed on the basic engine with the film cooled combustion chamber, except as noted in the following paragraphs.

Oxygen Injectors

The original oxygen injector was of the self-impinging type. It was designed for maximum momentum exchange with the radially injected hydrogen and to impinge at a point near the nozzle entrance (See Figure 1 and Drawing 1B). The injector consisted of a single ring of eight 1/16 inch diameter injection holes.

Pickitt designed a second injector which was a combination showerhead and self-impinging type. This was a modification of the original injector which added eight additional 1/16 inch diameter holes for axial injection. The purpose of this injector was to decrease the oxygen momentum and increase oxygen dispersion in order to bring the flame front closer to the injector face, improve mixing, and prevent hot spots in the nozzle. Pickitt found this design necessary since he determined that one of the major causes for burnout of his nozzle was due to the original injector not providing the desired spray pattern. The modified injector geometry is illustrated in Figure 1 and Drawing 2B.

In order to improve oxygen injection, two corrective steps were taken. First, the original injector design was corrected to provide closer tolerances in production. Second, the modified injector (not completed by Pickitt) was redesigned and built. Then the completed injectors were subjected to water tests to determine the spray patterns. The results of these tests are shown in Figures 2 and 3. The improved impingement and diffusion seen in the spray pattern of the modified injector is visibly apparent.

The oxygen injector used in this investigation was the improved version of the original injector. The requirement that combustion chamber configuration remain constant for all tests did not allow time to evaluate the performance of the modified injector.

Hydrogen Injector

The original hydrogen injector was designed for radial injection. Seventy-two 1/16 inch diameter holes were spaced circumferentially along the full length of the combustion chamber in order to provide chamber film cooling as well as fuel injection. The complete injector was made up of a forward and aft chamber liner designed to provide injection velocities near .4 Mach at a mixture ratio of about 1. This hydrogen injector, which conforms to Ow's configuration B, is shown in Figure 6 and Drawing 6B.

Some modifications to the aft chamber liner were necessary to facilitate nozzle film cooling. Therefore, to provide various configurations for coolant injection three aft chamber liners were designed as follows:

1. One liner was made to provide sixteen, equally-spaced, 1/16 inch diameter holes, which were drilled in the rear of the liner. These injector holes allowed 17.6% of the total hydrogen flow to be directed tangential to the nozzle entrance (convergent section). This liner is illustrated in Drawing 3B, and is shown mated to the forward chamber liner (hydrogen injector) in Figure 6.

2. A second liner was designed for sixteen 3/64 inch diameter injector holes, in a manner similar to the first. This liner permitted 10.9% of the total hydrogen flow to be directed tangential, or at an angle of 15 degrees, to the nozzle entrance — depending on the convergent angle of the nozzle.

a fairly optimum angle for conical nozzles when considering wall friction and radial component velocity losses (Ref 3:87-88).

The nozzles were designed with large convergent area ratios (greater than 25) to permit very low mainstream velocities at the nozzle entrance and to provide a value of L^* greater than 100. Static temperatures and pressures at the nozzle entrance would then more closely approach isentropic stagnation values of the combustion chamber and nozzle. In addition, by using values of L^* greater than 100, rocket engine performance parameters would not tend to be a function of different engine geometries; in effect, this ensured adequate residence time of the propellants for complete combustion in the chamber (Ref 3:102, 401-403).

All nozzles were designed to slightly overexpand the exhaust gases. For a costant chamber pressure (300 psia), this would result in a large exit pressure differential at the low mixture ratios but would approach optimum expansion as the mixture ratio was increased to higher values. See Figure 15. In any case, the designed over-expansion would not cause separation or shock wave interaction at the exit since the separation point for these nozzles is at an exit pressure ratio (P_e/P_a) of about .4 (Ref 3:77).

The original nozzle, Ow's configuration D, with an exit expansion ratio $\epsilon = 4.25$, was available and designated nozzle A for the purpose of testing (Figure 7). It had a convergent half-angle of 45 degrees, with a short straight throat section, and a constant wall thickness of 1/8 inches.

A second nozzle, designed by Pickitt, was designated nozzle B. For this nozzle, the throat section was rounded so that the diameter of the throat was equal to the throat radius of curvature (Ref 3:70). This ensured a more progressive velocity increase than that of nozzle A. Nozzle B, with $\epsilon = 4.41$, had a convergent half-angle of 45 degrees and a constant wall thickness of 3/16 inches. This nozzle is illustrated in Drawing 5B and Figure 7.

The third nozzle, designated nozzle C, was designed to provide film cooling near the nozzle throat (Drawing 4B and Figure 8). The half-angle of convergent was changed to 30 degrees to provide a smoother transition of gas flow from chamber to throat conditions. Also this convergent angle would permit the use of chamber liners for 15 degree coolant injection at the nozzle entrance. Nozzle C was designed with an exit expansion area ratio $\epsilon = 4.25$ and a throat similar to nozzle B. The wall thickness, however, was constant at 3/16 inches only from the exit to the coolant section. This created some difficulty in temperature measurement which will be discussed in the instrumentation section.

The throat coolant section, of nozzle C, was located at an area ratio $A/A_t = 7.43$. It consisted of twelve 3/64 inch diameter holes, equally spaced circumferentially, to provide film coolant injection at an angle of 45 degrees to mainstream flow direction. The coolant section was connected to the aft combustion chamber section by means of a short external line. See Figure 9.

All nozzles were made of copper primarily because of its high thermal conductivity. This enabled rapid temperature stabilization and small temperature gradients through the nozzle wall. In addition, the soft copper material facilitated nozzle instrumentation.

The variation in nozzle geometry resulting from modifications should not cause any major differences in performance parameters. Zucrow pointed out that: correctly designed conical nozzles with smooth polished interior surfaces have efficiencies between 96 and 98 percent; the exact geometry of convergent sections is not critical so that a smooth transition to the throat is sufficient; the throat section need not be well rounded and can be short; and that no measurable loss of thrust will result from a variation of the nozzle convergent half-angle between 30 and 60 degrees (Ref 28:375).

Initially, the nozzles were to be cooled externally with a water spray system. Then, if the film cooling schemes proved successful, the coolant water could be eliminated thereby permitting heat transfer only to the ambient atmosphere.

For easy reference, the design data for all nozzles is summarized in Table I. Illustrations are provided in Figures 7 and 8.

Propellant Feed System

The propellant lines leading to the rocket engine were modified to decrease run condition transient time and pressure loss. Pickitt found that the large volume in the hydrogen manifold plus the extensive network of small tubing and connectors gave a hydrogen pressure drop fifty times larger than that of oxygen. In addition, the transient time from hydrogen start pressure to run pressure was about two seconds longer than that for oxygen pressure. Pickitt indicated that these two factors were primary causes of nozzle burnout since the propellant mass flows surged to a high mixture ratio while only one percent coolant mass flow was available (Ref 20:20-22).

As a result of Pickitt's observations, the hydrogen manifolding was modified to provide larger diameter, but shorter length, feed lines and to substantially reduce the number of elbows, tees, and reducers. The results of a preliminary test showed that this modification corrected the surge problem, so that the transient time from start to run pressure was about the same for both hydrogen and oxygen feed systems.

Coolant Configurations

With three nozzles and three combustion chamber liners, a number of possibilities existed for applying the film cooling technique. The final combinations selected made up five basic coolant configurations.

Nozzle A was used with the two coolant chamber liners to provide tangential injection at the nozzle entrance for coolant flow ratios $\omega = .178$ and $\omega = .109$. These coolant configurations were designated A-A and A-B, respectively.

Nozzle B was used with all three chamber liners (one without cooling provisions). Similar to nozzle A, and with identical coolant flow ratios, two of the configurations enabled coolant injection tangential to the nozzle entrance. These coolant configurations were designated B-A and B-B, respectively. The third chamber liner provided a coolant flow ratio $\omega = 0$, and was designated configuration B-C. This configuration could then be used as a standard for comparing the rocket performance and cooling effectiveness of the other configurations.

Nozzle C was used with two of the chamber liners (A and C of nozzle B) to provide coolant mass flow ratios $\omega = .084$ and $\omega = .176$, and were designated coolant configurations C-D and C-E, respectively. These configurations differed from those of nozzle A and B in that part of the coolant flow was diverted to the throat cooling section. Thus, for configuration C-D all coolant flow was injected near the throat, while for configuration C-E part of the coolant flow was injected near the throat and part injected at an angle of 15 degrees to the nozzle entrance.

The five basic coolant configurations, with pertinent data, are illustrated in Table I.

Ignition

Ignition was accomplished in the same manner as that used by Ow (Ref 18:9); an initial hydrogen flow was ignited external to the rocket nozzle by means of an electric arc. Then the oxygen flow rate was increased until the flame flashed back into the combustion chamber. The pre-selected run settings were then electrically initiated to provide the desired run conditions. By using this ignition procedure, a fuel-rich mixture ratio was ensured and the danger of premature nozzle or combustion chamber burnout was prevented.

III. Instrumentation

The experimental work performed in this investigation was conducted in the Rocket Test Facility of the Mechanical Engineering Department.

The original design, construction, and calibration of the test facility was completed in a joint project by Keller, Macko and Pickitt. The results of their work were published in the Facility Operation Manual (Ref 15). This manual provided equipment lists, operation checklists, a description of the test facility, calibration procedures, and applicable wiring schematics.

In general, the Rocket Test Facility consisted of:

1. Two propellant manifolds for gaseous oxygen and gaseous hydrogen, and a gaseous nitrogen manifold to provide a purge and control system.

2. Check valves, dome valves and solenoids for control of mass flow rates and pressures.

3. Two Hershell venturis, with associated pressure transducers and thermocouples, for measurement of mass flow rates.

4. A test console to control and synchronize the test sequence, and to provide a continuous means of observing important measurements.

5. An oscillograph and visicorder for recording test sequence data.

6. Necessary piping, wiring, instrumentation, and calibration equipment.

A detailed description of the above components is given in the Facility Operation Manual.

Thrust measurements were obtained using a constant stress, cantilever mounted aluminum beam in a manner similar to that given by Ow (Ref 18:10-11). A bridge of four active strain guages was mounted on the engine thrust beam with two guages balanced on either side of the beam. The thrust signal was amplified and recorded on a visicorder where the trace deflection would be proportional to the thrust.

Two pressure transducers were used to measure chamber and coolant pressures. Chamber pressure was measured at the oxygen injector face as shown in Figure 1. The signal was sent directly to the visicorder and to the test console through a Microsen Electronic Pressure Transmitter. The coolant pressure was measured at the aft chamber liner and the signal furnished to the visicorder.

Nozzles A and B were instrumented with six iron constantan thermocouples, as illustrated in Figure 7 and Table I. The thermocouples were spaced axially and circumferentially on the surface of the nozzle to furnish a profile of nozzle wall temperatures for evaluation of coolant configuration effectiveness.

Nozzle C was provided with nine iron constantan thermocouples as shown in Drawing 7B and Figure 8; however, only three

thermocouples were mounted on the nozzle surface while six were installed approximately 1/32 inch from the inside nozzle wall. This installation method was required since the coolant section would cause inaccurate wall surface temperatures for comparison with those of other coolant configurations (nozzles A and B).

The two methods of mounting the thermocouples are shown in Figure 10. The installation method for each type is described below:

1. Surface Thermocouples. First, the leads of the thermocouple were fused together, into a spherical bead, by means of a jewelers torch. Then a small hole, the same size as the thermocouple bead, was drilled in the wall to a point just below the surface. After the thermocouple was inserted, the hole was closed with a punch. Finally, the thermocouple was sealed and insulated with glyptal or furnace cement.

2. Inside Wall Thermocouples. A small hole was drilled in the wall to within 1/32 inch of the inside surface. The thermocouple leads were silver soldered to a short piece of small copper tubing, which had the same diameter as the drilled hole. Then the thermocouple, with cylinder, was inserted into the hole, and pressed firmly into place with another piece of copper tubing. Finally, the installation was sealed and insulated with glyptal or furnace cement.

To provide a valid comparison of nozzle wall temperature profiles, all thermocouples were located at the same respective

area ratio of each nozzle. In addition, the thermocouples for each nozzle were spaced circumferentially in the same relative position, and the nozzles were mounted to the combustion chamber with the same orientation. Therefore, any error resulting from this type of thermocouple installation would be common to all tests. A summary of thermocouple data is given in Table I.

IV. Method of Evaluation

Engine Performance

The method of engine performance evaluation involves a comparision of experimental rocket parameters with those determined theoretically. The basic rocket performance paramenters are defined below:

1. Characteristic velocity (C^*), depends only on the characteristics of the reaction used, and is a function of chamber temperature (T_c) and molecular weight (M). It is relatively independent of chamber pressure (P_c), and indicates the energy available after combustion.

2. Thrust coefficient (C_F), measures the ability of the nozzle to convert the random thermal energy of gases in the combustion chamber into linear momentum, and therefore, directed thrust (F). C_F is nearly constant for a given nozzle.

3. Specific impulse (I_s), combines the first two parameters and is characteristic of overall rocket engine performance. It implies a knowledge of the expansion pressure ratio (P_c/P_e) or exit area ratio (ϵ), and is usually computed for optimum expansion ($P_e = P_a$).

Theoretical values of specific impulse, characteristic velocity and thrust coefficient were determined by a method quite different from that used by Ow (Ref 18:12). Briefly, Ow obtained thermochemical data and isentropic flow functions from the

experimental results of Bollinger and Edse (Ref 6). He first determined an average isentropic coefficient (k) from the isentropic equation, Pv^k = constant, for each mixture ratio. Then, pressure ratio (Pc/Pe) was found for the applicable area ratio (Ae/At) and average k. Hence, exit velocity (Ve) and, therefore, specific impulse (I_s) could be determined from the nozzle isentropic flow equation. Finally, (I_s) was corrected to account for non-optimum expansion (Pe ≠ Pa) by means of the thrust equation. These steps were followed for each test condition assuming average k, T_c and optimum expansion.

For this study theoretical values of I_s, C^* and C_F were determined by aerothermochemical methods (considering the high energy of the hydrogen-oxygen combination). These methods account for dissociation phenomena and allow for different combustion product characteristics in each section of the rocket engine. For each mixture ratio, and assumed temperature and pressure, the properties at a point are determined from equations of equilibrium constants and conservation of mass. Computed properties, in terms of enthalpy and entropy, are then applied to the perfect gas law and energy equation to provide values of velocity and specific impulse (Ref 3:130-188).

The results of these computations for the hydrogen-oxygen system are found in tables and Mollier diagrams published by Jet Propulsion Laboratory (Ref 2:App A). This report includes

data for liquid or gaseous injection of components under various conditions of chamber pressure and temperature. In addition, nozzle expansion properties are provided for equilibrium or constant composition flow.

For the aerothermochemical method the assumptions made in determining point properties are as follows:

1. There is complete combustion in the chamber.
2. The combustion process is adiabatic at constant pressure.
3. The combustion products are in equilibrium at the entrance to the nozzle.
4. Expansion through the nozzle takes place isentropically.
5. The perfect gas law applies.
6. The convergent area ratio of the nozzle is of such a value that the kinetic energy of the gases in the chamber is negligible ($V_c \rightarrow 0$).
7. The flow is steady, homogeneous, and one-dimensional.

Theoretical values of characteristic velocity, specific impulse, and thrust coefficient were computed from data of Ref 2: App A, for gaseous injection of components at 300 psi chamber pressure and expansion to 14.7 psia. These parameters were plotted as a function of mixture ratio (MR) as shown in Figure 14. Equilibrium flow was assumed for optimum expansion, and the small variations in nozzle area ratios (ϵ) and throat areas (A_t) were neglected.

Since specific impulse varies with chamber pressure, mixture ratio, exit velocity and exit pressure, it would be more accurate to determine theoretical values of I_s, for each test condition, from the thrust equation:

$$I_{sT} = \phi I_s - \frac{A_e}{\dot{w}} (P_a - P_e) \qquad (1)$$

where ϕ is a correction factor to account for 2-dimensional flow in the conical divergent section of the nozzle, and has a value of .983 when the half-angle of the divergent (α) is 15° (Ref 3:87-88). I_s is computed for the test conditions of area expansion ratio (ϵ), chamber pressure (P_c) and expansion pressure ratio (P_c/P_e). The second term in equation (1) accounts for overexpansion in the nozzle and is computed for each exit area (A_e), exit pressure (P_e), atmospheric pressure (P_a) and weight flow rate of propellants ($\dot{w}$).

A graphical analysis of equation (1), for each A_e and the assumed test conditions of $\dot{w}$ = .286 lb/sec and P_a = 14.4 psia, is shown in Figure 16. Because exit pressure is a function of mixture ratio for a given-geometry overexpanded nozzle, optimum expansion is approached as the mixture ratio is increased (See Figure 15). Therefore, the plotted curves show that corrections to optimum I_s can be neglected and still maintain accuracy near one percent in the operating range of mixture ratios. An analysis of equation (1) for constant composition flow provided similar results. In addition, actual flow conditions lie somewhere between constant

composition and equilibrium flow (Ref 7:385), and the chamber pressure varies somewhat from ideal (300 psia), so that a rigorous computation for each test condition was not considered worthwhile.

Experimental values of characteristic velocity (C_x^*) were determined, for each test condition, from measured values of chamber pressure (P_c), nozzle throat area (A_t), and total weight flow rate ($\dot{w}$):

$$C_x^* = \frac{P_c A_t g}{\dot{w}} \tag{2}$$

where $\dot{w} = \dot{w}_o + \dot{w}_f + \dot{w}_i$

Experimental values of specific impulse (I_{sx}) were calculated from the defining equation

$$I_{sx} = \frac{F}{\dot{w}} \tag{3}$$

Thrust coefficient (C_{Fx}) for each test condition, was computed from the equation

$$C_{Fx} = \frac{F}{P_c A_t} = \frac{I_{sx} g}{C_x^*} \tag{4}$$

Performance comparison, for each coolant configuration, was obtained by employing the quality factors given below:

(1) Characteristic velocity quality factor (η), a measure of combustion efficiency, is defined

$$\eta = \frac{C_x^*}{C_T^*} \tag{5}$$

(2) Thrust coefficient quality factor (λ), characteristic of nozzle efficiency, is given by

$$\lambda = \frac{C_{Fx}}{C_{FT}} \tag{6}$$

(3) Specific impulse quality factor (ξ), a measure of the overall rocket engine-propellant combination, is defined

$$\xi = \frac{I_{sx}}{I_{sT}} = \eta\lambda \tag{7}$$

Weight flow rates were computed from measured venturi pressures and temperatures by applying the equation

$$\dot{w} = 0.525\, Y_a\, C \frac{D^2}{\sqrt{1-\beta^4}} \sqrt{\rho(P_1 - P_2)}$$

from the ASME Fluid Meters Report (Ref 13: 65). Tables of flow rate for oxygen and hydrogen were provided in the Facility Operation Manual (Ref 15). The validity of these tables was verified by computing several arbitrary mass flows using a standard square-edged orfice. Values were found in agreement to within one percent accuracy.

For the computation of coolant flow rate ($\dot{w}_i$) incompressible flow was assumed so that flow rates would be a function of area only. Then the continuity equation

$$\dot{w}_h = \dot{w}_f + \dot{w}_i \tag{9}$$

becomes

$$\dot{w}_i = \dot{w}_h \left(\frac{A_i}{A_i + A_f} \right) \tag{10}$$

where $\dot{w}_h$ is the total flow rate of hydrogen, A_i is the coolant

area, and A_f is the fuel injection area. For this calculation all hydrogen flow directed radially into the combustion chamber was considered fuel flow rate ($\dot{w}_f$) even though a small portion of the hydrogen provided chamber wall cooling as determined by Ow (Ref 18:14). In addition, Ow found experimentally that

$$\left(\frac{\Delta P}{P}\right)_i \approx \left(\frac{\Delta P}{P}\right)_f$$

which was confirmed in this investigation. Therefore, equation (10) should give a close approximation to $\dot{w}_i$.

In applying equation (10) to nozzle C, the provision for coolant injection near the throat section required an additional assumption. An estimated calculation of mainstream static pressure (P_s), for coolant injection at $A/A_t = 7.43$, showed that

$$\frac{P_s}{P_o} \approx 1$$

where P_o is the mainstream isentropic stagnation pressure. This fact, coupled with a small pressure drop from the aft chamber liner to the nozzle coolant section, resulted in the assumption

$$P_s \approx P_c$$

Coolant injection velocities (V_i) were determined from the Bernoulli incompressible flow equation

$$V_i = \sqrt{2g\, T_o \frac{R}{M} \left(\frac{P_i}{P_c} - 1\right)} \qquad (11)$$

when $\Delta P/P < .1$, and from the compressible isentropic equation

$$V_i = \sqrt{2g\, T_o \frac{R}{M} \frac{k}{k-1} \left[\left(\frac{P_i}{P_c}\right)^{\frac{k-1}{k}} - 1 \right]} \qquad (12)$$

when $\Delta P/P > .1$. For the cases where low injection velocities were obtained using equation (11), the measured pressure differences approached the reading error so that computed velocities could not be considered accurate. These values are marked with a double asterisk in Table III.

Coolant Performance

The method of coolant performance evaluation involves the comparison of nozzle wall temperature profiles with those obtained from the uncooled nozzle. This method was selected because present analytical equations for determining wall temperatures give only approximate results. For example, Bartz, Colburn, Mayer, Sibulkin, Greenfield, and Long offer relationships for the nozzle local heat transfer coefficient (h) in the form

$$Nu = \frac{hD}{K} = C\,(Re)^a\,(Pr)^b\,\left(\frac{T_g}{T_w}\right)^c \qquad (13)$$

which is similar to the pipe flow heat transfer relation.

Equation (13) is generally used in conjunction with Newton's equation, $q = h\,(T-T_w)$, and measured specific rate of heat flow (q), to provide theoretical values of wall temperature (T_w). However, these equations apply to convective/conductive heat transfer only and assume the following conditions (Ref 4:49):

1. No gas or wall radiation.

2. No gaseous dissociation with subsequent recombination near the wall.

3. No high frequency flow instabilities.

4. No combustion product deposits on the wall.

5. Complete combustion in the chamber.

Welsh and Witte made a comparison of analytical and experimental local heat fluxes in a nozzle and found variations in analytical estimates from 45% below to 80% above those determined experimentally. They indicated that combustion and flow non-uniformities, resulting from propellant-injector flow characteristics and combustion chamber configuration, were a major factor in these deviations (Ref 27:14). Therefore, as a result of these non-uniformities and assumptions, theoretical determination of wall temperature profiles was not attempted.

Theoretical values of gas stream static temperatures that could be used in this analysis were obtained from Ref 2: App A. These values were plotted as a function of mixture ratio (MR) for the combustion chamber, nozzle throat, and nozzle exit, as shown in Figure 17. The main purpose of Figure 17, then, is to indicate temperature magnitudes and gradients that might be expected within the nozzle.

Experimental values of wall temperature were determined for each coolant configuration by measuring nozzle surface temperatures, as discussed in Section III, Instrumentation. These values can be

assumed to closely approximate the temperature of the nozzle inside wall. For this assumption the high thermal conductivity of copper and small wall thickness (t_w) coupled with a low film heat transfer coefficient of out-side air lead to a small temperature gradient through the nozzle wall. This assumption was confirmed with inside wall and surface thermocouples installed at the entrance, throat, and exit of nozzle C. Differences in temperature through the wall were only 5 - 50°F throughout the range of mixture ratios. Then, for all coolant configurations the wall temperature profiles could be compared with those obtained for configuration B-C (no film cooling) without introducing major errors in thermocouple installation and testing conditions.

Finally, the coolant configuration providing the greatest local and overall wall temperature decrease for the least coolant flow rate and loss in engine performance would be considered the optimum.

V. Discussion and Results

Test Procedure

A series of tests were made for each nozzle/coolant configuration by varying the propellant pressures, and therefore, mixture ratio for each test. The five basic coolant configurations comprising three nozzles and three chamber liners were used to provide various coolant flow ratios (ω). Two series of tests were made with each nozzle, A and B, for tangential coolant injection at the nozzle entrance (ω = .178 and .109). Two test sequences were made with nozzle C, for 45° coolant injection upstream of the throat (ω = .084), and for a combination of throat injection and 15° coolant injection at the nozzle entrance (ω = .176). A final test series was made with nozzle B in the uncooled condition to provide a basis for comparison. Mixture ratios ranged from 1.5 to 6.5 while total hydrogen flow rates and coolant flow rates varied from .126 lb/sec to .040 lb/sec, and .022 lb/sec to .004 lb/sec, respectively. Visicorder data was evaluated immediately after each test to ensure the attainment of the desired conditions of chamber pressure (300 psia) and mixture ratio. Also, the rocket engine was inspected for damage to components, signs of discoloration and oxidation, and change of critical dimensions. Discrepancies detected were corrected prior to the following test.

Calibration Procedure

Calibration of pressure channels was accomplished using amplifier precision resistors and checked by loading pressure transducers and calibrated pressure guages simultaneously. The linearity of the transducers and recorder galvanometers produced a trace deflection which was proportional to the calibration load, thereby providing a calibration factor. This calibration factor, when applied to trace deflections obtained during a test, would then yield corrected pressure readings.

The thrust channel was calibrated in a manner similar to that of the pressure channels. In this case, the thrust beam was loaded with known weights and the output from the strain guages was sent through the amplifier system to the recorder. This calibration was performed without propellant flow to the engine. However, a check was made for developed thrust due to propellant flow alone under prevailing conditions that occurred during the tests. The maximum thrust thus obtained was less than + .3 pounds. Therefore, this small variable error, caused by propellant flow in the feed lines, was neglected in the thrust calculations.

Temperature channel calibration was accomplished using a potentiometer in conjunction with a variable resistor bank and a specially devised calibration circuit. A known voltage corresponding to the thermocouple temperature equivalent was impressed on the thermocouple circuit, thereby providing a trace deflection on the recorder. No load and balance conditions were furnished by the special calibration

circuit. The variable resistors were used to establish circuit critical damping conditions for the recorder galvonometers. The trace deflections then provided calibration curves which could be used to determine thermocouple temperatures for each test.

After completion of each test series, load calibration of all data channels was reaccomplished. In addition, recalibration was accomplished whenever a channel component was changed or when experimental data showed unaccountable trends. Differences between initial calibration curves and those obtained after each test series where within $\pm$ .02 inch trace deflection, which is the attainable reading accuracy. Corresponding data errors for a $\pm$ .02 inch trace deflection are: $\pm$ 2 psia for pressures, $\pm$ 5°F for temperatures, $\pm$ .5% for thrust, $\pm$ 1.5% for mass flow rates, $\pm$ 2.0% I_{sx} , $\pm$ 3.5% C^*_x , and $\pm$ 3.5% C_{Fx}.

General Discussion

Experimental data for each test series is presented in Table II, Engine Performance Summary, and Table III, Coolant Performance Summary. A typical data test run is shown in Figures 35 and 36. All data listed was used in the experimental evaluation, except as noted under each coolant configuration. Tests 1-3 were not listed since burning occurred entirely outside of the nozzle and equilibrium chamber conditions were never reached. This problem was corrected by using larger oxygen start pressures to maintain combustion in the chamber when shifting from start to run conditions.

Tests 4-6 of 10 second duration were conducted for rocket engine shakedown and to evaluate the nozzle water cooling system. Tests 4 and 5 proved successful in demonstrating overall rocket engine operation, but the water cooling system froze during test 6 due to a 20°F ambient temperature. An indirect result of these tests was that the film cooling configuration effectively decreased nozzle wall temperature so that the water cooling scheme could be eliminated. Another result was that steady state engine operation and wall temperature stabilization occurred in about 3 seconds. Experimental data for tests 7, 8, 50 and 58 was not obtained because of a jammed oscillograph or visicorder, as indicated in Table II.

For some of the initial tests with nozzles A and B, an instability problem was encountered in that steady state engine operation could not be achieved at the low mixture ratios (high hydrogen flow rates). This instability was eventually traced to the hydrogen supply manifold. Although the hydrogen supply pressure available was 1200-1800 psia, and only 500-600 psia run pressure was required, the use of 2 hydrogen bottles was insufficient to fulfill volume/mass flow requirements. By placing 10 or more hydrogen bottles on the supply manifold, steady state conditions were obtained in less than 3 seconds for all mixture ratios. In addition, better utilization was made of available gas supplies since the pressure differential between available and

required hydrogen run pressures could be reduced to about 100 psia and still allow stable engine operation.

Several temperature and injection velocity discrepancies are noted in Table II. As explained in Section IV, the coolant injection velocities marked with a double asterisk are inaccurate due to a small injection pressure differential. However, these velocities can be definitely categorized in the low velocity class for coolant effect analysis. Various temperature points, indicated under "Remarks", were not obtained because of faulty thermocouple installation or an oscillograph channel malfunction. Since all temperature data was provided by the oscillograph, some delay was encountered in correcting temperature channel discrepancies due to lag time for development of oscillograph film. This is evident in the series of missing data points for a particular thermocouple channel.

Table III also shows several non-steady temperature readings, indicated by a single asterisk. These temperatures occurred at a mixture ratio near five for the coolant configurations and at a mixture ratio of four for the uncooled configuration. In both cases, the temperatures were increasing at a moderate rate. Except for the non-steady temperature points used to evaluate configuration B-C (no cooling) these temperatures were not used in the cooling effect analysis. Nevertheless, the non-steady temperatures of cooled configurations provided an estimate of higher mixture ratios attainable without nozzle failure.

required hydrogen run pressures could be reduced to about 100 psia and still allow stable engine operation.

Several temperature and injection velocity discrepancies are noted in Table II. As explained in Section IV, the coolant injection velocities marked with a double asterisk are inaccurate due to a small injection pressure differential. However, these velocities can be definitely categorized in the low velocity class for coolant effect analysis. Various temperature points, indicated under "Remarks", were not obtained because of faulty thermocouple installation or an oscillograph channel malfunction. Since all temperature data was provided by the oscillograph, some delay was encountered in correcting temperature channel discrepancies due to lag time for development of oscillograph film. This is evident in the series of missing data points for a particular thermocouple channel.

Table III also shows several non-steady temperature readings, indicated by a single asterisk. These temperatures occurred at a mixture ratio near five for the coolant configurations and at a mixture ratio of four for the uncooled configuration. In both cases, the temperatures were increasing at a moderate rate. Except for the non-steady temperature points used to evaluate configuration B-C (no cooling) these temperatures were not used in the cooling effect analysis. Nevertheless, the non-steady temperatures of cooled configurations provided an estimate of higher mixture ratios attainable without nozzle failure.

In order to ensure a valid comparison of nozzle wall temperatures, similarity of test operation conditions was maintained in addition to the thermocouple installation similarities previous described in Section IV. All engine test times were restricted to 4.5 $\pm$ .7 sec, and measured from the initiation of run settings to purge shutdown. Also, initial wall temperatures and ambient conditions of air velocity and temperature were approximately the same for each test. These conditions of similarity are particularly important where non-steady temperature occurred. Even so, the manner of thermocouple installation, the impossibility of reproducing identical engine operating conditions for each configuration and mixture ratio and the variation of test times created some errors in the coolant configuration comparisons. However, it is felt that the sum of these errors was not significant so that experimental results should provide a reasonably accurate evaluation of performance.

Burnout of nozzle A occurred during test 26, for coolant configuration A-B (ω = .109). The burnout was first detected by a gradual fall-off of chamber pressure. Subsequent inspection showed that melted copper had started to flow from the convergent section near the throat, as shown in Figure 11. A throat temperature of 1760°F was recorded at the test run time of 4.3 seconds. The falure of this nozzle did not necessarily signify film cooling ineffectiveness since this test was made under the non-steady operating conditions previously discussed. The rapid decrease of hydrogen flow rate (increasing MR) resulted in a decreasing coolant

flow rate while mainstream static temperature was rapidly increasing. Therefore, the performance data of this test was used only in estimating the mixture ratio (6.49) and associated failure conditions. A direct result of this test was the inadequacy of the film cooling scheme to provide required coolant flow rate at the high mixture ratios.

Nozzle B in the uncooled configuration (B-C) sustained a throat burnout during test 71, similar to that of nozzle A (See Figure 12). For this test (MR = 4.17) equilibrium chamber conditions were reached, but nozzle wall temperatures were rapidly increasing at the time of burnout (4.9 sec). The highest wall temperature recorded was 1780°F at the nozzle throat.* This nozzle wall temperature profile was used to evaluate coolant performance since the effect of a comparison with coolant configuration profiles would give conservative results.

Two test series consisting of 28 test runs were made with no apparent difficulties using nozzle C (coolant configurations C-D and C-E). For these tests the effects of film cooling were particularly noticable in the throat section of the nozzle. From the location of injected coolant in the convergent section to a point half-way through the divergent section the inside wall surface remained a bright copper color while other portions of the nozzle surface were coated with dark deposits. The lack of the dark

*The melting temperature of copper is 1981°F at standard conditions.

deposits in the film cooled area was attributed to the coolant effect of preventing such formations while providing a thermal insulating boundary layer. Additionally, the light-colored area showed the extent of the cooling film layer prior to diffusion into the main gas stream. The film cooling effects are shown in Figure 13 but are barely discernible due to poor photographic lighting. The film coolant stains indicate that the hole spacing is at a maximum for adequate cooling in the throat area. Therefore, an increase in hole spacing would lead to only partial film cooling coverage.

The effects of film cooling in the combustion chamber are illustrated in Figure 4. Here, the discoloration around the fuel injector holes show that this film cooling scheme is at a minimum acceptable level for the higher hydrogen flow rates (high injection velocities).

Some questions may arise as to the manner of determining mixture ratio in this investigation. It should be noted that all hydrogen injected radially into the combustion chamber was considered fuel flow rate ($\dot{w}_f$), for computing mixture ratio ($MR = \dot{w}_o/\dot{w}_f$), while hydrogen flow that entered the nozzle by tangential or 45° radial injection was considered coolant flow rate ($\dot{w}_i$). However, it is likely that some portion of the injected coolant diffused immediately into the main gas stream, especially near the nozzle entrance, where it probably reacted with the oxygen to slightly

alter the mixture ratio, and therefore, theoretical data. This would result in a fuel-rich mixture ratio, particularly in the neighborhood of the wall, and increase the possibilities of recombination (energy release). For the extreme condition, if all hydrogen flow ($\dot{w}_f + \dot{w}_i$) had been considered as fuel flow in the mixture ratio calculation, the experimental mixture ratios would have been lower than those shown in the data tables by 8% for configuration C-D, 11% for configurations A-B and B-B, and 17% for configurations A-A, B-A and C-A (the maximum at the low mixture ratios). Nevertheless, it was felt that the actual case was much closer to the assumed conditions of no coolant reaction so that only small deviations would result at the low mixture ratios and practically no variations would occur in the high mixture ratio range.

Experimental Performance

For each test condition characteristic velocity, specific impulse and thrust coefficient were computed from the data presented in Table II. These experimental values were compared with theoretical values (Figure 14) and expressed as the quality factors η, λ, and ξ. The results were then plotted to provide the curves of Figures 18-26.

For nozzle A (coolant injection at the entrance) the characteristic velocity performance level η was about 83% for $\omega = .109$ and 81% for $\omega = .178$ at the lower mixture ratios (Figure 18). The increase in performance with increasing mixture

ratio was attributed to the decreasing cooling flow rate ($\dot{w}_1$) which resulted in improved combustion. Since the thrust coefficient quality factor, λ , for this nozzle was near 99% (Figure 24), combustion inefficiencies were the major factors affecting the specific impulse performance level, as shown in Figure 21. Here, the performance quality factor ξ , was on the order of 82% for ω = .109 and 80% for ω = .178. The similarity of the η and ξ curves should be noted. The decrease in performance level for the higher coolant flow ratio was only about 2%. The small decrease indicated that the low overall performance level of 83% must be a result of some factor other than coolant flow. This fact became apparent in the experimental evaluation of nozzle B.

The performance results for nozzle B are shown in Figures 19, 22 and 25. For this nozzle (coolant injection at the entrance) coolant flow ratios were identical to that of nozzle A, but the mixture ratio range was extended to lower values; in addition, engine performance with no cooling was evaluated. The results again show the dependency of characteristic velocity and specific impulse on coolant flow ratio. Especially noticable is the fall-off in the performance curves at the lower mixture ratios where coolant flow rates were greatest. However, a portion of this performance fall-off is probably due to the manner in which mixture ratio was computed; considering hydrogen reaction near the nozzle entrance at the high coolant flow rates with subsequent change in mixture ratio.

This would cause a leftward shift in the performance curves (C^*, I_s and C_F) at the low mixture ratios and result in a smaller decrease in performance efficiencies (η , ξ , and λ) below a mixture ratio of about 2.5.

Performance efficiencies of nozzle B were about 2% higher than those of nozzle A. This higher performance efficiency arises mainly from improved nozzle design which increased the thrust coefficient quality factor to the 100% level (See Figure 24 and 25).

Figure 19 provides another important result concerning combustion efficiency. The characteristic velocity quality factor, for the uncooled configuration (B-C) was at a performance level of about 87%. This revealed that 13% of the performance loss associated with the coolant configurations was caused by combustion inefficiencies in the combustion chamber, separate from those due to nozzle coolant injection. These combustion inefficiencies were explained by Ow in his analysis of the film cooled combustion chamber (Ref 18:20). Ow found that the radial method of fuel injection plus the fact that a portion of the injected fuel also provided some film cooling effects, led to maximum combustion efficiencies near 88%. Therefore, these effects were reflected in the coolant configuration performance levels of this investigation.

Nozzle C performance results are shown in Figures 20, 23 and 26. The coolant configurations for coolant injection near the nozzle throat (C-D) as well as coolant injection at both nozzle throat and entrance (C-D) demonstrated performance levels and curve shapes

similar to those of nozzles A and B. However, λ for nozzle C was about 1% higher than that of nozzle B. The slightly higher thrust coefficient most likely resulted from the difference in expansion area ratios for the two nozzles since all other geometry factors and test conditions were equal. Thus, the expansion area ratio for nozzle C, being closer to optimum thoroughout the mixture ratio range, enabled somewnat higher performance efficiencies.

Since specific impulse is dependent upon characteristic velocity and thrust coefficient, the loss in overall performance is best represented by this parameter. Therefore, the specific impulse of each coolant configuration was compared with that of the uncooled configuration and the resulting difference plotted as a function of coolant flow ratio. See Figure 27. A mixture ratio of three was selected since experimental and theoretical results have proved this mixture ratio to be near the optimum for the H_2-O_2 system. The performance loss curves clearly indicate that specific impulse decreases with increasing coolant flow ratio. However, in all cases the performance loss was relatively low, a maximum of 3.5% for ω = .187 (nozzle B). This result points out the advantage of using reactive coolants. Also, it was observed (Figure 27) that cooling configurations C-D and C-E provided the desired larger coolant flow ratios for the least reduction in performance, about 1% and 2.5% respectively. This can be explained by noting that the thrust coefficient of nozzle B was about 2% higher than that of nozzle A and 1% lower than that of nozzle C. Since comparisons were based on the

uncooled nozzle B, nozzle A and C thrust efficiencies were reflected in the performance loss curves. In addition, higher performance appears to be dependent upon injection location, although not significantly. This possibly accounts for the 1% difference in curves for coolant injection at the nozzle entrance (coolant configurations B-B), and coolant injection near the nozzle throat (coolant configuration C-D). See also Figures 19 and 20. Finally, it should be noted that the performance loss curves of Figure 27 represent coolant flow ratios based on total hydrogen flow rates, $\dot{w}_i/\dot{w}_h$, which are somewhat higher than those based on total propellant flow rates, $\dot{w}_i/\dot{w}$. The $\dot{w}_i/w$ scale was provided to show this relationship. The latter flow ratio percentages are approximately 6% for coolant configurations A-A, B-A, and C-E, 4% for coolant configurations A-B and B-B, and 3% for coolant configuration C-D.

Nozzle wall temperatures for the entrance, throat and exit were plotted as a function of mixture ratio in Figures 28, 29, and 30, respectively. These figures show that wall temperature increases with increasing mixture ratio (increasing mainstream static temperature), but at a level dependent upon the coolant flow ratio. Note that the wall temperature curves in Figure 28 for coolant configuration B-A (tangential injection) and C-E (15 degree angle of injection) are nearly identical. The small difference in wall temperature arises mainly from different coolant mass flows for each case, recalling that part of the coolant flow (about 1/3 for configuration C-E) was injected near the nozzle throat. Apparently, coolant injection at

small angles to mainstream flow, as compared with tangential injection, has little effect on wall temperature for the same coolant flow rate.

The slopes of the curves in Figures 28 and 29 demonstrate the influence of injection velocity on wall temperature; since coolant injection area was constant, injection velocity decreased with increasing mixture ratio (decreasing hydrogen flow rate). No velocity influence was noted until a mixture ratio of about three was reached where injection velocities approached 800 ft/sec. Then, the wall temperature remained nearly constant until a mixture ratio of about four was reached, although mainstream static temperature and wall temperature of the uncooled nozzle (B-C) were rapidly increasing at this mixture ratio. Evidently, injection velocities below 800 ft/sec improve the stability of the coolant film due to decreasing diffusion into the main gas stream. Absolute wall temperatures were much lower than expected, as indicated by uncooled configuration B-C. These lower temperatures apparently arise from lower mainstream gas temperatures and are attributed to the 85% combustion efficiencies previously discussed.

Nozzle wall temperature profiles for mixture ratios 2.0, 3.0, and 4.0 are provided in Figures 31-33. These profiles were plotted as a function of area ratio rather than axial distance since axial distance varied for each nozzle while area ratio, where temperature was measured, remained constant. The wall temperatures are seen to be proportional to the quantity of coolant injected. Also, it should

be observed that wall temperature continually increased with distance from the point of coolant injection. This brings out the fact that a constant wall temperature is not possible using a gaseous film coolant. The slopes of these temperature profiles, as compared with the uncooled nozzle (configuration B-C), demonstrated the persistance and extent of the film coolant with distance from the point of injection, i.e., coolant injection at the nozzle entrance had little affect on wall temperature at the nozzle throat, whereas coolant injection near the nozzle throat considerably lowered the throat wall temperature. However, the difference in wall temperature levels was not as great as might be expected. This evidently resulted from the lower coolant flow rate near the throat and the fact that the coolant was injected at 45° to the mainstream flow direction, rather than tangentially. Even so, the decrease in throat wall temperature emphasizes the importance of renewing the gaseous coolant film at various locations along the nozzle.

The influence of injection velocity was again noted in the wall temperature profiles of Figures 31 and 33. Here, the coolant effects were greatest at the higher mixture ratio where coolant injection velocities were lowest.

Cooling effectiveness of the various coolant configurations is summarized in Figure 34, for a mixture ratio of 3.0. This analysis was derived from a comparison of wall temperatures for each coolant configuration with those of the uncooled nozzle. Wall temperature

reductions at the nozzle entrance were about 38% for 15° and tangential injection (coolant configurations C-E and B-A), while a decrease of 28% was noted at the nozzle throat for 45° injection (coolant configurations C-D and C-E). Practically no reductions occurred at the nozzle exit for any of the coolant configurations. In addition, it was observed that coolant configuration C-E, with coolant injection at both nozzle entrance and throat, provided the largest overall wall temperature reductions throughout the nozzle.

In the final analysis reference is made to Figures 27 and 34 which show the effects of coolant flow ratio on engine performance and cooling effectiveness. It is apparent, that coolant configurations C-E (ω = .176) for coolant injection at the nozzle entrance and throat provided the best cooling method for the least loss in engine performance. For a performanne loss near 3% this cooling scheme reduced average wall temperatures about 30% from the nozzle entrance to a point past the nozzle throat. In addition, some wall temperature reductions were realized in the latter half of the nozzle divergent section (approximately 10%).

Because of the assumptions imposed on performance calculations and the manner of determining cooling effectiveness discussed in other sections of this study, the values given above should be considered conservative estimates. Also, it is felt that film cooling configuration C-E can be considerably improved to provide wall temperature reductions greater than 40% without additional loss in performance (no increase in coolant flow rate). This could

be accomplished by reducing the 45° radial injection angle to a point nearer the tangential direction, decreasing the spacing of injection holes, and maintaining injection velocities below 800 ft/sec. Nevertheless, coolant configuration C-E fulfills the cooling requirements established for this study, i.e., to effectively and efficiently reduce the wall temperature throughout the nozzle, especially in the most critical area——the nozzle throat.

VI. Conclusions

1. A small rocket engine nozzle can be effectively film-cooled with a gaseous coolant.

2. Rocket engine overall performance is only slightly affected by the injection of a reacting coolant gas in the nozzle.

3. Cooling effectiveness increases proportional to the coolant flow rate.

4. Engine performance is relatively independent of coolant injection location for equal coolant flow rates, but is dependent upon the coolant quantities injected.

5. Tangential coolant injection at the nozzle wall is the most effective means of establishing a gaseous cooling film.

6. Coolant injection near the nozzle throat provides the greatest decrease in throat wall temperatures.

7. Good cooling effectiveness and high rocket engine performance can be obtained over a wide range of mixture ratios.

8. Low injection velocities at the nozzle entrance increase cooling effectiveness.

9. Overall nozzle cooling is improved by increasing the number of axial coolant injection locations.

VII. Recommendations

It is recommended that:

1. Further work be conducted to optimize the gaseous film cooling technique. This could be accomplished by providing additional coolant injection locations in the convergent and divergent sections of the nozzle.

2. Work be performed to investigate optimum coolant flow rates, injection velocities, and injection hole spacing at a constant mixture ratio.

3. The wall temperature data provided in Table III be analysed to determine nozzle heat transfer coefficients and fluxes for the H_2-O_2 system. Subsequently, a comparison with theoretical heat transfer equations could be made and an applicable equation fitted to the experimental data. Such an analysis would be of value in predicting future heat transfer rates.

4. The engine be modified to investigate gaseous transpiration cooling in the combustion chamber.

In addition, efforts should be made to improve combustion efficiencies. The modified impinging/showerhead oxygen injector was not evaluated but an investigation of this part could possibly lead to improved engine performance. Also, unfinished spare injectors are available to permit investigation of other types of injection.

BIBLIOGRAPHY

1. Abramson, Andrew E. "Investigation of Internal Film Cooling of Exhaust Nozzles of a 1000-Pound Thrust Liquid-Ammonia/Liquid-Oxygen Rocket." NACA Research Memorandum, RM E52C26 (June 17, 1952).

2. Baker, Dwight I. "Mollier Diagrams for the Hydrogen-Oxygen System and Experimental Results of Tests on a Rocket Motor of 500-Pound Thrust." Jet Propulsion Laboratory Report, No. 20-127. California Institute of Technology, Pasadena, California (May 4, 1959).

3. Barrere, M., Jaumotte, A., Deveubeke, B., and Vandenkerckhove, J. Rocket Propulsion. New York: Elsevier Publishing Company, 1960.

4. Bartz, D. R. "A Simple Equation for Rapid Estimation of Nozzle Convective Heat Transfer Coefficients." Jet Propulsion, 27: 49-51. (January 1957).

5. Boden, R. H. "Heat Transfer in Rocket Motors and Applications of Film and Sweat Cooling." Jet Propulsion, 73: 385-390. (May 1951).

6. Bollinger, L. E. and Edse, R. "Research on a Premixed Gaseous Rocket Propellant." WADC TN 55-388. (August 1955).

7. Bollinger, L. E. et al. "Non-equilibrium Chemical Conduction Recombination Effects in Exhaust Nozzle Flow." Liquid Rockets and Propellants. New York: Academic Press, 1960. pp 385-403.

8. Eckert, E. R. G. Heat and Mass Transfer (Second Edition). New York: McGraw Hill Book Company, Inc. (1959).

9. Eckert, E.R. G. "Transpiration and Film Cooling." Heat Transfer Symposium. University of Michigan: University of Michigan Press, (1952) pp 173-192.

10. Eckert, E. R. G. and Livingood, J. B. "Comparison of Effectiveness of Convection-, Transpiration-, and Film-Cooling Methods with Air as a Coolant." NACA Technical Note, TN 3010 (October 1953).

11. Eckert, E. R. G. and Schneider, P. J. "Mass Transfer Cooling of a Laminar Boundary Layer by Injection of a Light-Weight Foreign Gas." Jet Propulsion, 28: 34. (January 1958).

BIBLIOGRAPHY - (Continued)

12. Ferri, A. and Libby, P. A. "The Use of Helium for Cooling Nozzles Exposed to High Temperature Gas Streams." WADC TN 55-318 (July 1955).

13. ..... American Society of Mechanical Engineers Fluid Meters. ASME Research Publication of Fluid Meters - Their Theory and Application.

14. Hyman, S. C., et al. "Transpiration and Film Cooling for Solid Propellant Rocket Nozzles." United Nuclear Corporation Report, NDA 2150-1. United Nuclear Corporation Development Division, White Plains, New York (1961).

15. Keller, R. G., Macko, R. F. and Pickitt, J. L. Operations Manual for the Rocket Engine Test Facility of the Department of Mechanical Engineering. Air Force Institute of Technology. Wright-Patterson Air Force Base, Dayton, Ohio (August 1961).

16. Knuth, E. L. "The Mechanics of Film Cooling." Jet Propulsion, 24: 359-365. (November-December 1954).

17. Morrell, G. "Investigation of Internal Film Cooling of a 1000-Pound Thrust Liquid-Ammonia Liquid-Oxygen Rocket-Engine Combustion Chamber." NACA Research Memorandum, RM E51E04 (July 17, 1951).

18. Ow, Y. W. An Evaluation of a Film Cooled Gaseous Hydrogen and Oxygen Rocket Engine of 100 Pounds Thrust. An unpublished thesis for degree of Master of Science in Astronautical Engineering at the Air Force Institute of Technology, (August 1960).

19. Papell, S. and Trout, A. M. "Experimental Investigation of Air Film Cooling Applied to an Adiabatic Wall by Means of an Axially Discharging Slot." NASA TN-D-9 (August 1959).

20. Pickitt, J. L. Design of, and Proposed Test Program for a Film-Cooled Nozzle. An unpublished thesis for degree of Master of Science in Aeronautical Engineering at the Air Force Institute of Technology, (August 1961).

21. Schmidt, D. L. "Ablation of Plastics". ASD-TR-61-650 February 1962).

BIBLIOGRAPHY - (Continued)

22. Seban, R. A., Chan, H. W., and Scesa, S. "Heat Transfer to a Turbulent Boundary Layer with Tangential Fluid Injection" ASME 59-A-177 (August 1959).

23. Sibulkin, M. "Heat Transfer to an Incompressible Turbulent Boundary Layer and Estimation of Heat Transfer Coefficients at Supersonic Nozzle Throats." Journal of the Aero. Sciences, 23: 162-172 (February 1956).

24. Sutton, G. P. Rocket Propulsion Elements (Third Edition). New York: John Wiley and Sons Inc. (1963).

25. ..... "Thermal Erosion of Ablative Materials." ASD-TR-61-307 (April 1962).

26. Welsh, W. E. Jr. "Review of Results of an Early Rocket Engine Film-Cooling Investigation at the Jet Propulsion Laboratory." Jet Propulsion Laboratory Technical Report, No. 32-58. California Institute of Technology, Pasadena, California (1961).

27. Welsh, W. E. Jr. and Witte, A. B. "A Comparison of Analytical and Experimental Local Heat Fluxes in Liquid-Propellant Rocket Thrust Chambers". Jet Propulsion Laboratory Technical Report, No. 32-43. California Institute of Technology, Pasadena, California (1961).

28. Zucrow, M. J. Aircraft and Missile Propulsion (Volume I). New York: John Wiley and Sons, Inc. (1958).

29. Zucrow, M. J. and Graham, A. R. "Some Considerations of Film Cooling for Rocket Motors." Jet Propulsion, 27: 650-656 (June 1957).

APPENDIX A

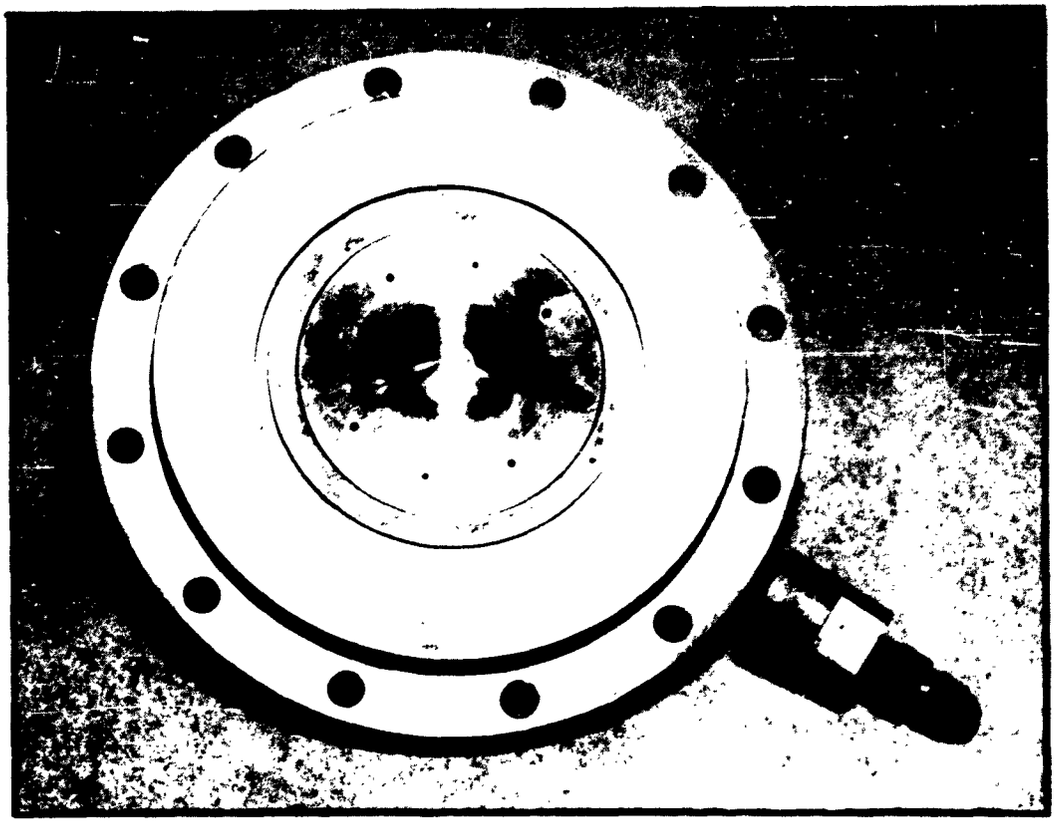

Assembled modified injector showing chamber pressure tap

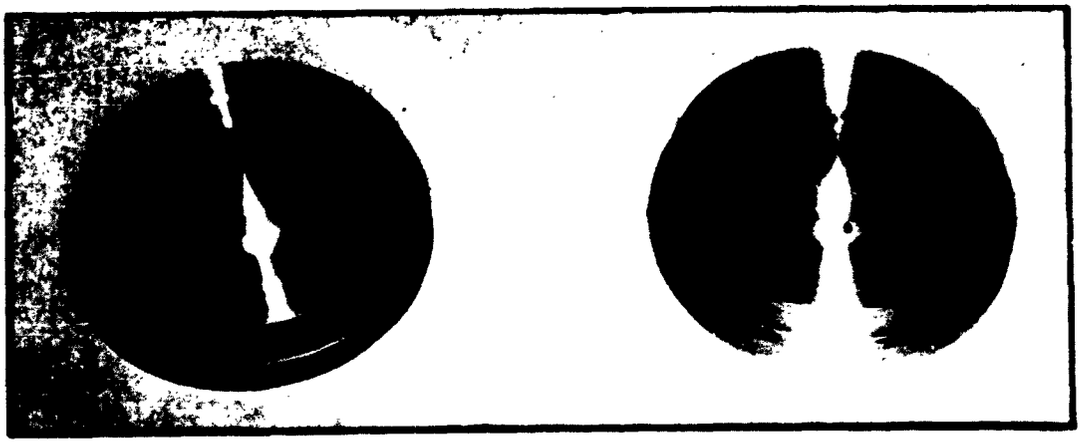

Original impinging injector Impinging/showerhead injector

Figure 1 - Oxygen Injectors and Assembly

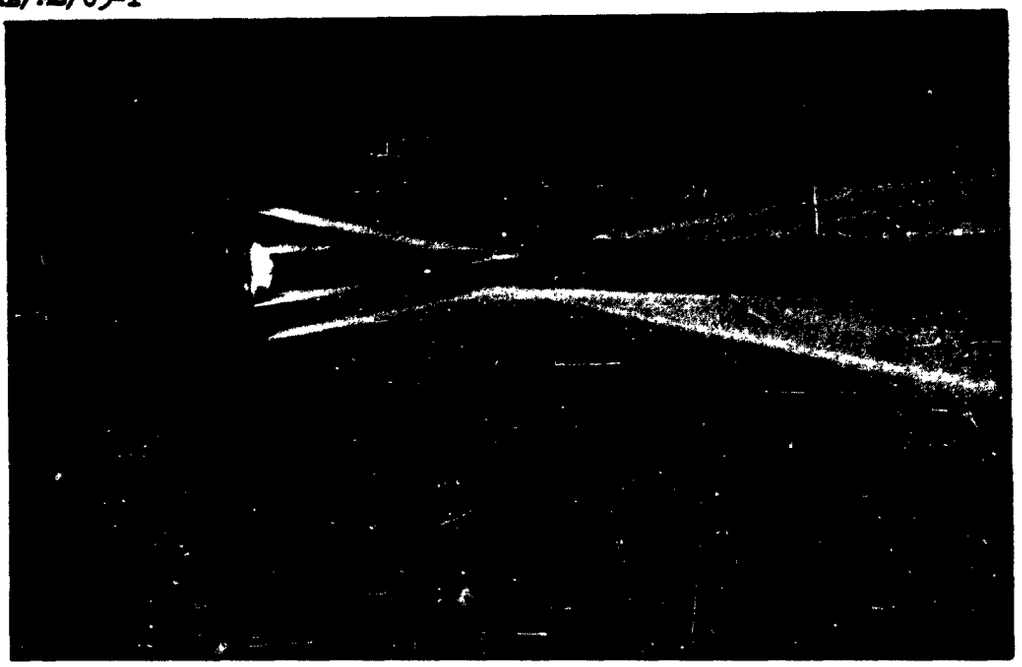

Original injector

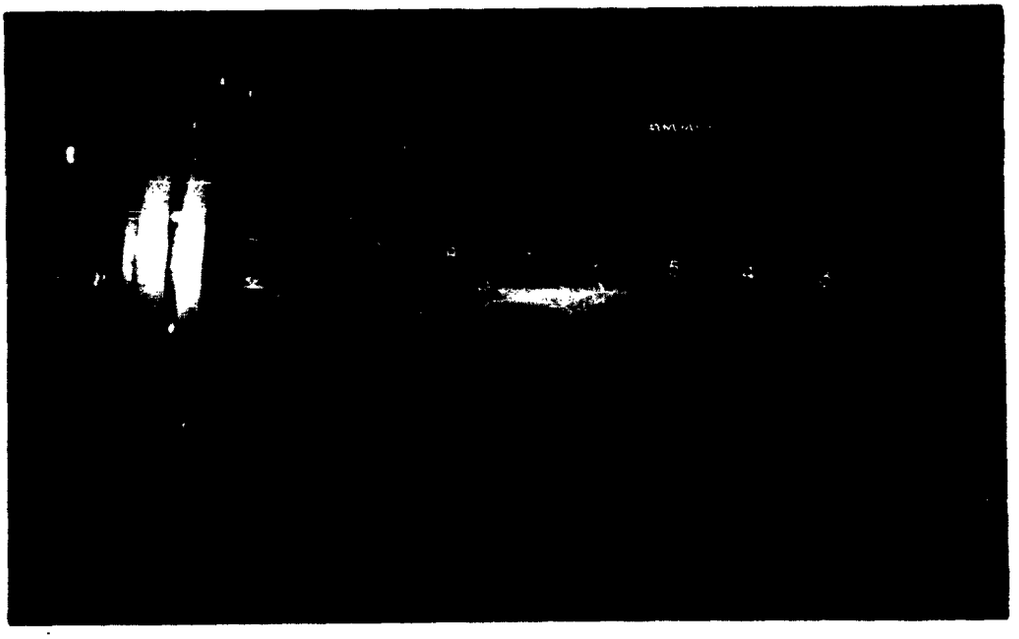

Modfied injector

Figure 2 - Oxygen Injector Water Spray Tests

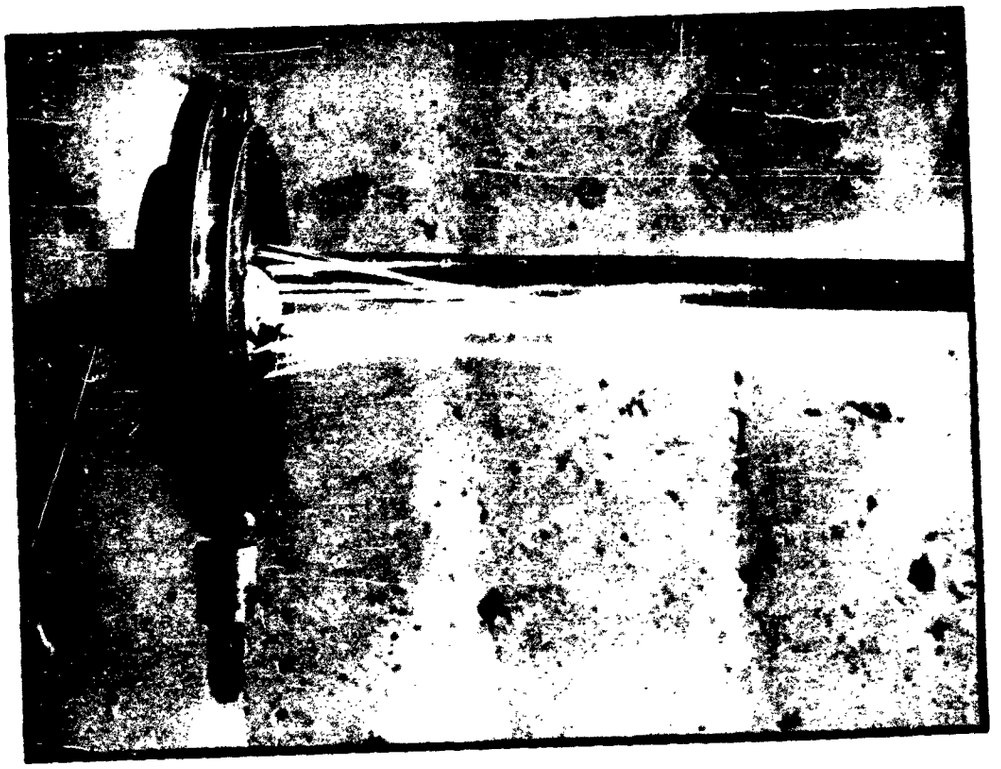

Figure 3 - Water Spray Test -- Inpinging/showerhead Oxygen Injector

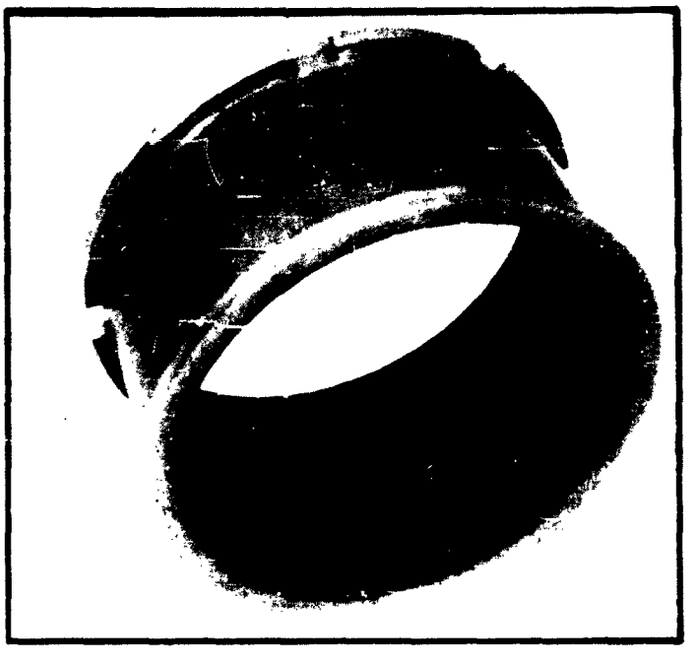

Liner used with coolant configurations A-B, B-B and C-E.
(Taken after completion of test 61)

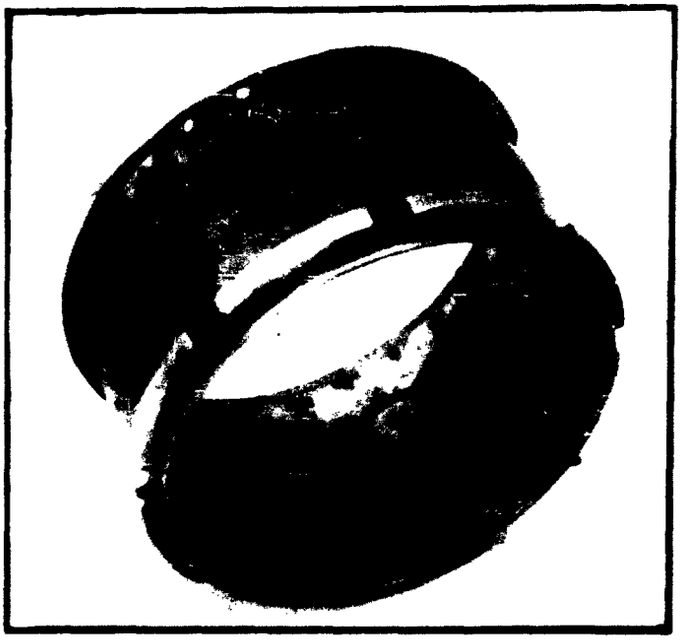

Liner used with coolant configurations A-A and B-A.
(Taken after completion of test 41)

Figure 4 - Hydrogen Injector Aft Chamber Liners

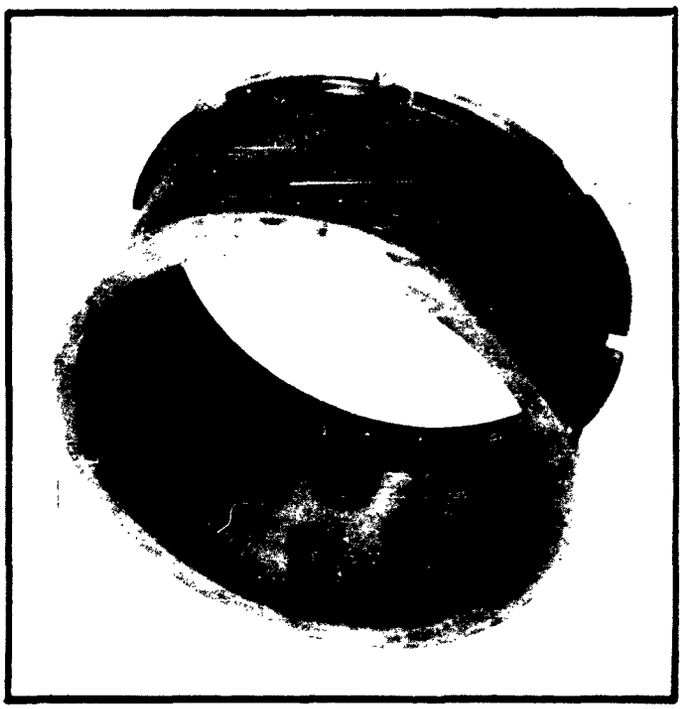

Liner used with uncooled configuration B-C.
(Taken after completion of test 71)

Figure 5 - Hydrogen Injector Aft Chamber Liner

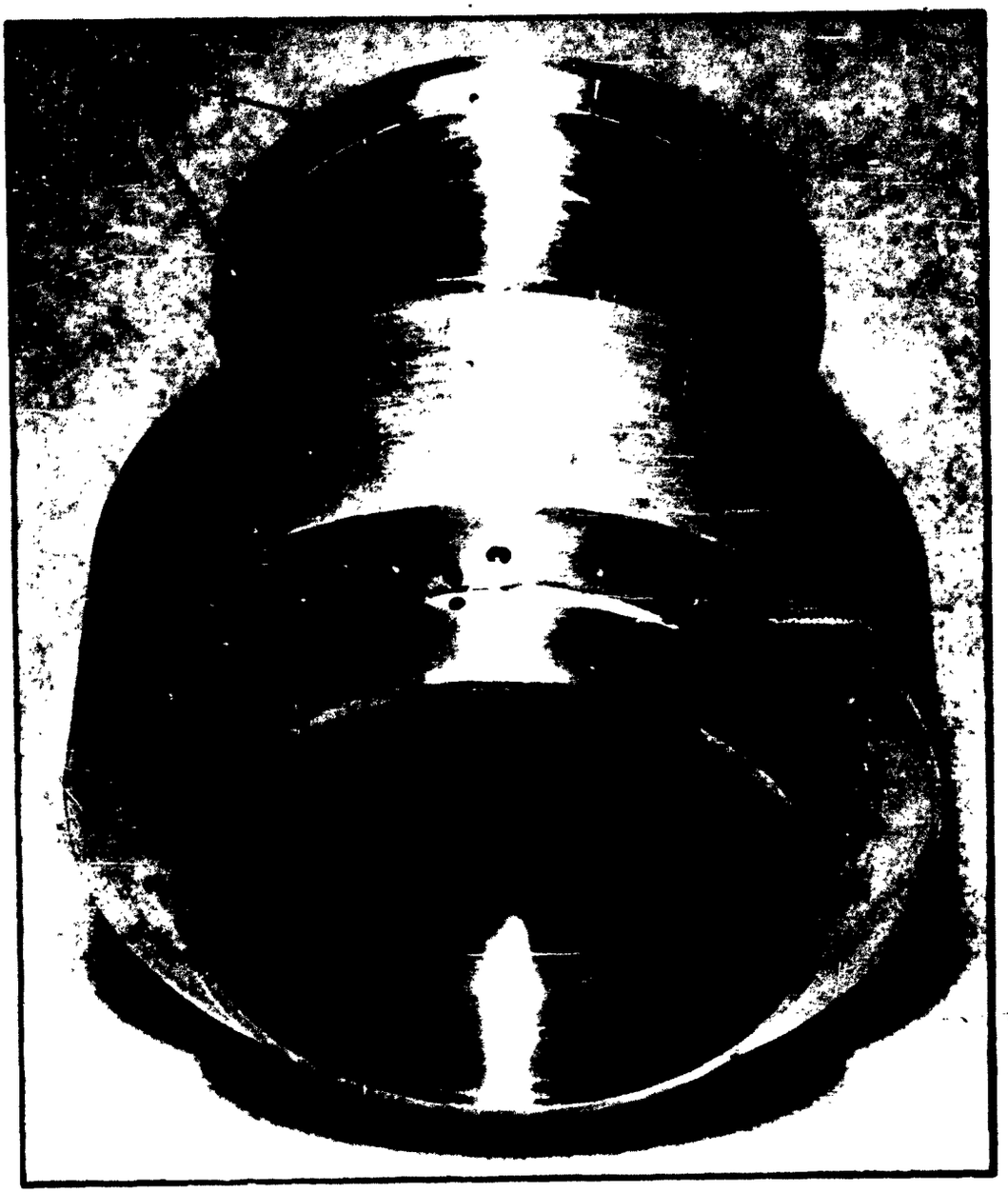

Figure 6 - Assembled Chamber Liners Showing Fuel and Coolant Injectors.

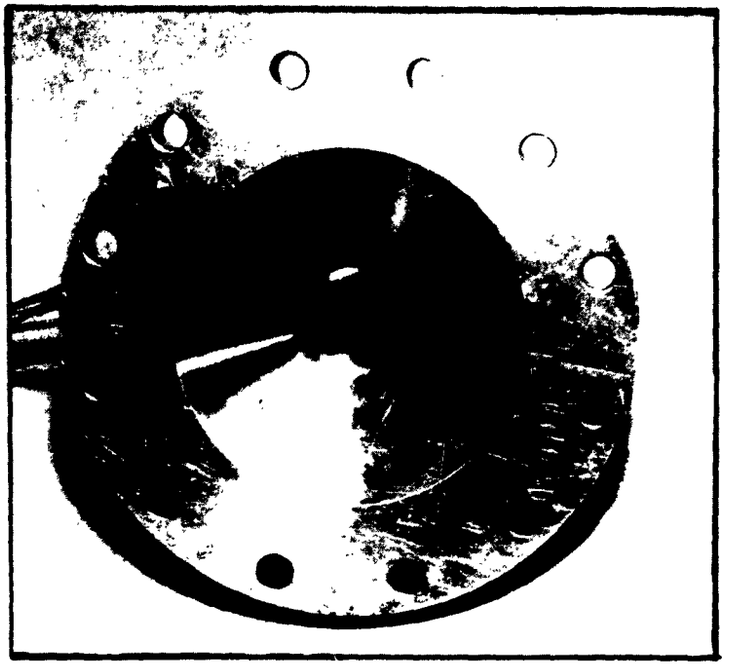

Convergent section -- Nozzle B

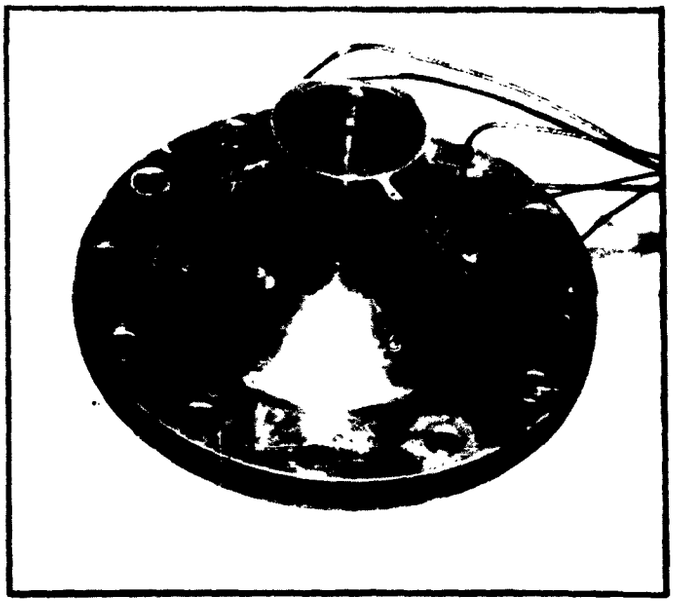

Divergent section -- Nozzle A

Figure 7 - Nozzles A and B

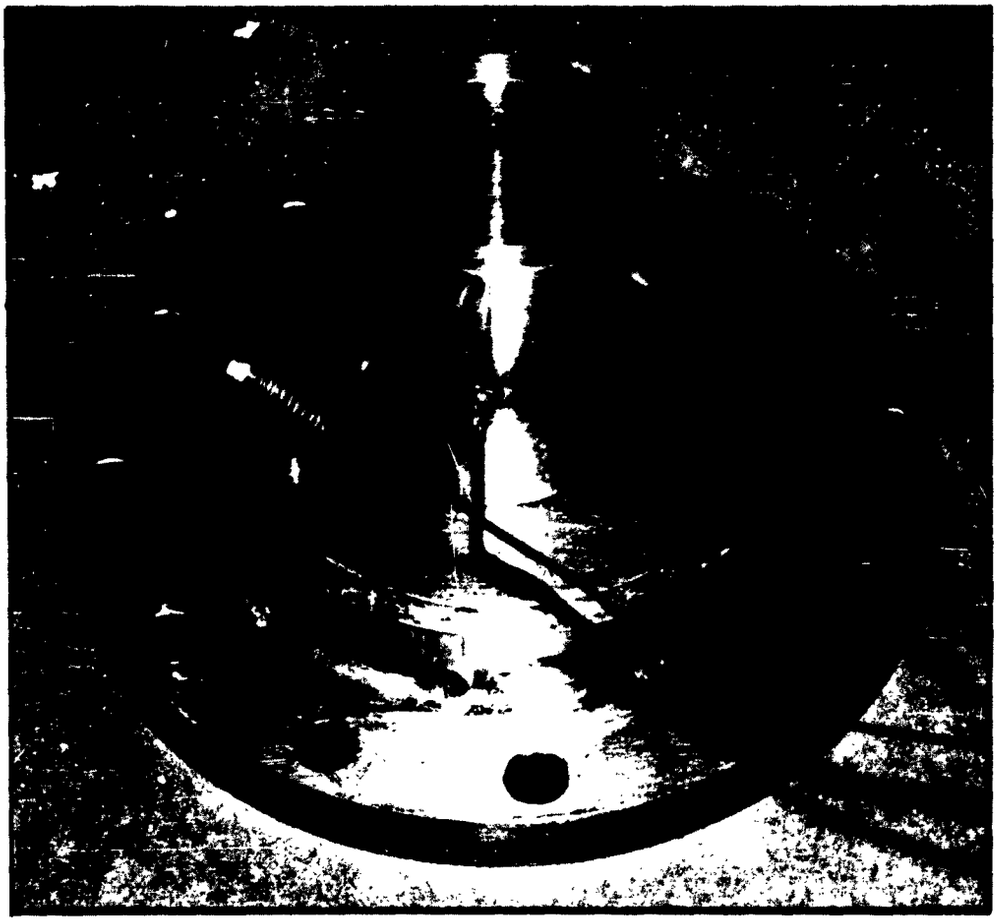

Figure 8 - Nozzle C with Coolant Section

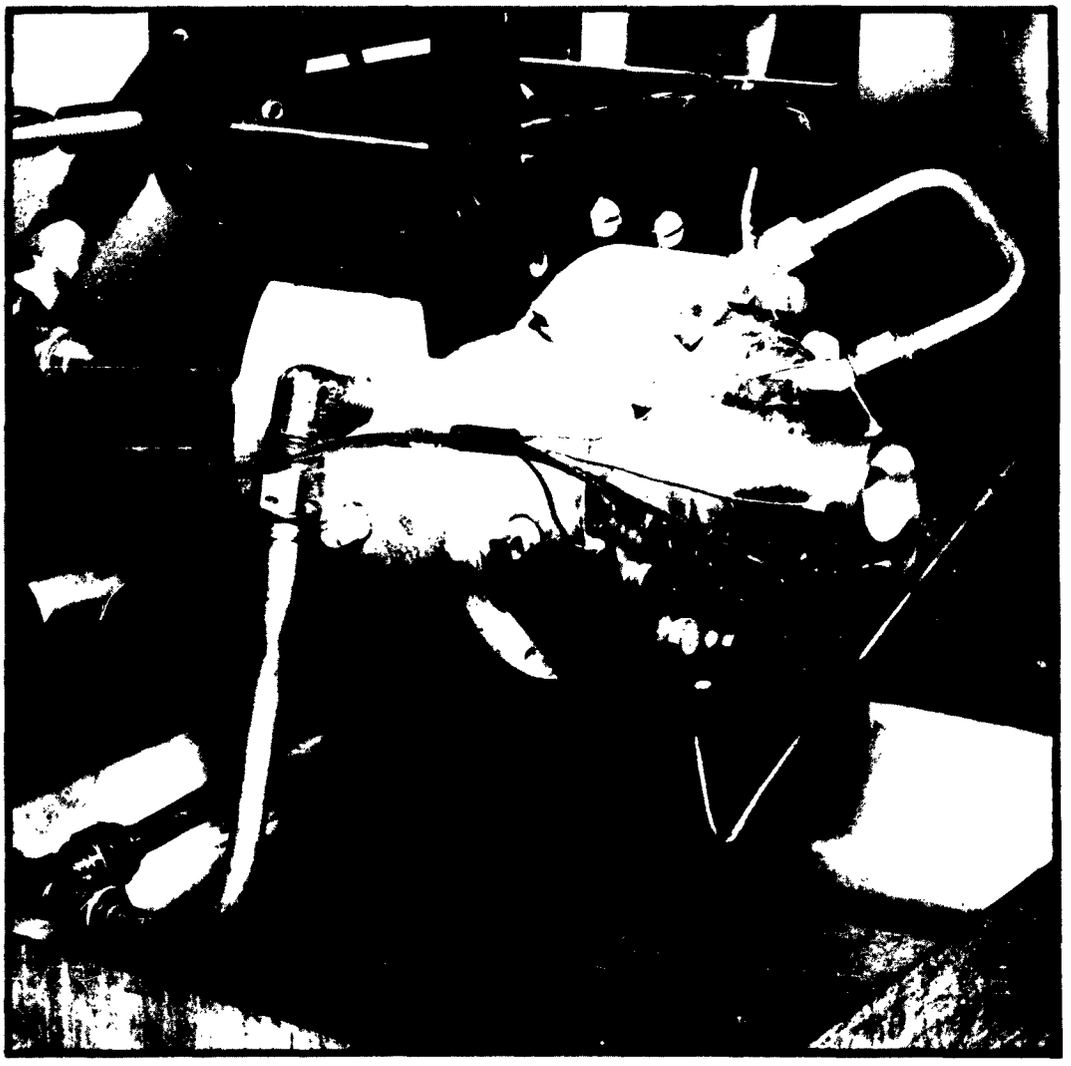

Figure 9 - Assembled Rocket Engine on Thrust Stand

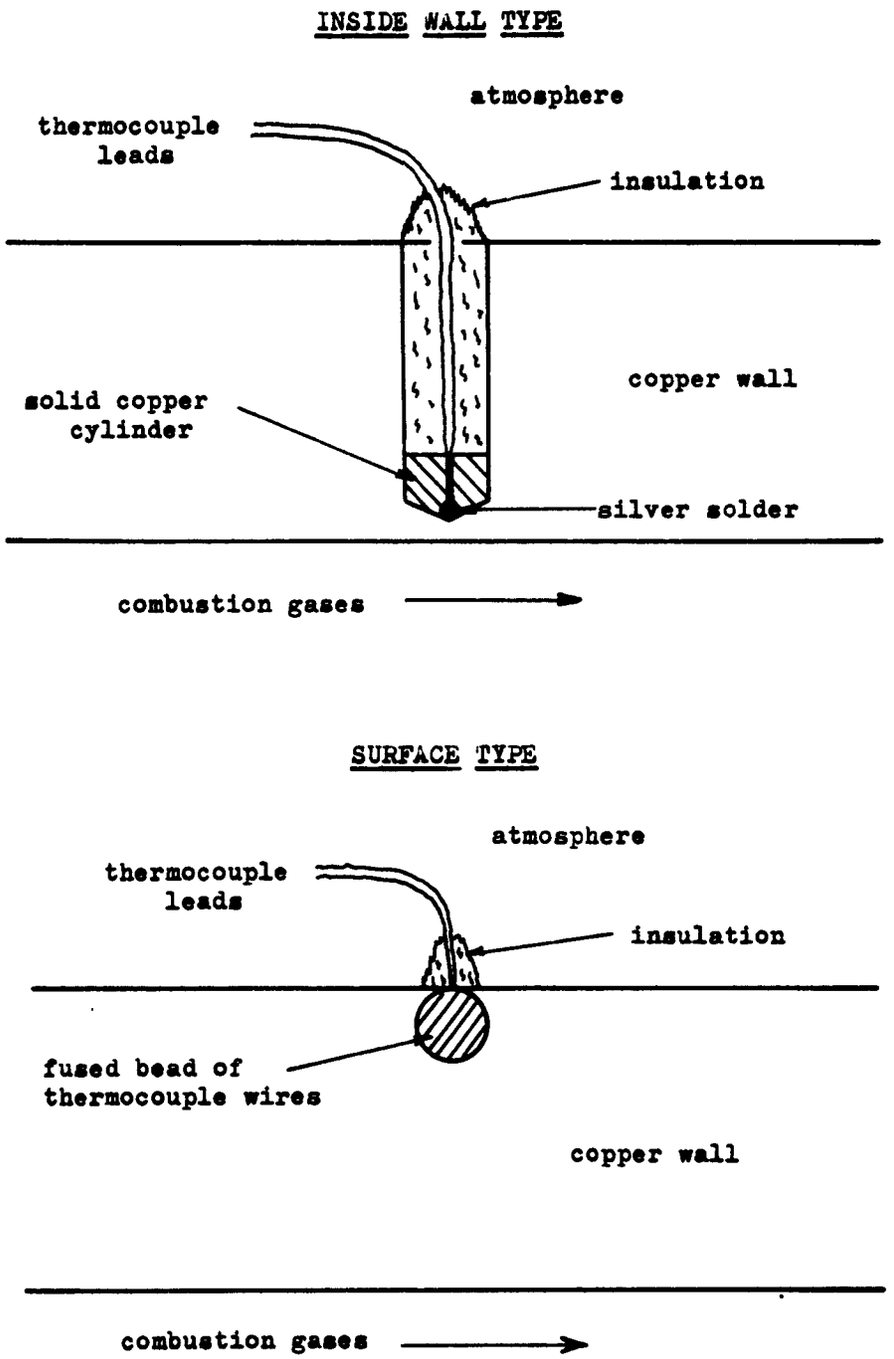

Figure 10 - Thermocouple Installations

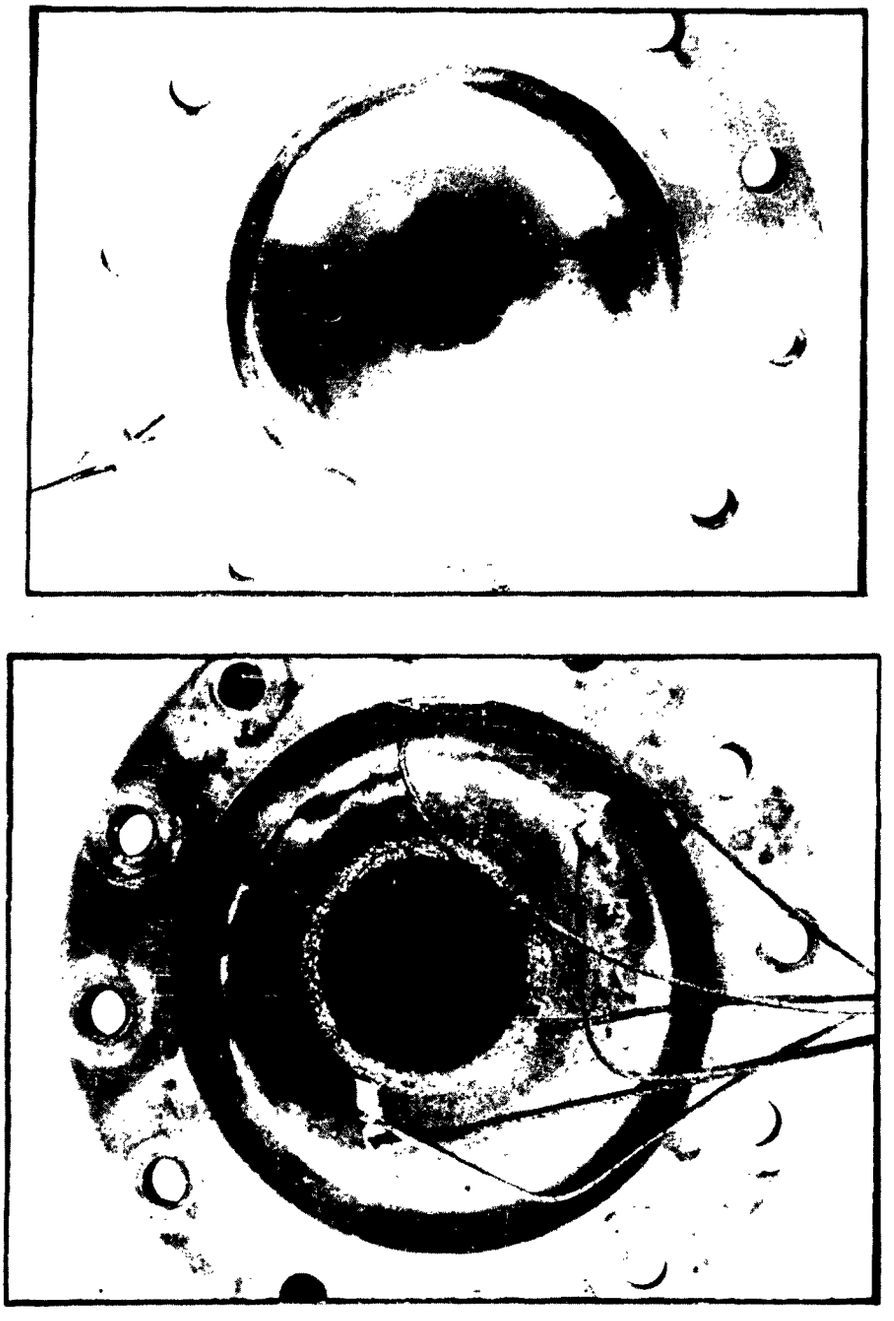

Figure 11 - Nozzle A, Burnout. Throat Melted During Test 26

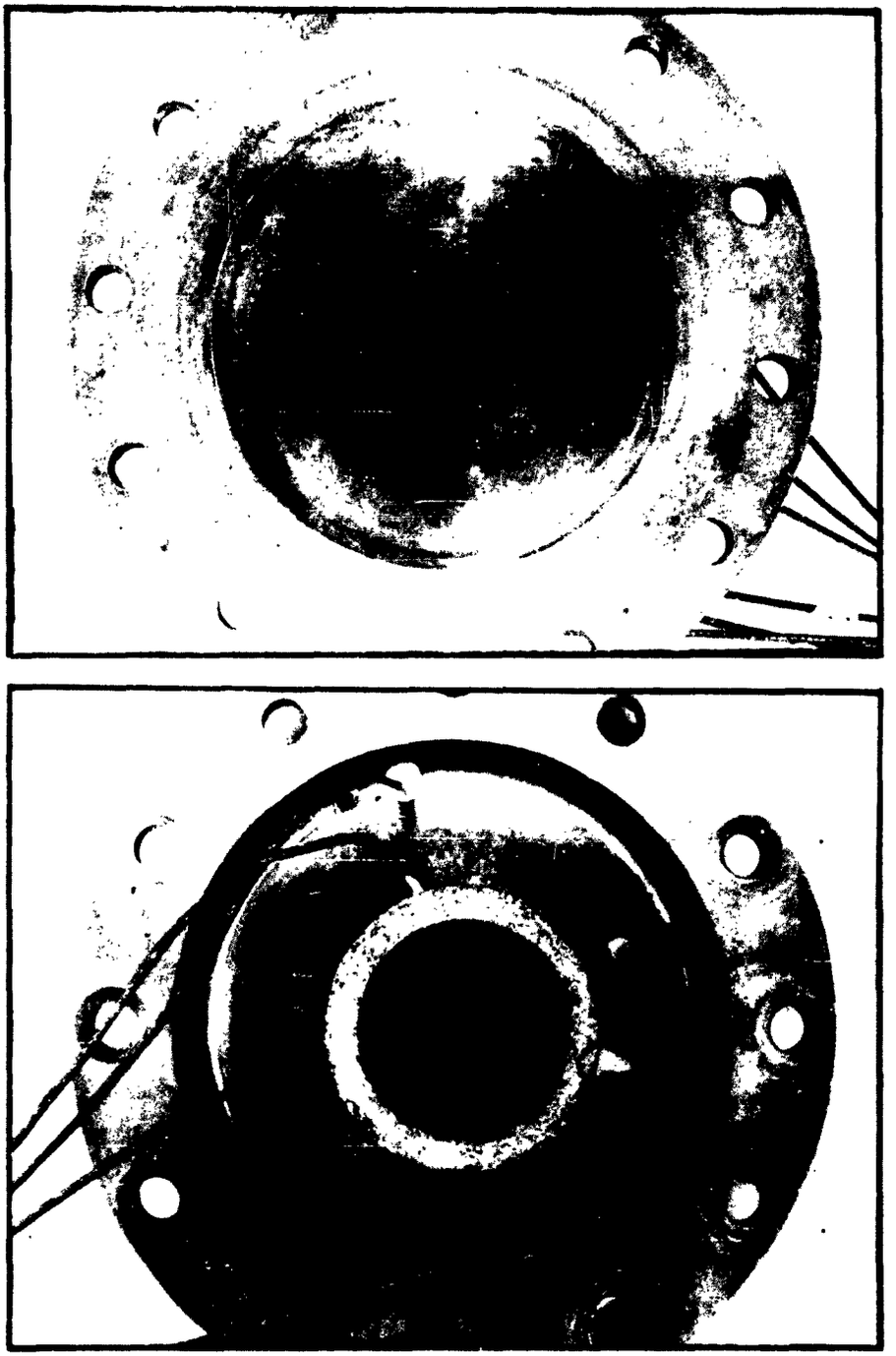

Figure 12 - Nozzle B, Burnout. Throat Melted During Test 71

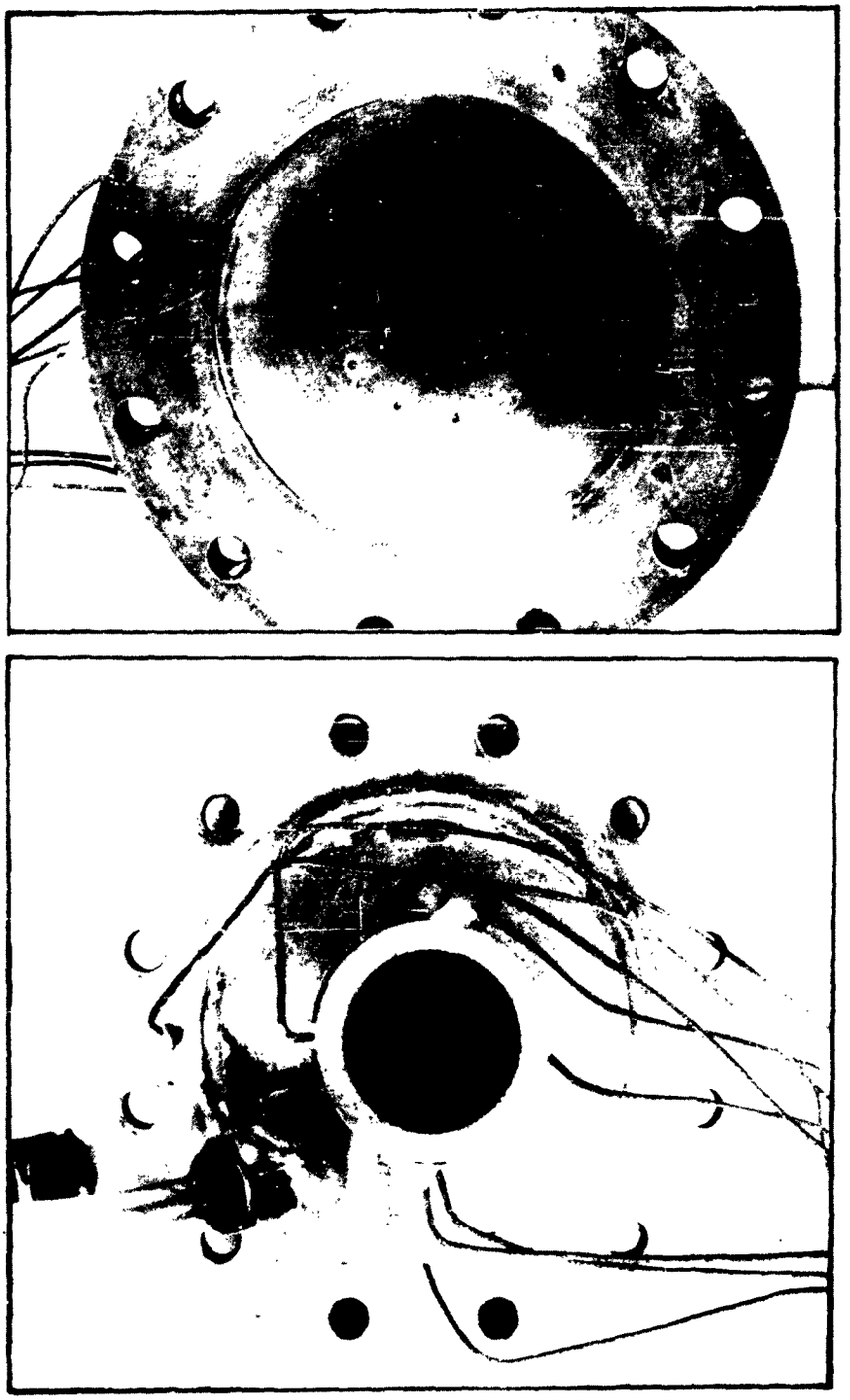

Figure 13 - Nozzle C, Cooling Effects. Taken After Completion of Test 99

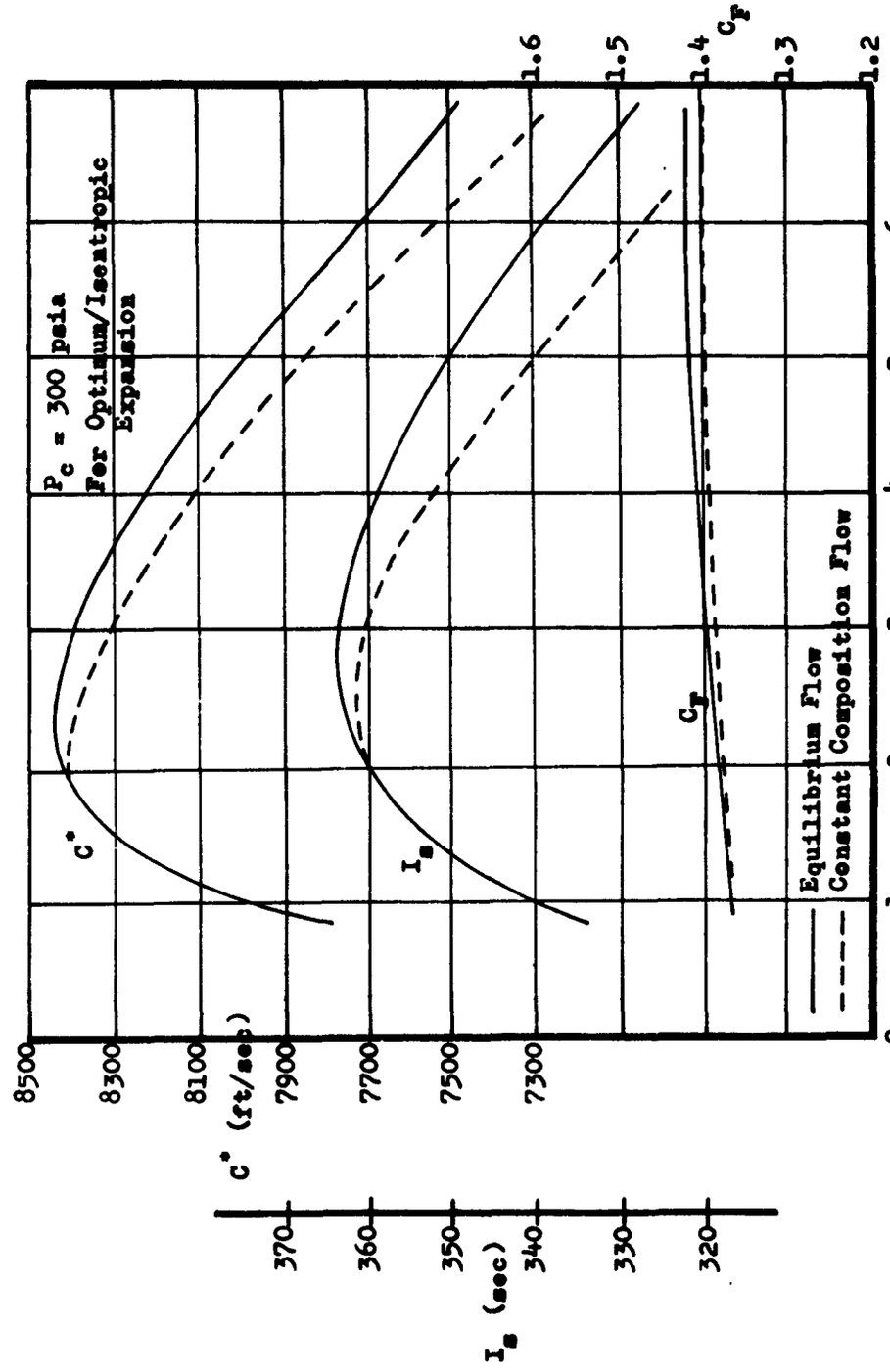

Figure 14 - Theoretical Performance for Gaseous Injection of H_2/O_2 Propellants. (Data Obtained from Ref 2:App A)

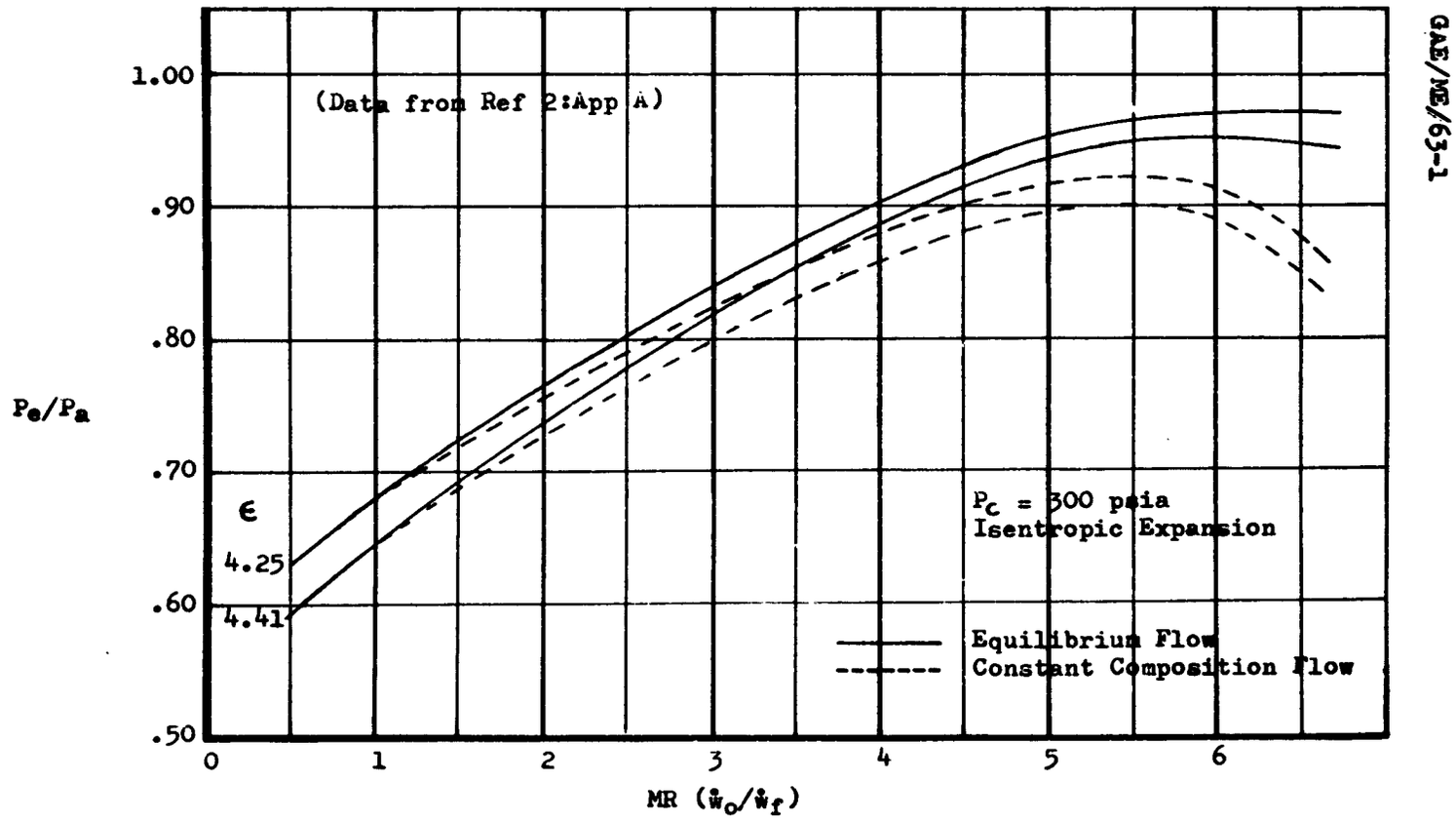

Figure 15 - Theoretical Exit Pressure Ratio vs. Mixture Ratio

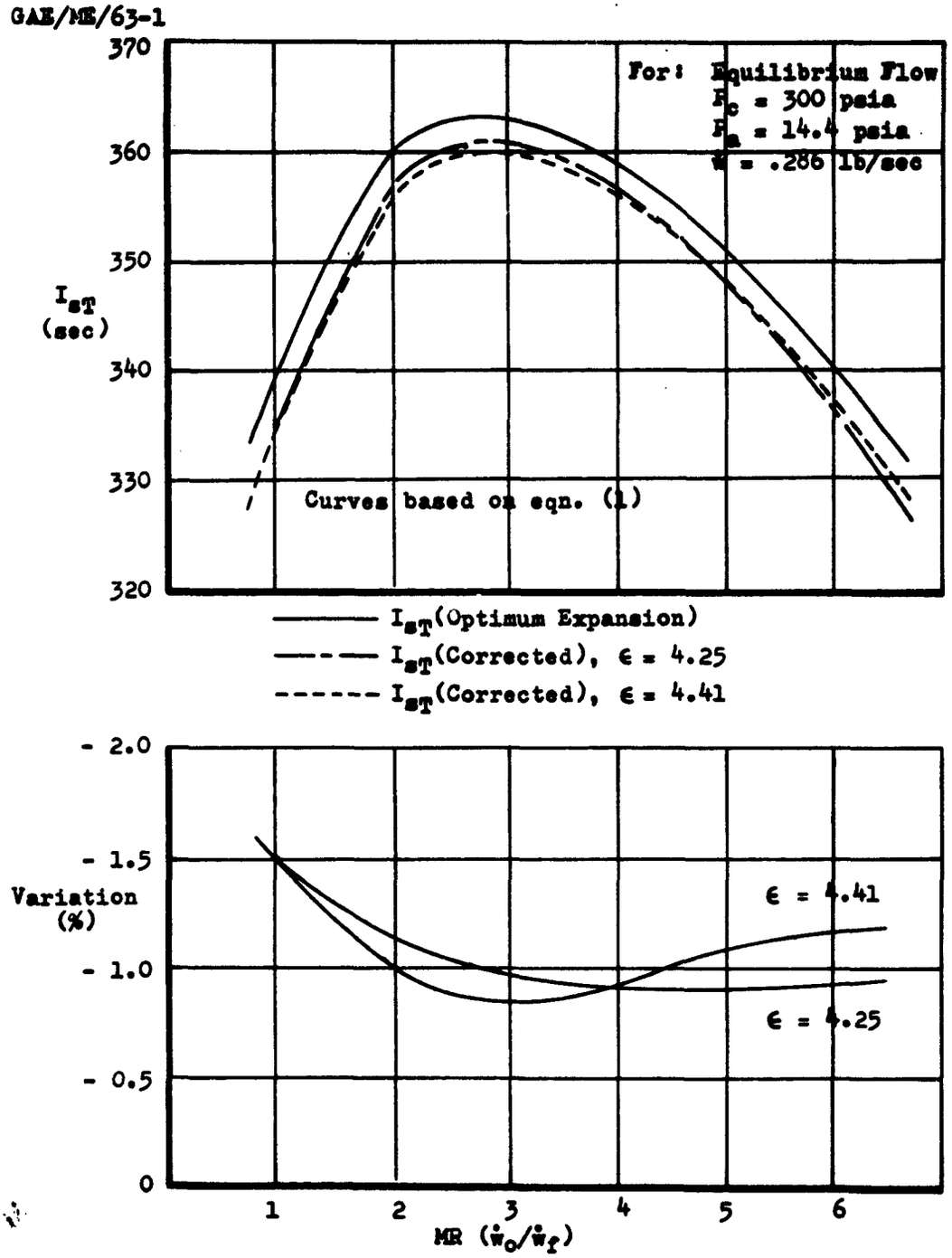

Figure 16 - Variation of Theoretical Specific Impulse from Optimum Expansion

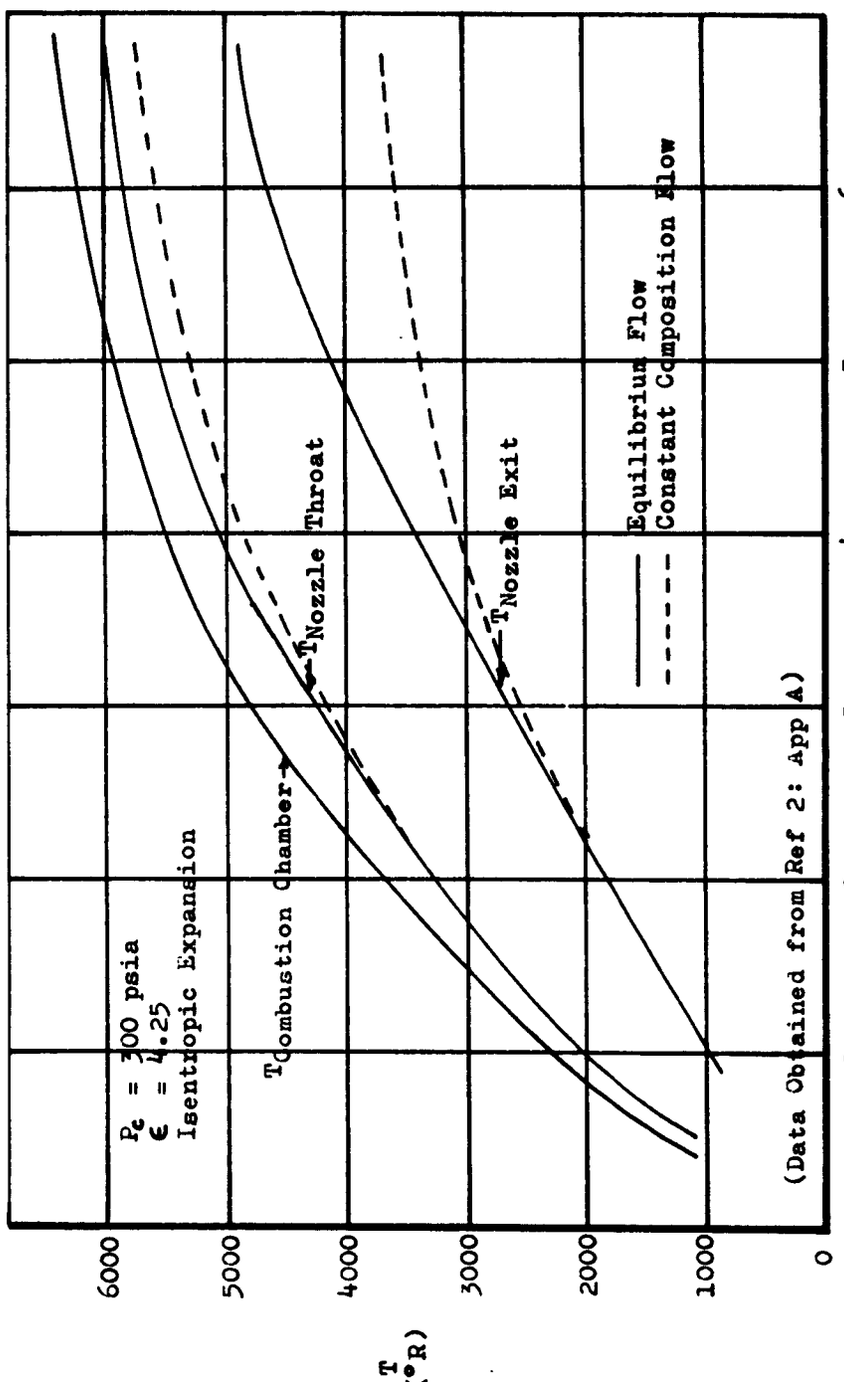

Figure 17 - Theoretical Gas Temperatures for Gaseous Injection of H_2/O_2 Propellants

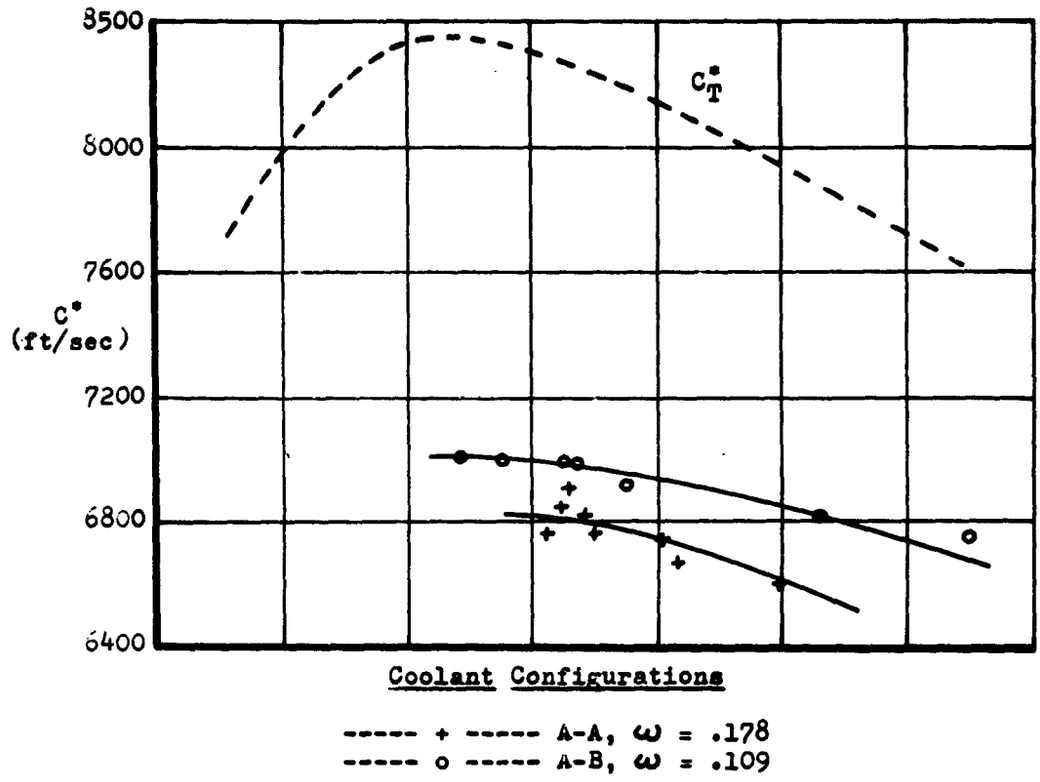

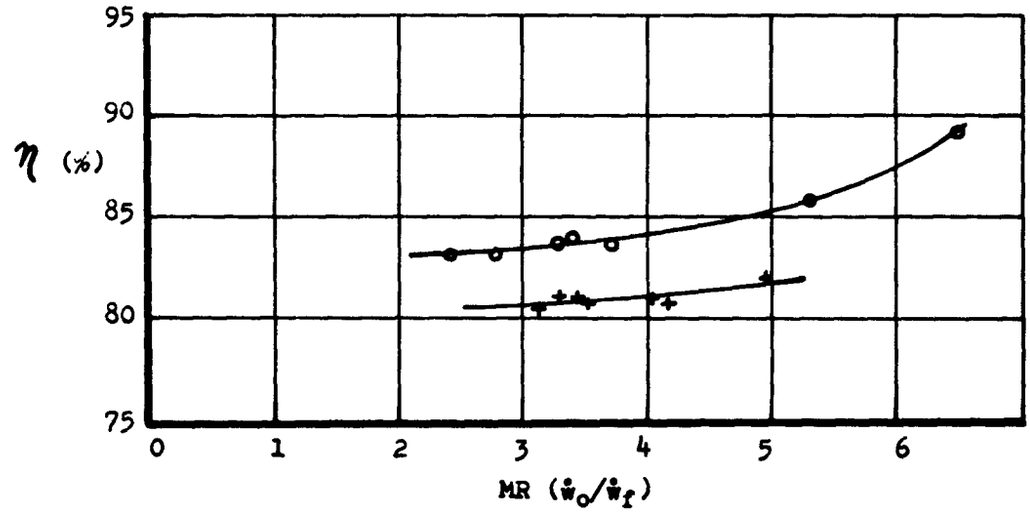

Figure 18 - Engine Performance for Nozzle A
(Characteristic Velocity)

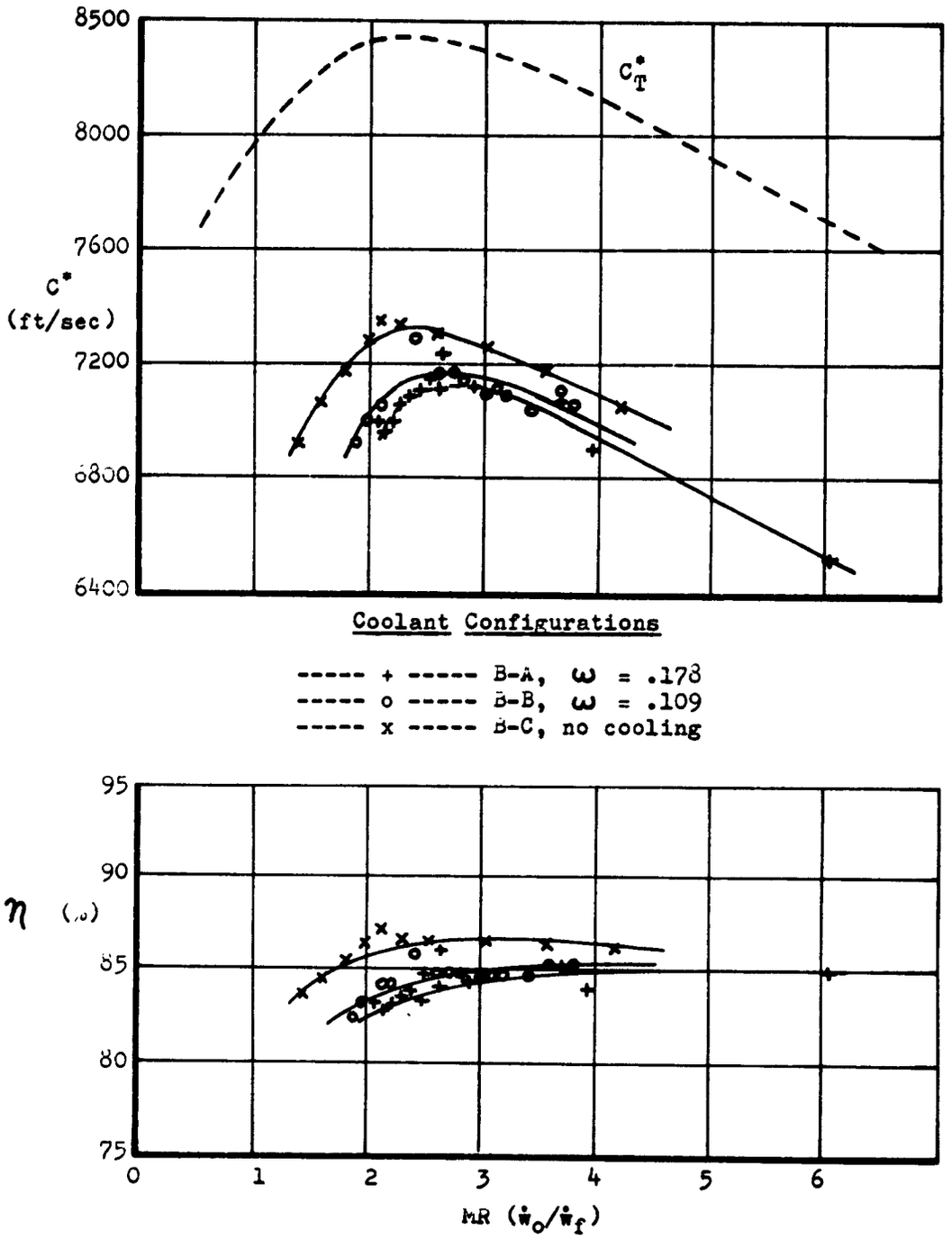

Figure 19 - Engine Performance for Nozzle B
(Characteristic Velocity)

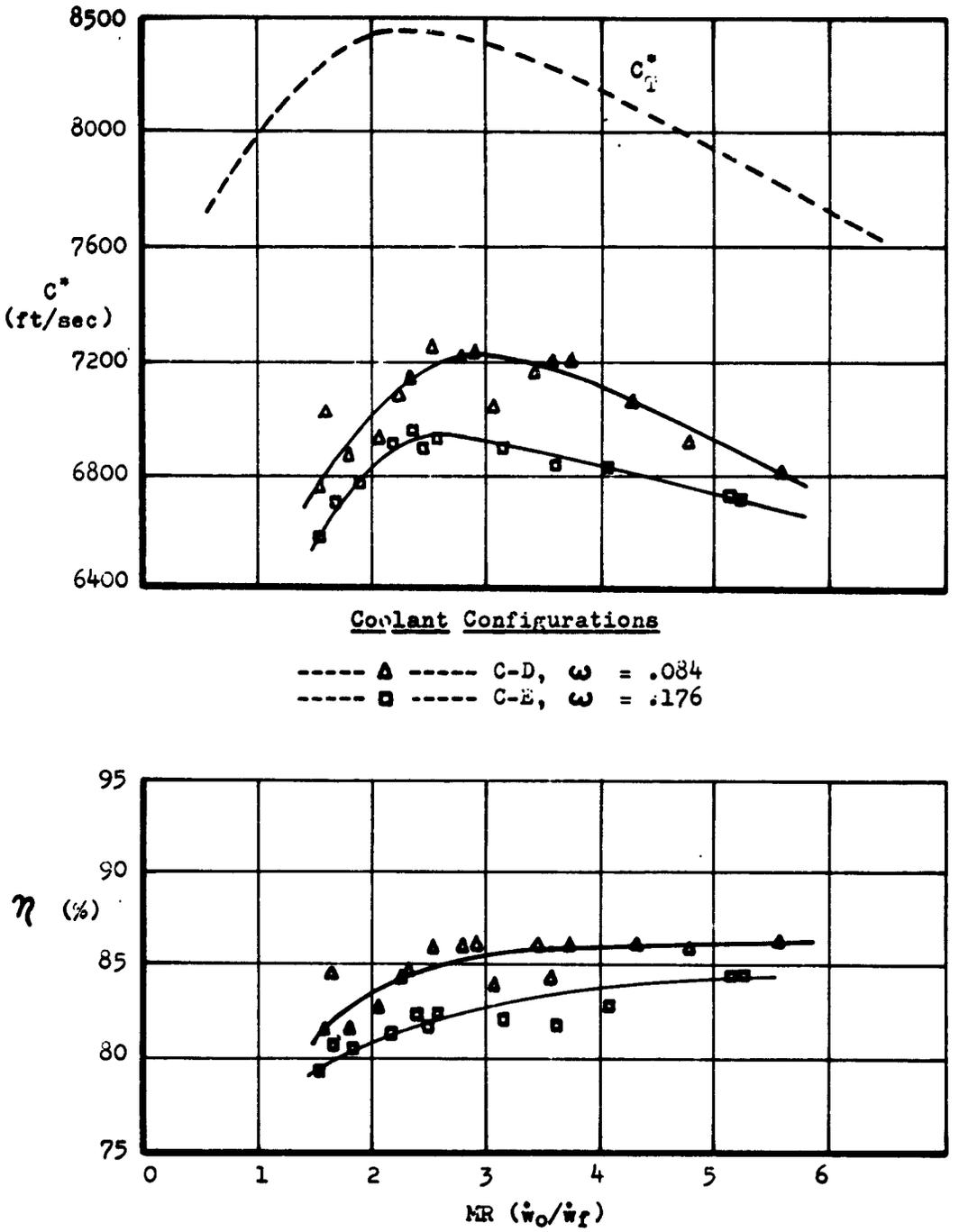

Figure 20 - Engine Performance for Nozzle C
(Characteristic Velocity)

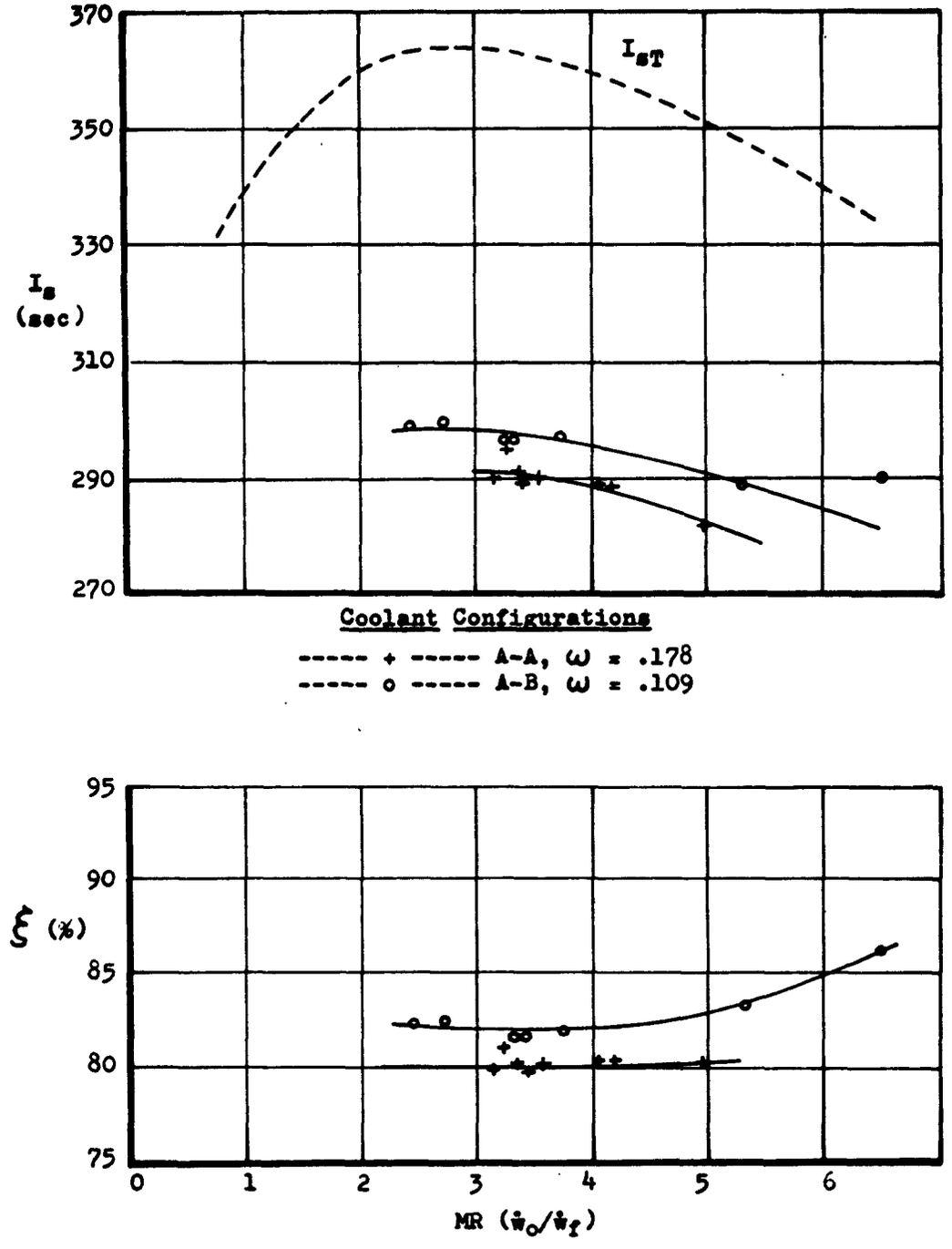

Figure 21 - Engine Performance for Nozzle A
(Specific Impulse)

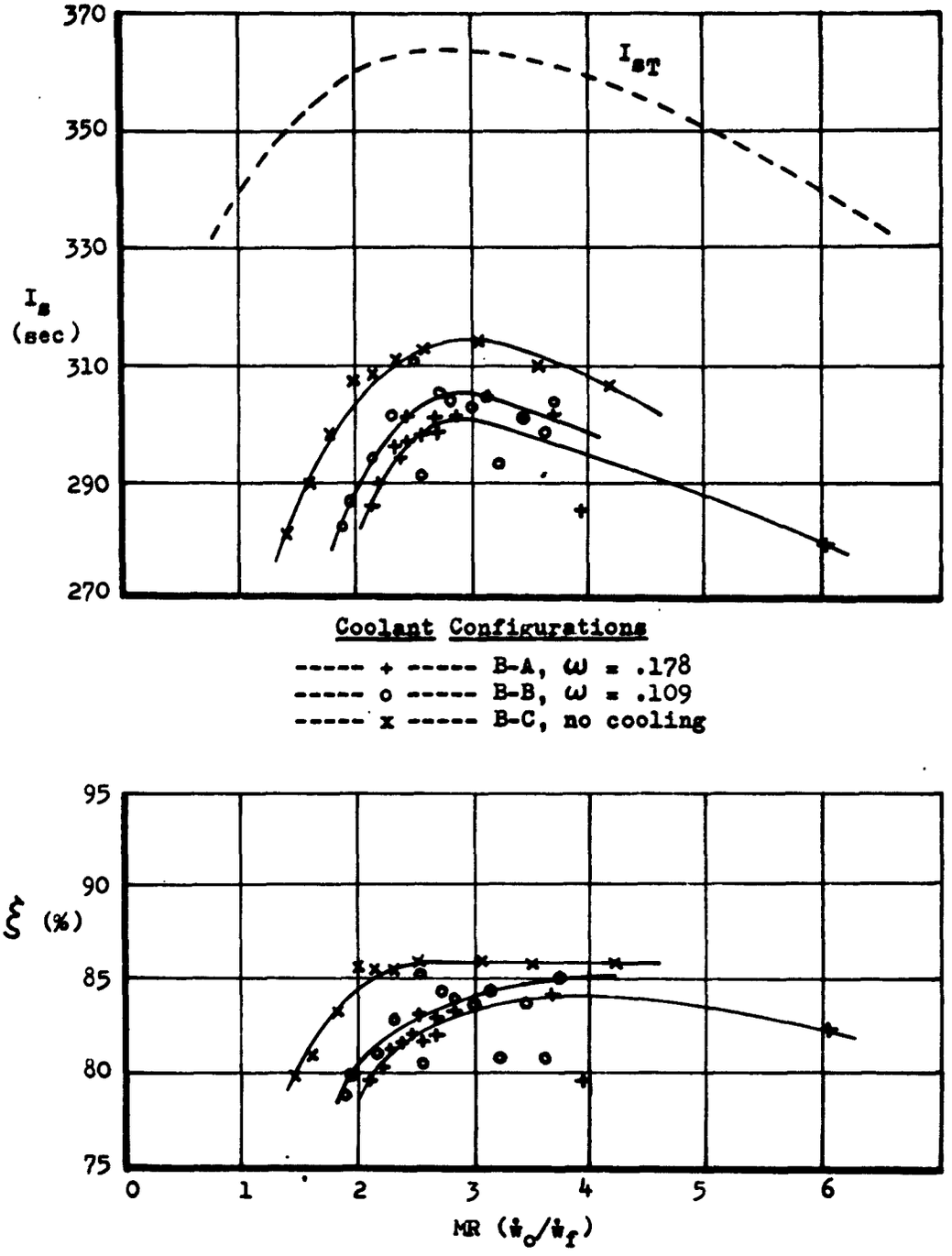

Figure 22 - Engine Performance for Nozzle B
(Specific Impulse)

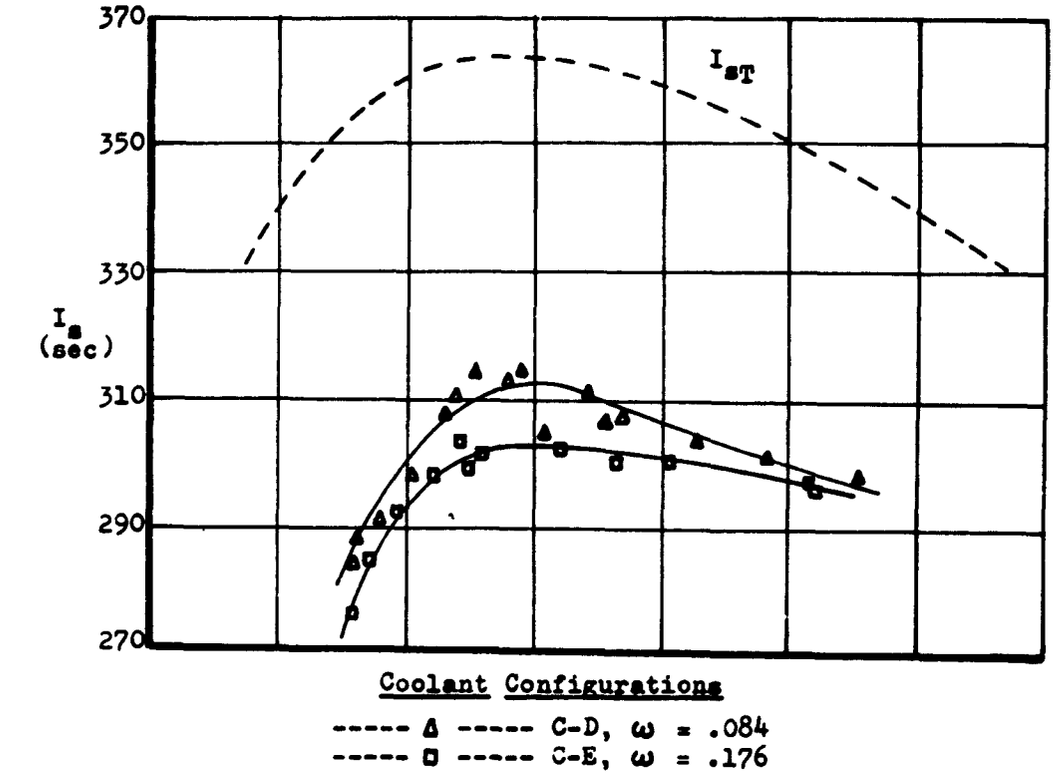

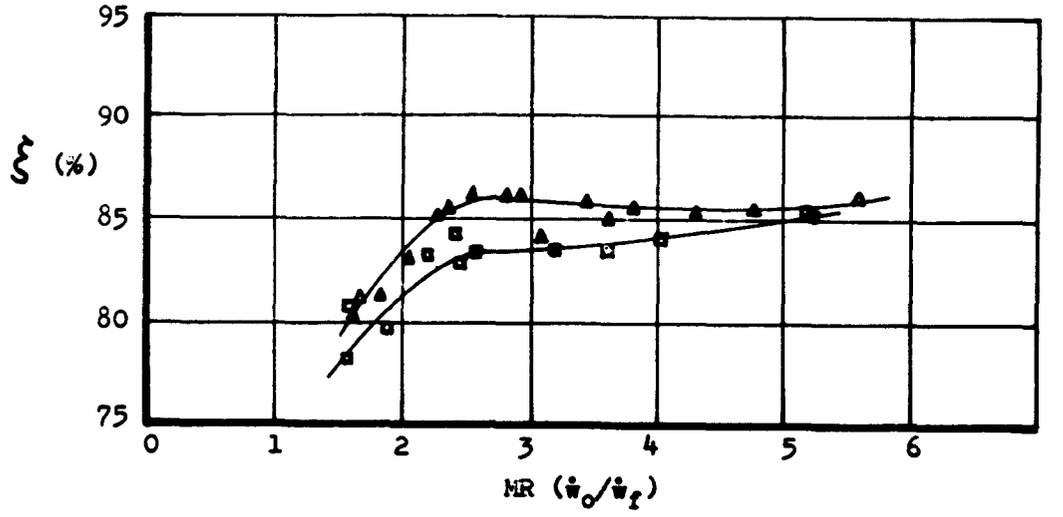

Figure 23 - Engine Performance for Nozzle C (Specific Impulse)

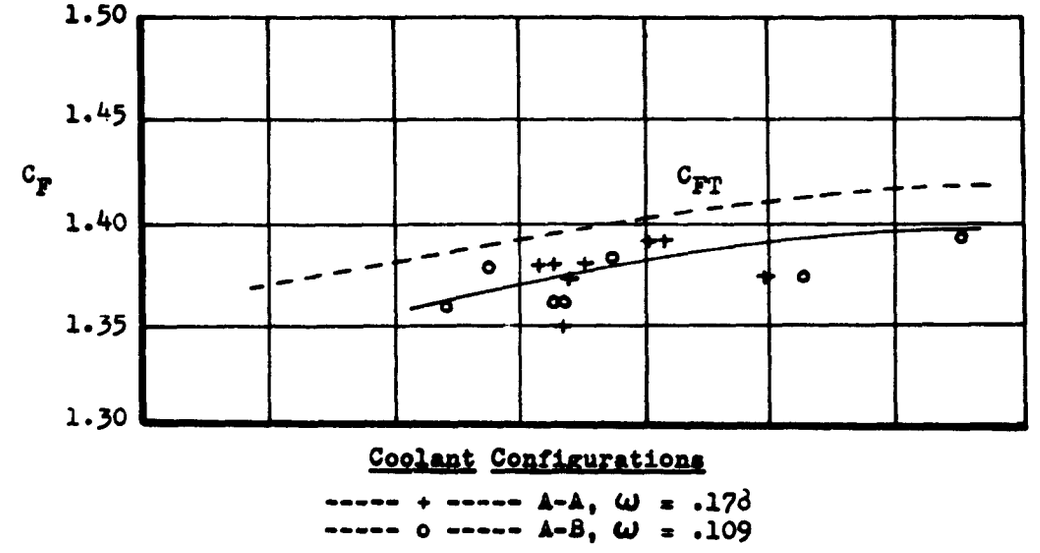

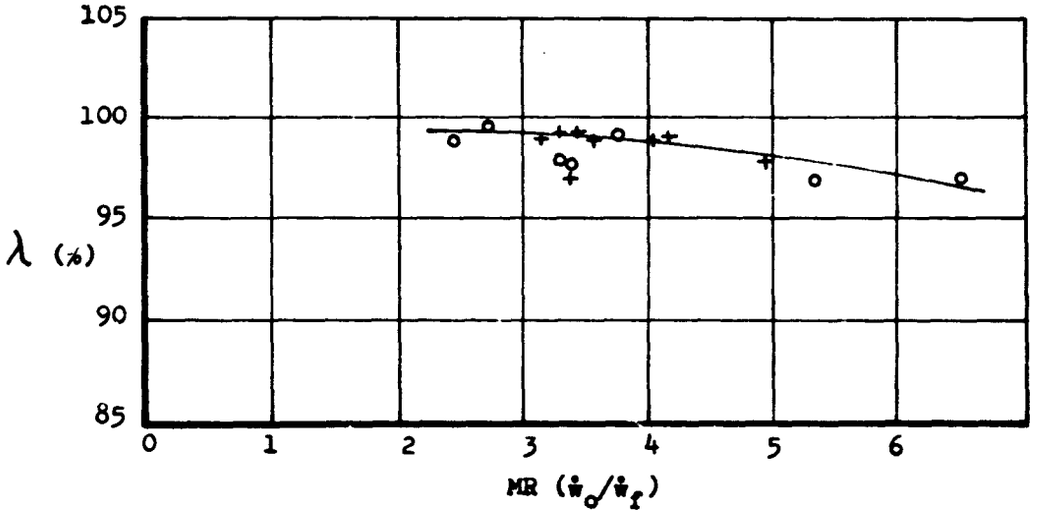

Figure 24 - Engine Performance for Nozzle A
(Thrust Coefficient)

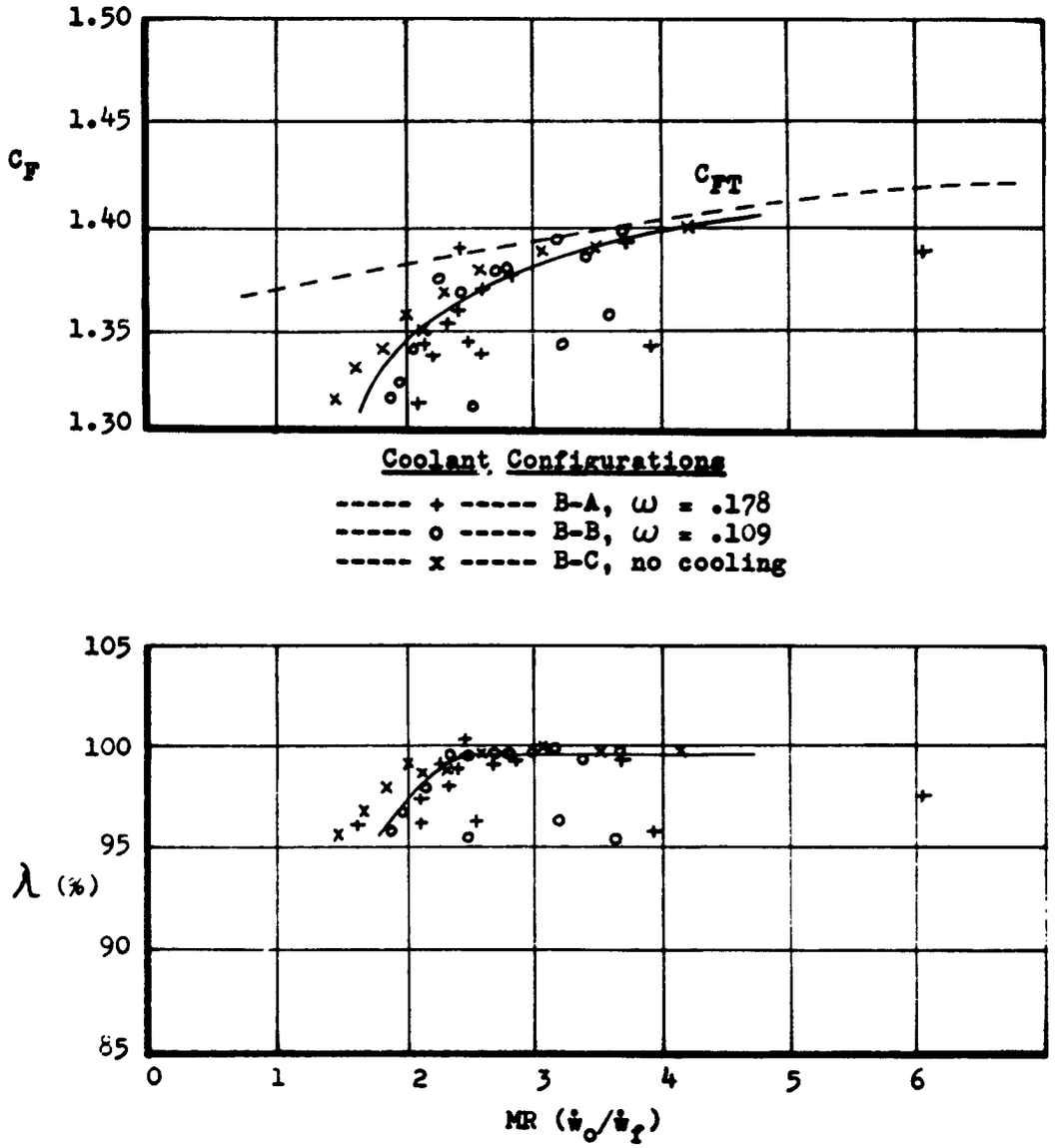

Figure 25 - Engine Performance for Nozzle B
(Thrust Coefficient)

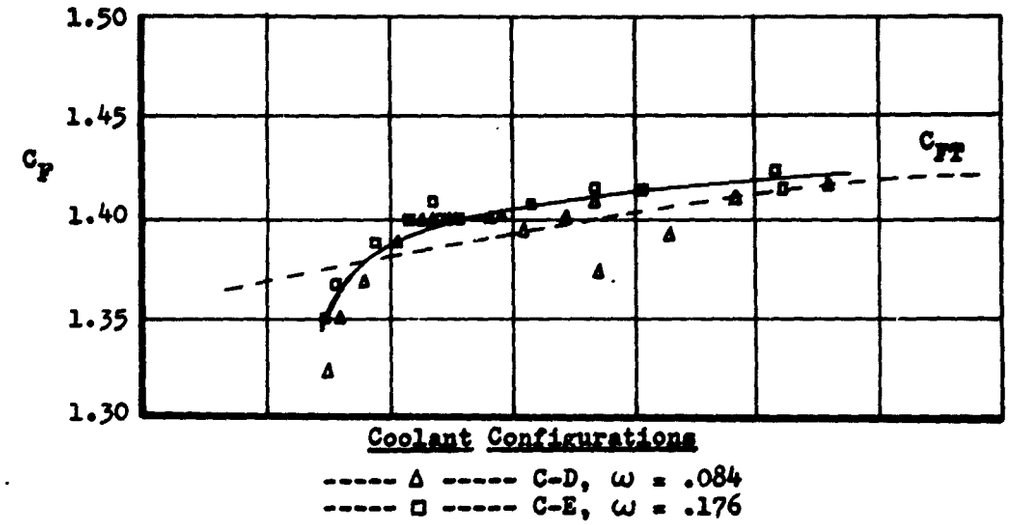

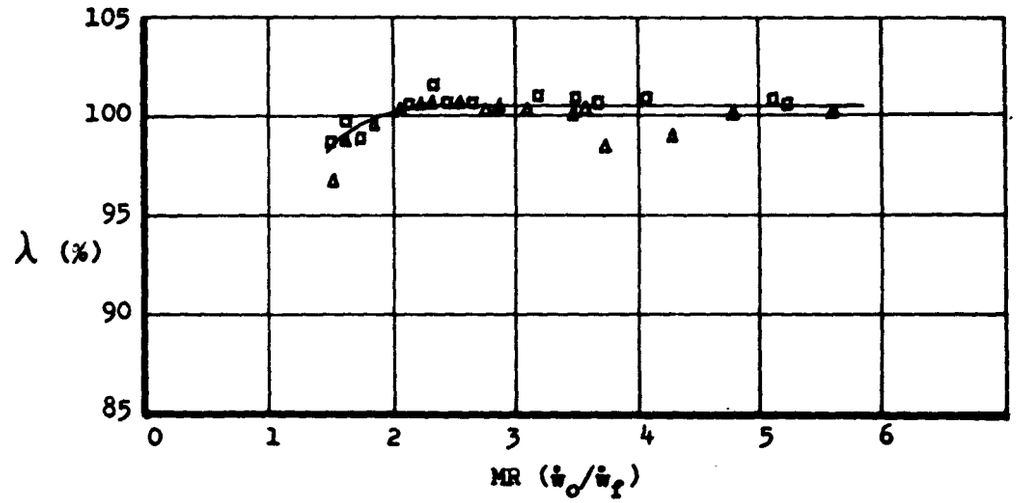

Figure 26 - Engine Performance for Nozzle C
(Thrust Coefficient)

$$\phi = \frac{I_{sx}(\omega=0) - I_{sx}}{I_{sx}(\omega=0)}$$

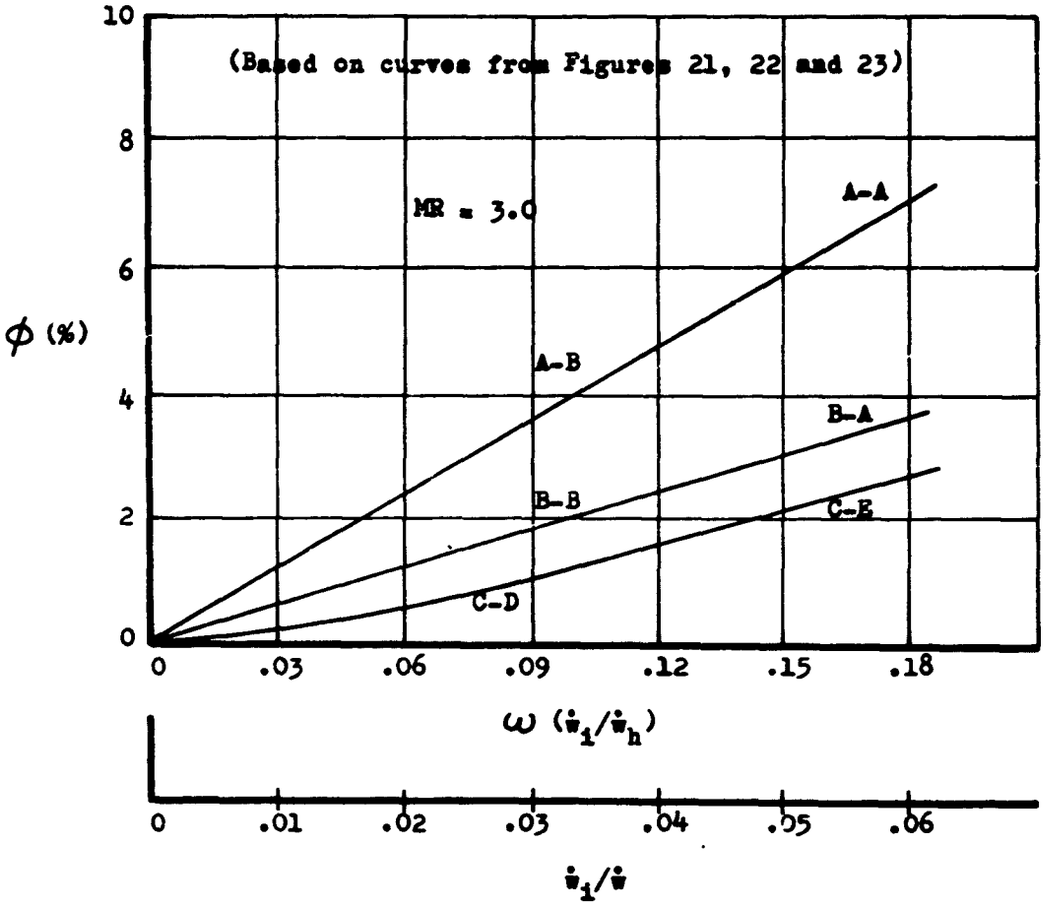

Figure 27 - Performance Loss vs. Coolant Flow Ratio

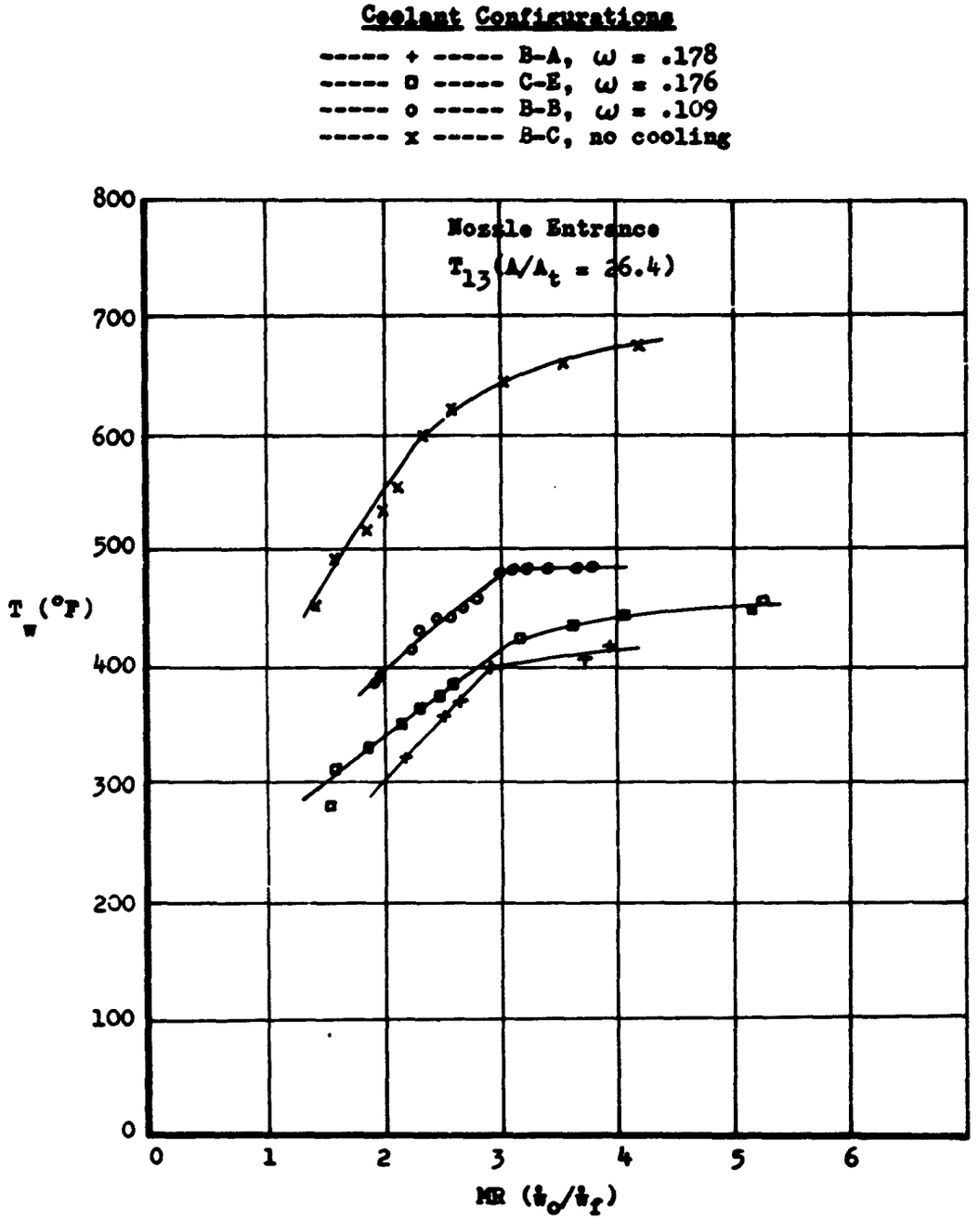

Figure 28 - Wall Temperature vs. Mixture Ratio (Nozzle Entrance)

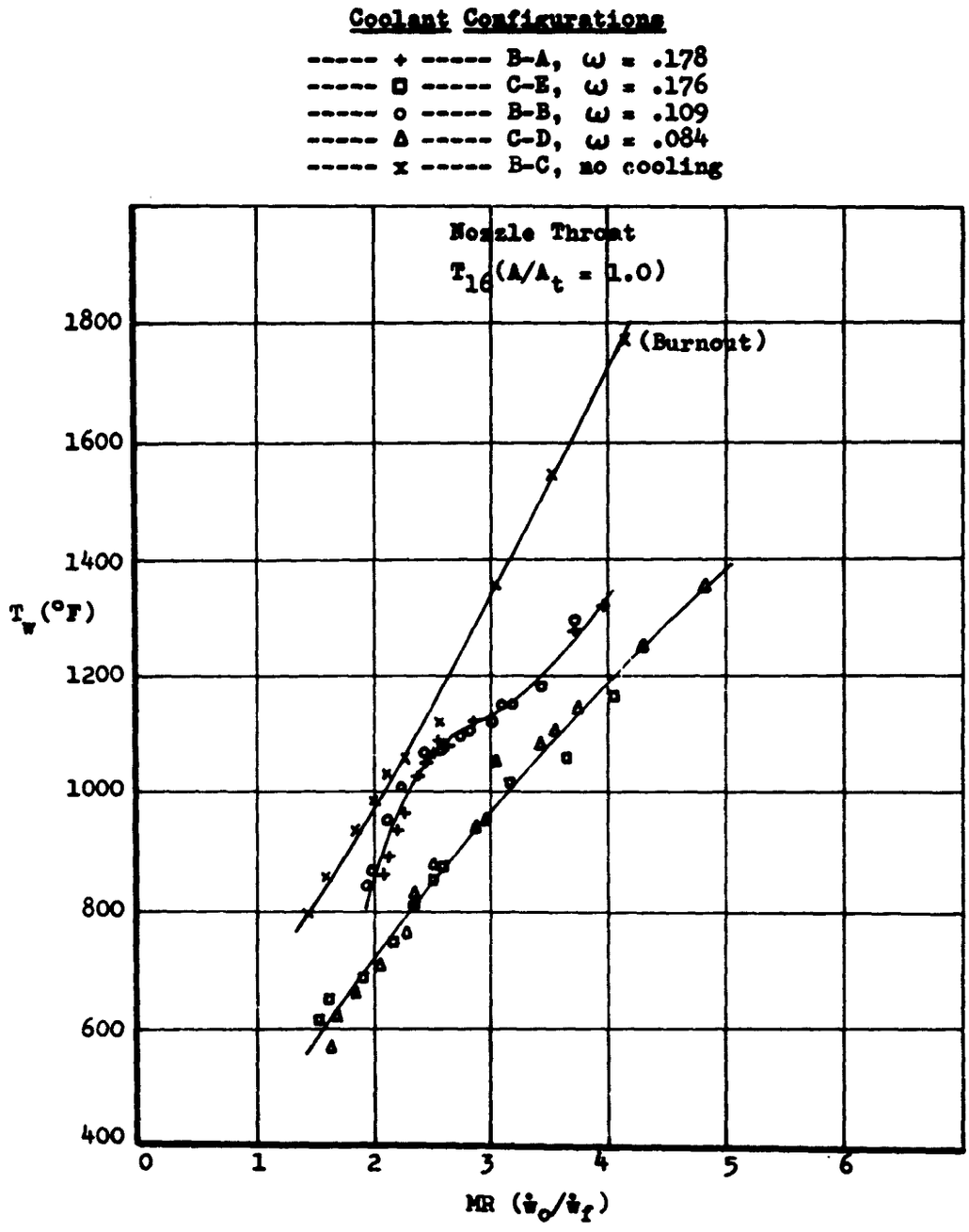

Figure 29 - Wall Temperature vs. Mixture Ratio (Nozzle Throat)

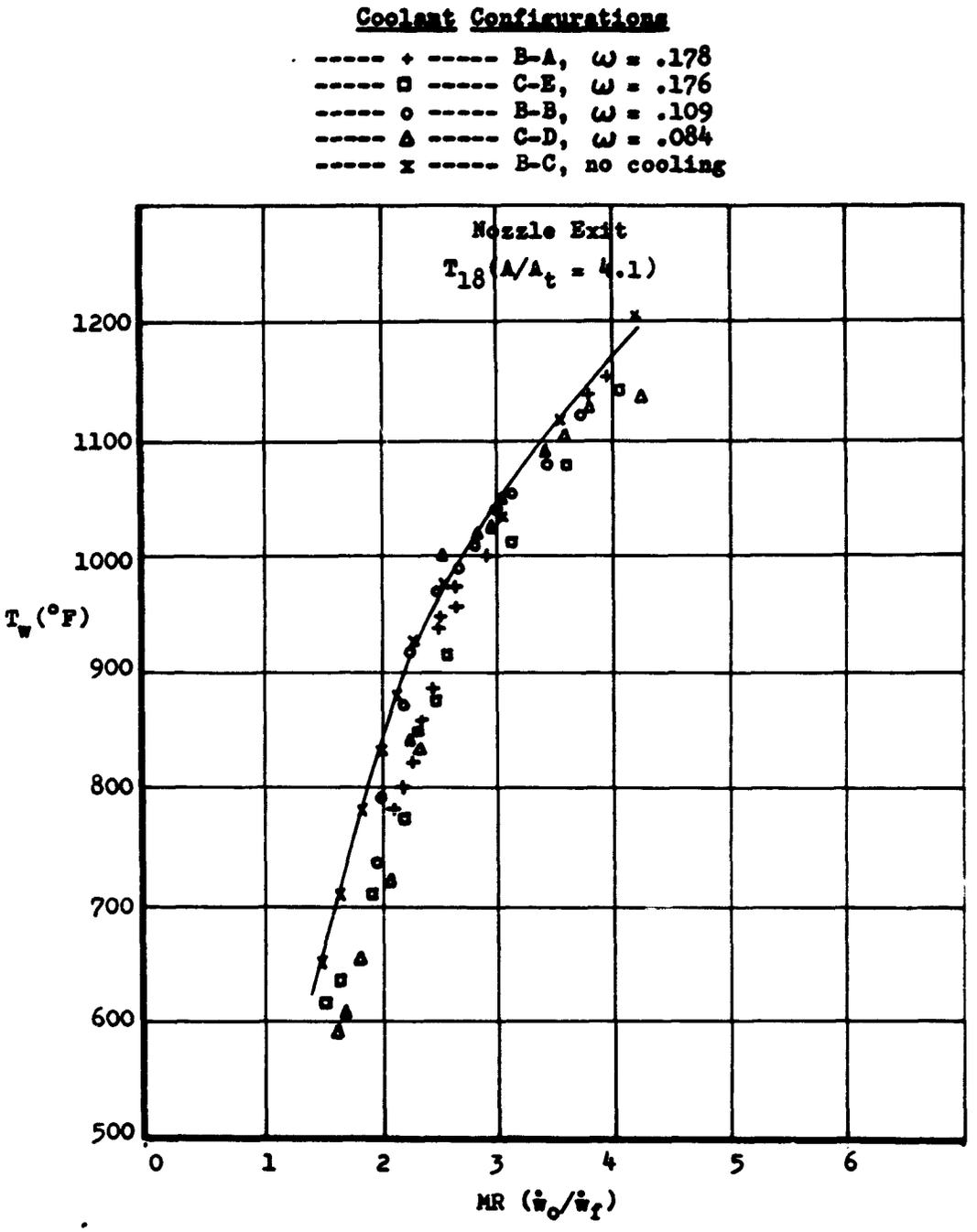

Figure 30 - Wall Temperature vs. Mixture Ratio (Nozzle Exit)

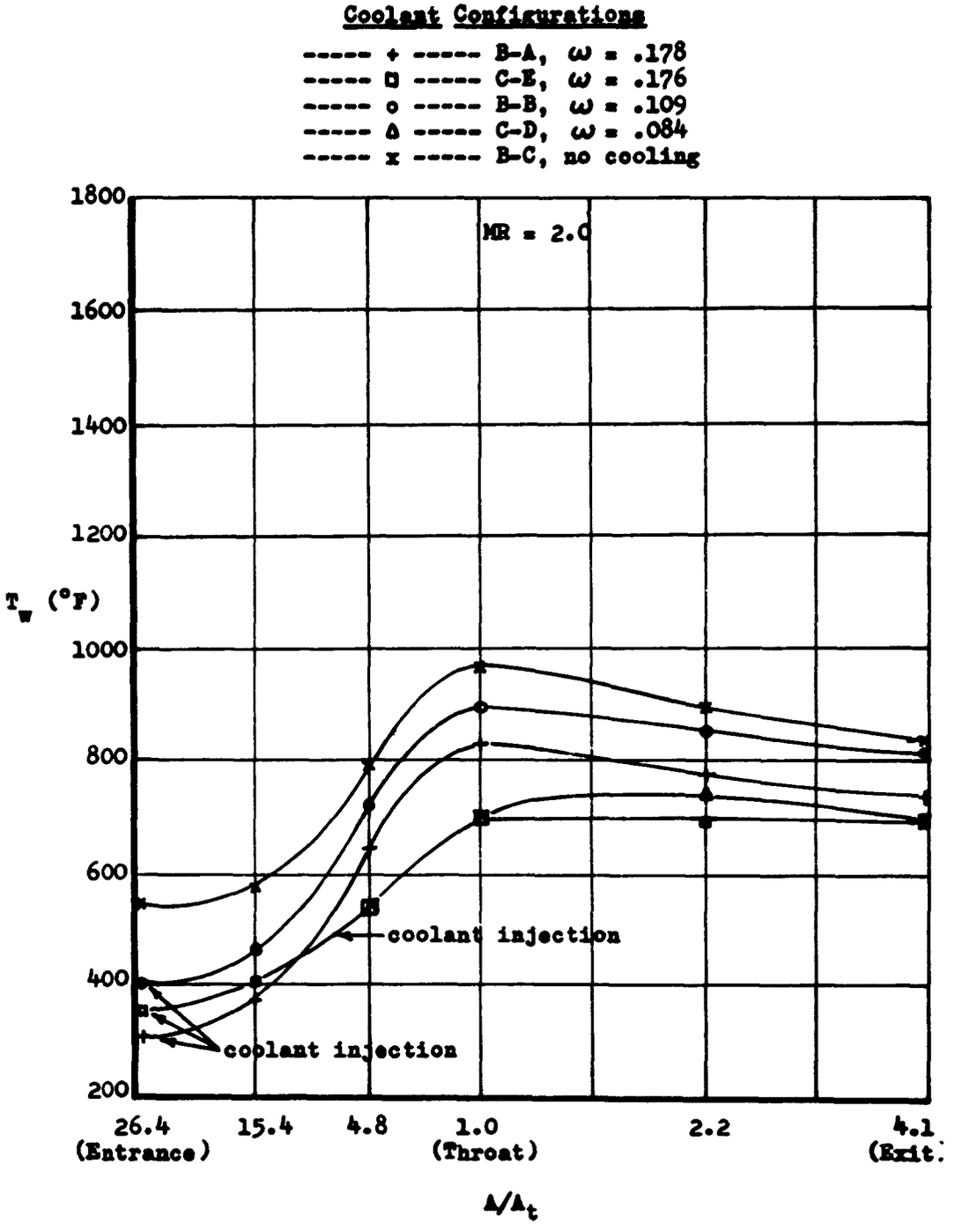

Figure 31 - Nozzle Wall Temperature vs. Area Ratio (MR = 2.0)

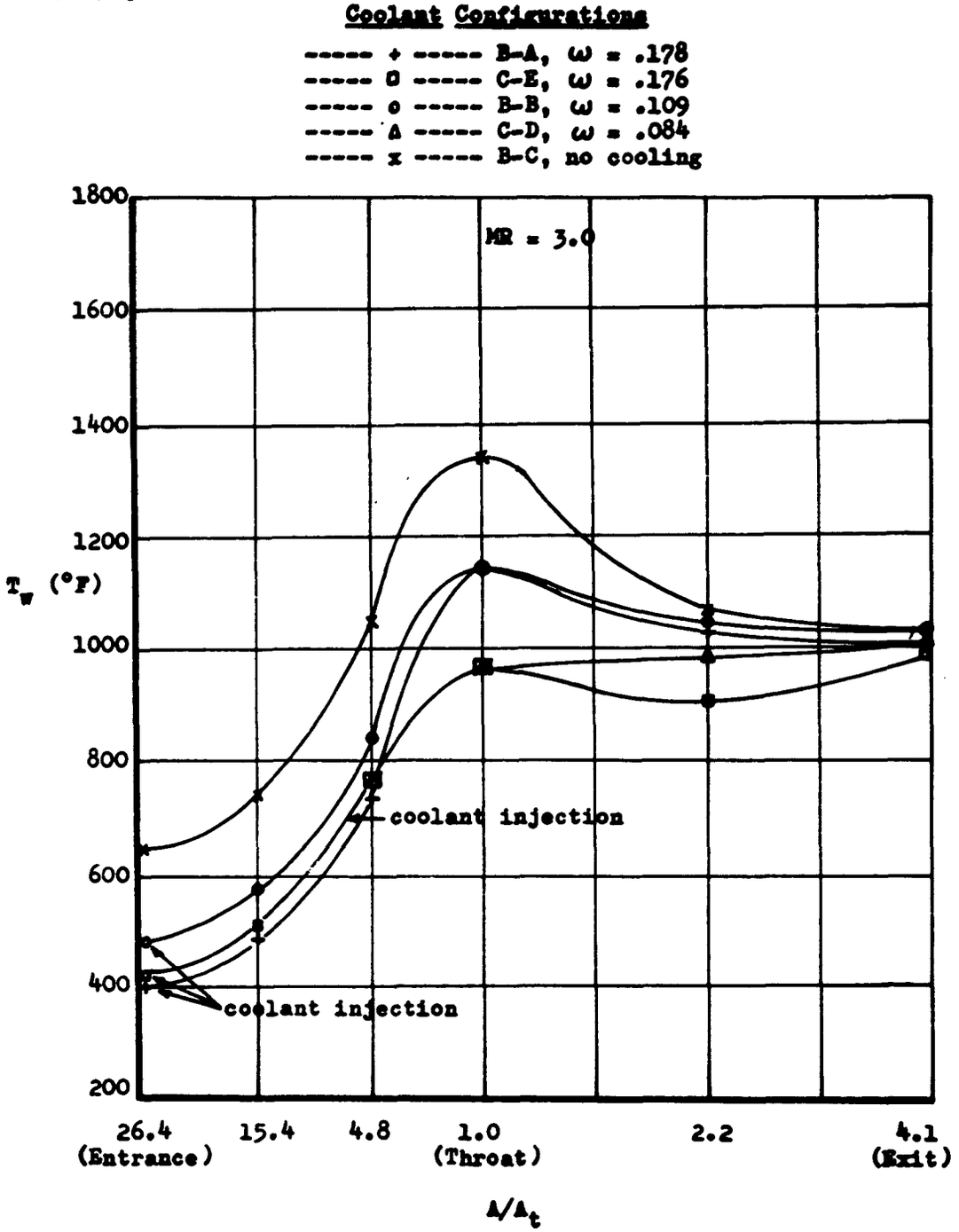

Figure 32 - Nozzle Wall Temperature vs. Area Ratio (MR = 3.0)

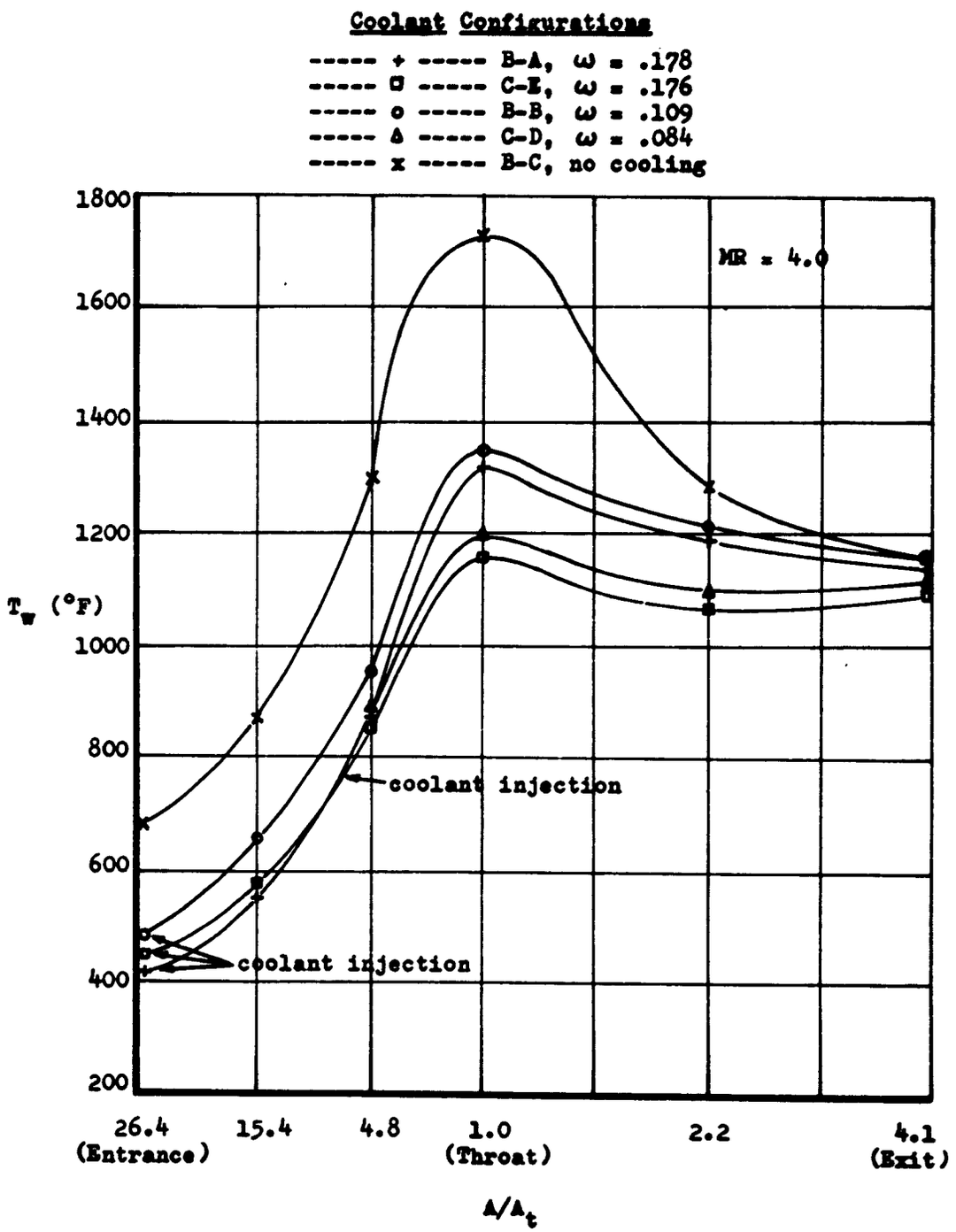

Figure 33 - Nozzle Wall Temperature vs. Area Ratio (MR = 4.0)

$$\theta = \frac{T_w(\omega=0) - T_w}{T_w(\omega=0)}$$

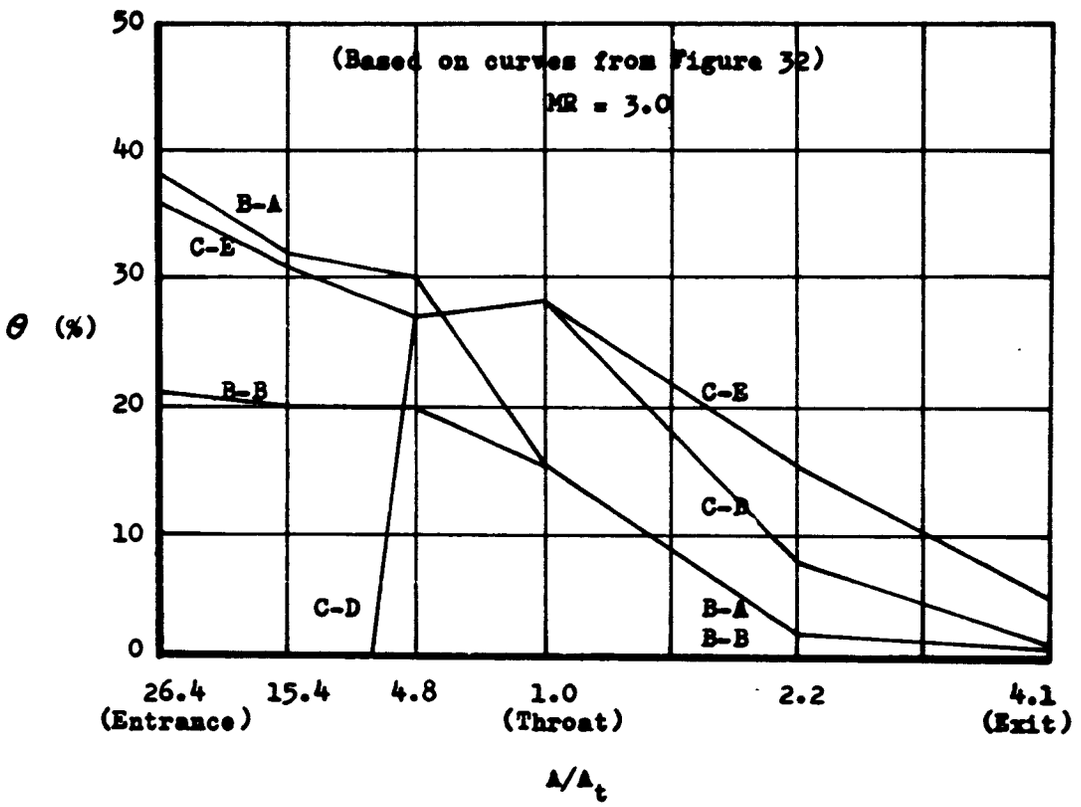

Figure 34 - Cooling Effectiveness for Various Coolant Configurations (MR = 3.0)

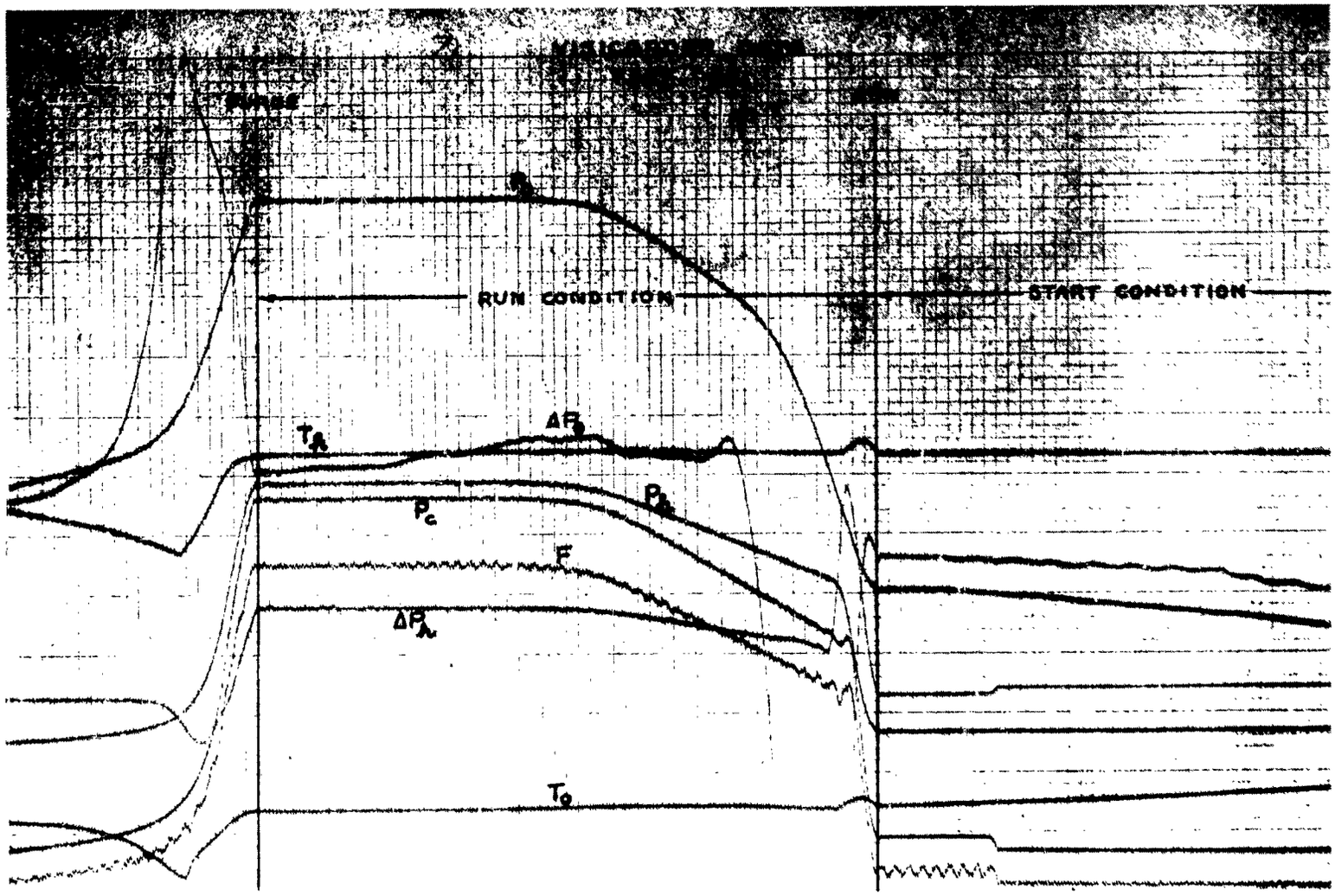

FIGURE 35 - VISICORDER DATA (TEST # 82)

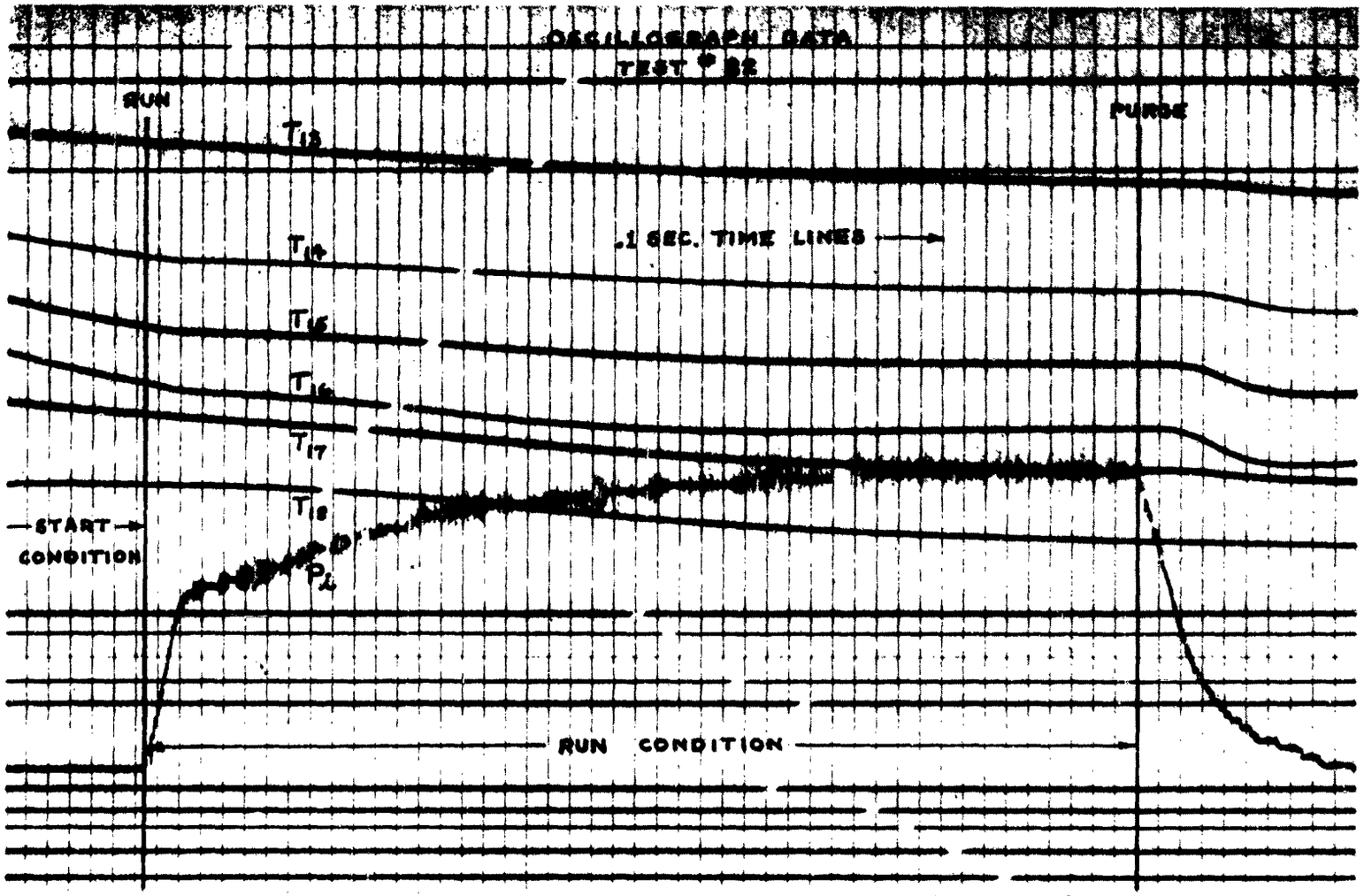

FIGURE 36 - OSCILLOGRAPH DATA (TEST 82)

TABLE I. ROCKET ENGINE DATA

Design Criteria: F = 100 lb P_c = 300 psia $\dot{w}$ = .286 lb/sec I_{sp} = 350 sec

Engine Configuration

Nozzle Code Symbol	D_c (in)	V_c (in^3)	ϕ (deg)	$V_{c(TOTAL)}$ (in^3)	α (deg)	D_t (in)	D_e (in)	r	ε	L* (in)	t_w (in)
A	2.75	23.5	60	25.1	15	.500	1.032	30.2	4.25	128	.125
B	2.75	23.5	60	25.1	15	.512	1.078	28.7	4.41	121	.188
C	2.75	23.5	45	26.2	15	.514	1.058	28.7	4.25	127	.188

Propellant Injector Data

Injector	Type	A_{in} (in^2)
Oxygen	Impinging: 8- $\frac{1}{16}$ Dia. holes	.0246
Hydrogen	Radial: 72- $\frac{1}{16}$ Dia. holes	
	8- $\frac{1}{32}$ Dia. holes	.2273

Table I. (Cont'd) Rocket Engine Data

Coolant Configurations

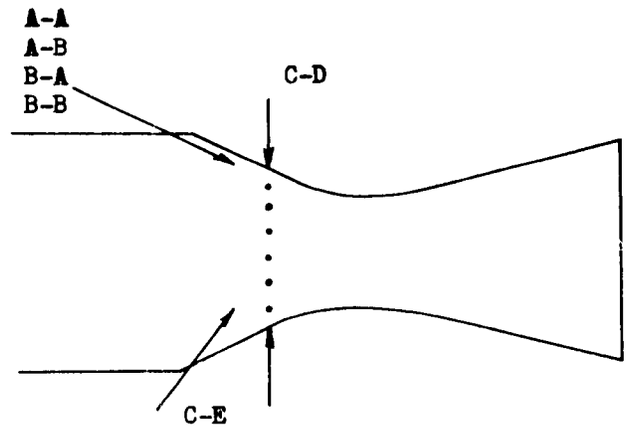

Coolant Code Symbol	Coolant Configuration (Nozzle-Coolant)	Nozzle Injection Location	Type Injection	A_i (in^2)	ω
A	A-A , B-A	entrance	tangential: 16- $\frac{1}{16}$ Dia holes	.0491	.1776
B	A-B , B-B	entrance	tangential: 16- $\frac{3}{64}$ Dia holes	.0277	.1087
C	B-C	no cooling		-	0
D	C-D	convergent (β = 7.43)	45° radial: 12- $\frac{3}{64}$ Dia holes	.0207	.0835
E	C-E	entrance + convergent (β = 7.43)	15° tangential: 16- $\frac{3}{64}$ Dia holes 45° radial: 12- $\frac{3}{64}$ Dia holes	.0484	.1755

TABLE I. (Cont'd) ROCKET ENGINE DATA

Thermocouple Location

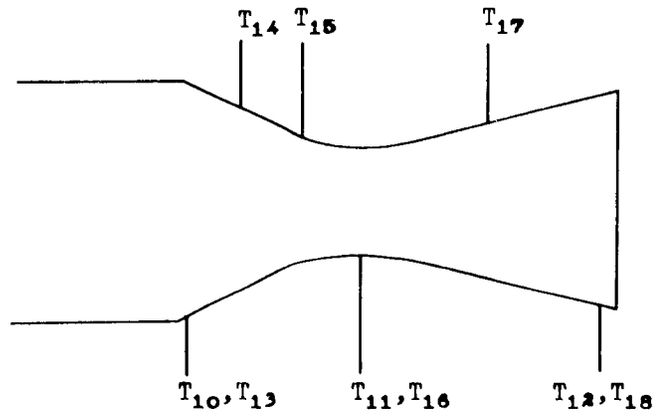

Thermocouple	Section Location	A/A_t
T_{10} , T_{13}	entrance	26.4
T_{14}	convergent	15.4
T_{15}	convergent	4.8
T_{11} , T_{16}	throat	1.0
T_{17}	divergent	2.2
T_{12} , T_{18}	exit	4.1

TABLE II. ENGINE PERFORMANCE SUMMARY

Coolant Configuration A-A; w = .178

Test No.	MR	$\dot{w}_h$	$\dot{w}_f$	$\dot{w}_o$	$\dot{w}$	F	P_c	I_{sx}	C^*_x	C_{Fx}	η	ξ	λ
		(lb / sec)				(lb)	(psia)	(sec)	(ft/sec)		(%)	(%)	(%)
9	3.36	.0688	.0566	.190	.257	75.2	272	291	6930	1.35	82.9	80.3	96.9
10	3.53	.0693	.0570	.201	.270	78.7	278	290	6765	1.38	81.3	80.2	98.8
11	3.15	.0790	.0650	.205	.284	82.7	292	290	6760	1.38	80.7	79.9	99.0
12	3.28	.0763	.0628	.206	.282	83.7	294	295	6855	1.38	81.9	81.4	99.4
13	3.43	.0713	.0586	.201	.272	79.2	282	289	6815	1.37	81.6	79.9	99.4
14	4.02	.0620	.0510	.205	.267	78.0	274	289	6745	1.39	81.8	80.5	98.5
15	4.14	.0558	.0459	.190	.247	71.2	250	288	6670	1.39	81.3	80.4	98.9
16	4.98	.0499	.0410	.204	.254	72.2	255	281	6600	1.37	82.4	80.2	97.5

Remarks: (a) Tests 1-3; Burning outside nozzle.
(b) Test 4, 5, 6; Shakedown and nozzle water cooling.
(c) Test 7, 8; Oscillograph malfunction, non-steady operation.

TABLE II. (Cont'd) ENGINE PERFORMANCE SUMMARY

Coolant Configuration A-B; w = .109

Test No.	MR	$\dot{w}_h$	$\dot{w}_f$	$\dot{w}_o$	$\dot{w}$	F	P_c	I_{sx}	C^*_x	C_{Fx}	η	ξ	λ
		(lb / sec)				(lb)	(psia)	(sec)	(ft/sec)		(%)	(%)	(%)
18	2.45	.0815	.0726	.178	.260	77.5	288	298	7010	1.36	83.0	82.1	98.9
19	3.29	.0628	.0560	.184	.247	73.2	273	296	7000	1.36	83.6	81.6	97.7
21	5.32	.0420	.0374	.199	.241	69.7	261	289	6810	1.37	86.2	83.2	96.6
22	3.33	.0681	.0607	.202	.270	79.8	298	296	6990	1.36	83.9	81.6	97.4
24	3.72	.0681	.0607	.226	.294	87.2	321	297	6910	1.38	83.3	82.3	99.2
25	2.73	.0748	.0667	.182	.257	77.2	274	301	7005	1.38	83.0	82.8	99.8
26	6.49	.0400	.0356	.231	.271	78.5	290	290	6775	1.39	89.4	86.4	96.7

Remarks: (a) Tests 17, 20, 23: Non-steady.
(b) Test 26: Nozzle throat burn-out, non-steady.

TABLE II.- (Cont'd) ENGINE PERFORMANCE SUMMARY

Coolant Configuration B-A; w = .178

Test No.	MR	$\dot{w}_h$	$\dot{w}_f$ (lb / sec)	$\dot{w}_o$ (lb / sec)	$\dot{w}$	F (lb)	P_c (psia)	I_{sx} (sec)	C^*_x (ft/sec)	C_{Fx}	η (%)	ξ (%)	λ (%)
27	2.65	.0874	.0717	.190	.277	82.7	301	299	7255	1.33	86.1	82.3	95.7
28	2.55	.0864	.0709	.181	.267	79.7	287	298	7175	1.34	84.9	82.1	95.7
30	3.95	.0603	.0490	.195	.255	73.0	264	286	6910	1.33	83.7	79.7	95.3
32	6.04	.0431	.0353	.213	.256	71.4	251	279	6540	1.38	84.9	82.3	96.9
33	2.16	.0971	.0798	.172	.269	78.0	281	290	6970	1.34	82.7	80.3	97.1
34	2.11	.0995	.0818	.173	.273	78.0	287	286	7010	1.31	83.2	79.3	95.3
35	2.18	.1018	.0836	.182	.284	84.7	298	298	7000	1.37	83.1	82.3	99.0
36	2.29	.0994	.0816	.187	.286	85.0	303	297	7060	1.35	83.7	81.8	97.8
37	2.39	.0986	.0810	.193	.292	87.7	310	300	7080	1.36	83.8	82.7	98.8
38	2.45	.0990	.0814	.199	.298	90.7	317	304	7100	1.38	83.0	83.8	101.0
39	2.65	.0926	.0761	.202	.295	89.3	314	303	7100	1.37	84.5	83.4	98.7
40	2.89	.0851	.0700	.202	.287	87.7	307	306	7140	1.38	84.8	84.1	99.3
41	3.71	.0677	.0556	.206	.274	83.7	291	305	7090	1.39	85.2	84.6	99.4

Remarks: (a) Tests 29, 31: Non-steady.

TABLE II. (Cont'd) ENGINE PERFORMANCE SUMMARY

Coolant Configuration B-B; ω = .109

Test No.	MR	$\dot{w}_h$	$\dot{w}_f$	$\dot{w}_o$	$\dot{w}$	F (lb)	P_c (psia)	I_{sx} (sec)	C^*_x (ft/sec)	C_{Fx}	η (%)	ξ (%)	λ (%)
		(lb / sec)											
42	2.57	.0753	.0671	.172	.247	72.0	265	292	7160	1.31	84.8	80.5	95.0
47	3.18	.0731	.0641	.204	.277	81.3	294	294	7080	1.34	84.5	81.0	95.9
48	3.65	.0643	.0573	.209	.274	81.7	292	299	7110	1.36	85.5	80.8	94.6
49	1.93	.1054	.0940	.181	.286	80.7	296	282	6910	1.31	82.4	78.5	95.3
51	1.97	.1053	.0940	.185	.290	83.3	304	287	6990	1.32	83.2	79.9	96.1
52	2.16	.0986	.0879	.190	.289	85.3	306	295	7065	1.34	83.8	81.7	97.5
53	2.27	.0968	.0862	.196	.293	88.4	310	302	7060	1.38	83.8	83.4	99.5
54	2.46	.0935	.0833	.205	.299	93.0	327	311	7295	1.37	86.3	85.7	99.4
55	2.70	.0881	.0785	.212	.300	92.2	322	307	7160	1.38	84.9	84.5	99.7
56	2.80	.0858	.0765	.214	.300	91.7	321	306	7140	1.38	84.7	84.3	99.5
57	3.00	.0806	.0718	.215	.296	90.3	314	305	7080	1.39	84.2	83.9	99.7
59	3.12	.0782	.0697	.217	.295	90.7	314	307	7105	1.39	84.6	84.6	100.0
60	3.44	.0714	.0636	.219	.290	87.4	306	301	7040	1.38	84.3	83.2	98.8
61	3.73	.0662	.0590	.220	.286	87.7	304	307	7090	1.40	85.4	85.1	99.8

Remarks: (a) Runs 43-46: Non-steady.
(b) Runs 50, 58: Visicorder malfunction.

TABLE II. (Cont'd) ENGINE PERFORMANCE SUMMARY

Coolant Configuration B-C; no cooling

Test No.	MR	$\dot{w}_h$	$\dot{w}_f$ (lb/sec)	$\dot{w}_o$ (lb/sec)	$\dot{w}$ (lb/sec)	F (lb)	P_c (psia)	I_{sx} (sec)	C^*_x (ft/sec)	C_{Fx}	η (%)	ξ (%)	λ (%)
62	1.46	-	.1096	.160	.270	75.6	279	280	6895	1.31	83.7	79.8	95.4
63	1.67	-	.1033	.172	.275	79.7	290	290	7040	1.33	84.5	81.7	96.8
64	1.87	-	.1003	.187	.287	85.8	308	299	7160	1.34	85.4	83.6	97.9
65	2.00	-	.0954	.191	.286	88.0	312	308	7280	1.36	86.5	85.6	99.0
66	2.13	-	.0910	.193	.284	87.9	313	309	7360	1.35	87.3	85.5	98.0
67	2.32	-	.0858	.199	.285	88.5	313	311	7330	1.37	86.8	85.7	98.8
68	2.60	-	.797	.207	.287	89.8	314	313	7300	1.38	86.5	86.3	99.8
69	3.04	-	.711	.216	.287	90.0	313	314	7280	1.39	86.6	86.5	99.9
70	3.58	-	.0620	.222	.284	88.0	306	310	7185	1.39	86.3	85.7	99.3
71	4.17	-	.0543	.226	.280	86.0	296	307	7060	1.40	86.0	85.8	99.8

Remarks: (a) Test 71: Nozzle throat burnout.

TABLE II. (Cont'd) ENGINE PERFORMANCE SUMMARY

Coolant Configuration C-D; ω = .084

Test No.	MR	$\dot{w}_h$	$\dot{w}_f$	$\dot{w}_o$	$\dot{w}$	F	P_c	I_{sx}	C^*_x	C_{Fx}	η	ξ	λ
		(lb / sec)				(lb)	(psia)	(sec)	(ft/sec)		(%)	(%)	(%)
72	1.66	.1061	.0973	.162	.268	76.2	272	284	6760	1.35	81.3	80.1	98.6
73	1.84	.1022	.0937	.172	.274	79.7	281	291	6840	1.37	81.7	81.3	99.5
74	2.05	.0979	.0897	.184	.282	84.0	292	298	6910	1.39	82.1	82.6	100.6
75	2.23	.0928	.0851	.190	.283	87.2	301	308	7100	1.40	84.2	85.2	101.2
76	2.27	.0926	.0849	.193	.286	89.0	307	311	7160	1.40	84.8	85.9	101.3
77	2.51	.0843	.0773	.194	.278	87.6	302	315	7250	1.40	85.8	86.8	101.2
78	2.93	.0755	.0692	.203	.279	87.7	302	315	7225	1.40	85.9	86.7	101.0
79	2.84	.0754	.0691	.196	.271	84.8	293	313	7210	1.40	85.6	86.2	100.7
80	3.05	.0736	.0675	.206	.280	85.2	295	304	7030	1.39	83.6	83.8	100.2
81	3.44	.0662	.0607	.209	.275	85.6	295	311	7160	1.40	85.7	85.9	100.1
82	3.58	.0661	.0606	.217	.283	86.7	297	306	7000	1.41	84.1	84.7	100.7
83	1.69	.1048	.0961	.162	.267	77.0	282	288	7050	1.32	84.7	81.1	95.9
84	3.70	.0643	.0589	.218	.282	86.7	305	307	7210	1.37	86.8	85.1	98.1
85	4.26	.0593	.0543	.231	.290	88.0	306	303	7040	1.39	86.0	84.9	98.8
86	4.84	.0554	.0508	.246	.301	91.0	311	302	6895	1.41	85.8	85.7	99.9
87	5.54	.0489	.0448	.248	.297	89.3	303	300	6805	1.42	86.7	86.9	100.1

TABLE II. (Cont'd) ENGINE PERFORMANCE SUMMARY

Coolant Configuration C-E; ω = .176

Test No.	MR	$\dot{w}_h$	$\dot{w}_f$	$\dot{w}_o$	$\dot{w}$	F (lb)	P_c (psia)	I_{sx} (sec)	C^*_x (ft/sec)	C_{Fx}	η (%)	ξ (%)	λ (%)
		(lb / sec)											
88	1.57	.1258	.1037	.163	.289	79.8	285	276	6580	1.35	79.4	78.3	98.7
89	1.63	.1233	.1016	.165	.288	82.7	291	287	6745	1.37	81.2	81.0	99.8
90	1.88	.1142	.0941	.177	.291	85.3	298	293	6790	1.39	80.9	79.5	98.3
91	2.15	.1062	.0877	.189	.295	88.8	306	301	6920	1.40	82.1	83.3	101.4
92	2.36	.0997	.0822	.194	.294	89.8	308	306	6990	1.41	82.8	84.6	102.1
93	2.47	.0942	.0777	.192	.286	85.8	296	300	6910	1.40	81.8	82.7	101.1
94	2.54	.0937	.0773	.196	.290	87.7	302	303	6950	1.40	82.3	83.5	101.4
95	3.15	.0815	.0672	.212	.294	89.0	304	303	6900	1.41	82.2	83.5	101.6
96	3.63	.0737	.0608	.221	.295	89.0	302	301	6830	1.42	82.1	83.3	101.3
97	4.03	.0680	.0561	.226	.294	89.0	301	302	6830	1.42	82.9	84.2	101.6
98	5.13	.0556	.0458	.235	.291	87.2	294	299	6745	1.43	84.7	85.6	101.1
99	5.16	.0570	.0470	.242	.299	89.3	302	298	6740	1.42	84.8	85.3	100.6

TABLE III. COOLANT PERFORMANCE SUMMARY

Coolant Configuration A-A; ω = .178

Test No.	MR	V_i (ft/sec)	T_{13} (°F)	T_{14} (°F)	T_{15} (°F)	T_{16} (°F)	T_{17} (°F)	T_{18} (°F)	T_a (°F)	Pa (psia)	Test Time (sec)
9	3.36	1145	-	535	705	1220	1085	1055	55	14.5	4.5
10	3.53	1210	-	545	715	1245	1145	1110	57	14.5	4.1
11	3.15	1025	-	525	710	1145	1045	1030	57	14.5	4.0
12	3.28	834	-	530	700	1175	1075	1045	59	14.5	4.0
13	3.43	846	-	530	705	1235	1100	1065	59	14.5	4.0
15	4.14	639**	-	530	775	1280	1200	1140	59	14.5	4.0
16	4.98	438**	-	615	880*	1460*	1230*	1180*	59	14.5	4.0
14	4.02	679	-	535	765	1265	1180	1125	59	14.5	4.0

* Non-steady temperature reading.

** Inaccurate due to small ΔP_{in}

Remarks: (a) Tests 9-16: T_{13} thermocouple faulty.

TABLE III. (Cont'd) COOLANT PERFORMANCE SUMMARY

Coolant Configuration A-B; ω = .109

Test No.	MR	V_i (ft/sec)	T_{13} (°F)	T_{14} (°F)	T_{15} (°F)	T_{16} (°F)	T_{17} (°F)	T_{18} (°F)	T_a (°F)	P_a (psia)	Test Time (sec)
18	2.45	1215	420	630	710	1070	955	925	45	14.5	3.5
19	3.29	1030	445	655	765	1180	1085	1025	45	14.5	3.7
21	5.32	627**	480*	765*	885*	1380*	1260*	1130*	44	14.5	3.9
22	3.33	869	450	675	770	1200	1100	1040	43	14.5	3.9
24	3.72	773	455	700	790	1265	1160	1125	42	14.5	3.8
25	2.73	953	430	640	725	1120	995	965	42	14.5	5.7
26	6.49	715	600*	960*	1075*	1760*	1610*	1310*	42	14.5	4.3

* Non-steady temperature reading.

** Inaccurate due to small ΔP_{in}

Remarks: (a) Test 26: Nozzle throat burnout, non-steady.

TABLE III. (Cont'd) COOLANT PERFORMANCE SUMMARY

Coolant Configuration B-A; ω = .178

Test No.	MR	V_i (ft/sec)	T_{13} (°F)	T_{14} (°F)	T_{15} (°F)	T_{16} (°F)	T_{17} (°F)	T_{18} (°F)	T_a (°F)	P_a (psia)	Test Time (sec)
27	2.65	1080	375	470	685	1080	990	965	52	14.4	5.4
28	2.55	1060	360	460	680	1060	980	960	52	14.4	5.4
30	3.95	898	415	560	870	1330	1200	1160	41	14.5	5.3
32	6.04	440**	515*	795*	1000*	1430*	-	945*	42	14.5	4.0
33	2.16	1345	320	415	670	895	845	800	78	14.4	4.1
34	2.11	1290	-	405	670	865	825	785	78	14.4	4.4
35	2.18	1235	-	430	675	945	865	830	78	14.4	4.6
36	2.29	932	-	440	680	975	895	860	77	14.4	4.5
37	2.39	1295	-	445	690	1030	930	890	77	14.4	4.6
38	2.45	1220	-	460	690	1050	980	950	77	14.4	4.5
39	2.65	1120	-	480	690	1090	995	975	76	14.4	4.5
40	2.89	1125	400	485	690	1120	1020	1000	76	14.4	4.5
41	3.71	1270	410	525	815	1270	1170	1140	76	14.4	5.1

* Non-steady temperature reading.

** Inaccurate due to small ΔP_{in}

Remarks: (a) Tests 34-39: T_{13} oscillograph channel faulty.
(b) Tests 30, 32: T_{17} thermocouple faulty.

TABLE III. (Cont'd) COOLANT PERFORMANCE SUMMARY

Coolant Configuration B-B; ω = .109

Test No.	MR	V_i (ft/sec)	T_{13} (°F)	T_{14} (°F)	T_{15} (°F)	T_{16} (°F)	T_{17} (°F)	T_{18} (°F)	T_a (°F)	P_a (psia)	Test Time (sec)
42	2.57	443**	445	505	750	1075	995	-	46	14.5	4.6
47	3.18	648**	490	595	860	1160	1070	-	46	14.4	4.0
48	3.65	649**	485	635	900*	1085*	1030*	-	46	14.4	4.0
49	1.93	831	390	455	710	840	780	740	50	14.5	4.2
51	1.97	1050	395	455	720	880	820	795	50	14.5	4.1
52	2.16	1010	415	465	735	960	890	875	50	14.5	4.3
53	2.27	1110	430	480	745	1005	930	915	50	14.5	4.2
54	2.46	973	440	495	750	1065	990	980	50	14.5	4.4
55	2.70	981	455	510	760	1095	1005	990	50	14.5	4.3
56	2.80	927	465	535	790	1100	1020	1010	50	14.5	4.4
57	3.00	277**	485	580	825	1125	1055	1040	50	14.5	4.4
59	3.12	641**	485	585	850	1150	1065	1050	50	14.5	4.5
60	3.44	506**	485	600	880	1185	1100	1080	50	14.5	4.5
61	3.73	300**	485	645	945	1300	1170	1125	50	14.5	4.4

* Non-steady temperature reading.

** Inaccurate due to small ΔP_{in}.

Remarks: (a) Tests 42, 47, 48: T_{18} oscillograph channel faulty.

TABLE III. (Cont'd) COOLANT PERFORMANCE SUMMARY

Coolant Configuration B-C; no cooling

Test No.	MR	V_i (ft/sec)	T_{13} (°F)	T_{14} (°F)	T_{15} (°F)	T_{16} (°F)	T_{17} (°F)	T_{18} (°F)	T_a (°F)	P_a (psia)	Test Time (sec)
62	1.46	-	450	500	695	795	725	660	54	14.4	4.5
63	1.67	-	495	515	710	855	765	710	54	14.4	4.5
64	1.87	-	515	545	750	940	860	785	54	14.4	4.5
65	2.00	-	535	565	795	990	895	835	55	14.4	4.5
66	2.13	-	560	595	845	1015	940	880	55	14.4	4.5
67	2.32	-	600	625	860	1055	960	920	55	14.4	4.5
68	2.60	-	625	660	890	1130	990	970	56	14.4	4.6
69	3.04	-	645	745	1060	1360	1055	1030	56	14.4	4.5
70	3.58	-	660	805	1165	1565	1170	1115	57	14.4	4.2
71	4.17	-	675*	900*	1330*	1780*	1320*	1205*	58	14.4	4.9

* Non-steady temperature reading.

Remarks: (a) Test 71: Nozzle throat burnout.

TABLE III. (Cont'd) COOLANT PERFORMANCE SUMMARY

Coolant Configuration C-D; ω = .084

Test No.	MR	V_i (ft/sec)	T_{13} (°F)	T_{14} (°F)	T_{15} (°F)	T_{16} (°F)	T_{17} (°F)	T_{18} (°F)	T_a (°F)	P_a (psia)	Test Time (sec)
72	1.66	1715	365	480	505	585	615	590	53	14.3	4.5
73	1.84	1385	440	485	525	650	700	650	54	14.3	5.0
74	2.05	1365	475	500	550	710	765	715	55	14.3	5.0
75	2.23	1110	505	550	645	770	845	855	55	14.3	5.1
76	2.27	1235	510	560	655	820	920	945	56	14.3	5.1
77	2.51	1015	525	590	730	890	960	1000	56	14.3	5.8
78	2.93	1210	540	615	760	960	980	1030	56	14.3	5.0
79	2.84	1190	535	605	750	950	970	1020	71	14.3	4.9
80	3.05	1070	555	625	785	1050	990	1050	73	14.2	4.3
81	3.44	1040	590	695	835	1075	1010	1090	75	14.2	4.5
82	3.58	903	600	705	880	1110	1035	1105	76	14.2	4.5
83	1.69	1825	400	-	515	615	665	610	68	14.4	6.2
84	3.70	1085	610	-	885	1160	1055	1125	67	14.4	5.4
85	4.26	1045	630	-	920	1250	1145	1140	68	14.4	4.5
86	4.84	913	665	-	990	1370*	1235*	1155*	68	14.4	4.2
87	5.54	1250	690	-	1035	1440*	1260*	1200*	68	14.4	4.2

* Non-steady temperature reading.

Remarks: (a) Tests 83-87: T_{14} oscillograph channel faulty.

TABLE III. (Cont'd) COOLANT PERFORMANCE SUMMARY

Coolant Configuration C-E; ω = .176

Test No.	MR	V_i (ft/sec)	T_{13} (°F)	T_{14} (°F)	T_{15} (°F)	T_{16} (°F)	T_{17} (°F)	T_{18} (°F)	T_a (°F)	P_a (psia)	Test Time (sec)
88	1.57	1005	285	340	465	610	590	620	72	14.2	5.1
89	1.63	1000	310	350	485	650	615	645	72	14.2	6.0
90	1.88	926	330	385	510	695	655	710	72	14.2	5.3
91	2.15	882	345	430	580	760	745	775	72	14.2	5.4
92	2.36	835	365	445	655	810	770	850	72	14.2	5.2
93	2.47	772	375	450	675	860	800	885	72	14.2	5.1
94	2.54	662	385	460	720	880	830	915	72	14.2	5.5
95	3.15	653	425	510	825	1010	945	1005	71	14.2	5.1
96	3.63	278**	435	535	845	1065	1055	1080	70	14.2	5.1
97	4.03	832	445	570	860	1170	1085	1145	70	14.2	5.2
98	5.13	732	445	685	910	1215*	1125*	1165*	60	14.1	4.9
99	5.16	277**	455	695	935	1240*	1135*	1170*	60	14.1	4.7

* Non-steady temperature reading.

** Inaccurate due to small ΔP_{in}.

APPENDIX B

GAE/ME/63-1

NOTICE: WHEN GOVERNMENT DRAWINGS, SPECIFICATIONS, OR OTHER DATA ARE USED FOR ANY PURPOSE OTHER THAN IN CONNECTION WITH A DEFINITELY RELATED GOVERNMENT PROCUREMENT OPERATION, THE UNITED STATES GOVERNMENT THEREBY INCURS NO RESPONSIBILITY, NOR ANY OBLIGATIONS WHATSOEVER; AND THE FACT THAT THE GOVERNMENT MAY HAVE FORMULATED, FURNISHED, OR IN ANY WAY SUPPLIED THE SAID DRAWINGS, SPECIFICATIONS, OR OTHER DATA IS NOT TO BE REGARDED BY IMPLICATION OR OTHERWISE AS IN ANY MANNER LICENSING THE HOLDER OR ANY OTHER PERSON OR CORPORATION, OR CONVEYING ANY RIGHTS OR PERMISSION TO MANUFACTURE, USE, OR SELL ANY PATENTED INVENTION THAT MAY IN ANY WAY BE RELATED THERETO.

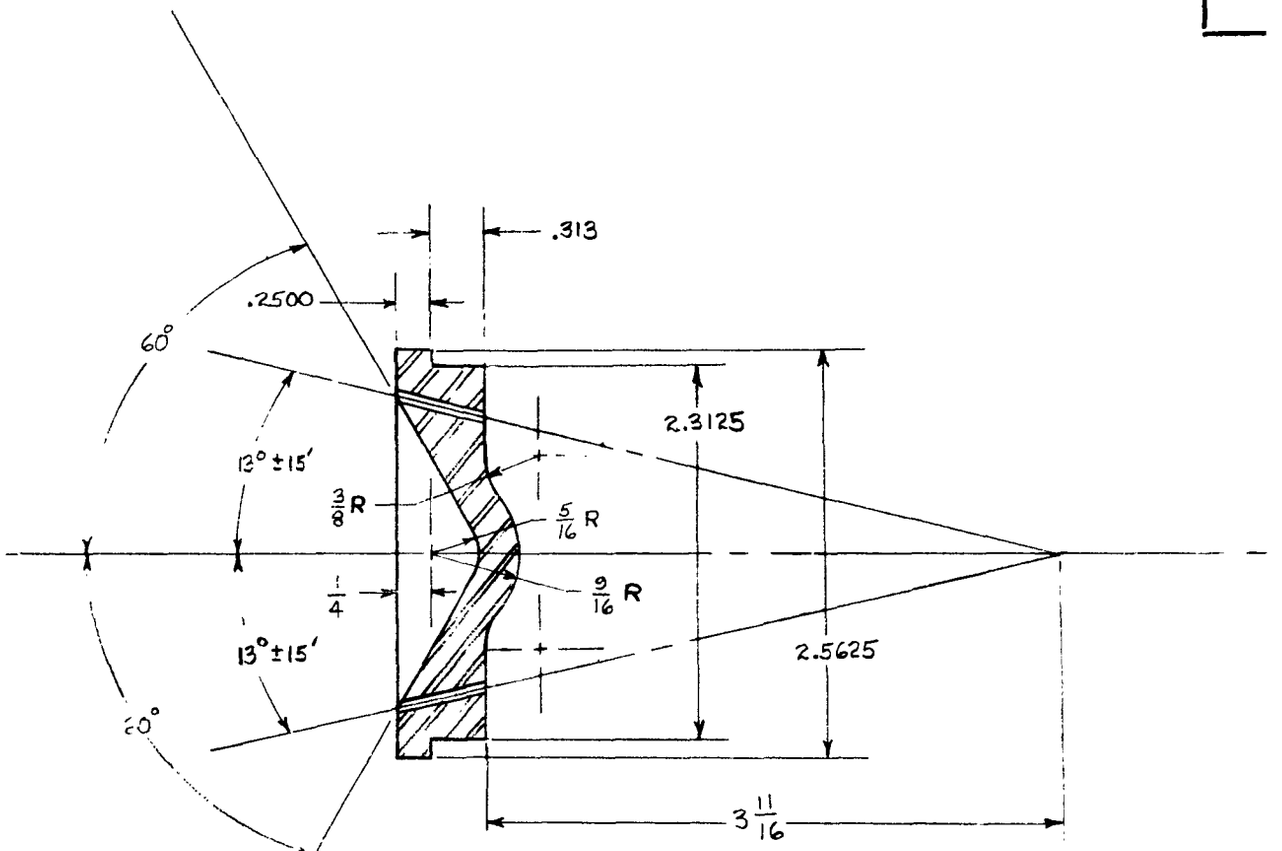

1

① BUFF	④ ROUGH MACH. FINISH	
② HAND FINISH	⑤ ROUGH FILE OR GRIND	
③ SMOOTH MACH. FINISH	⑥ SAND BLAST	
⑦ REMOVE FINS AND SPRUES		
⑧ FINISH ALL SURFACES NOT OTHERWISE SPECIFIED		

UNLESS OTHERWISE SPECIFIED DIMENSIONS ARE IN INCHES. TOLERANCES ON FRACTIONS.	DECIMALS.	ANGLES.	DRAFTSMAN D.J.
1/64	0.0005	15'	CHECKER
MATERIAL STAINLESS STEEL 302 OR 303 OR K-MONEL			ENGINEER G.O.
TREATMENT			EXAMINED
FINISH ③ ② ALL OVER			PRO. APPR

AMC Form No. 1168 (30 Nov 47)

This Form replaces AMC Form No. 97-4-38, existing stock of which will be used until exhausted.

SYMBOL	ALTERATION	DATE	APPROVED

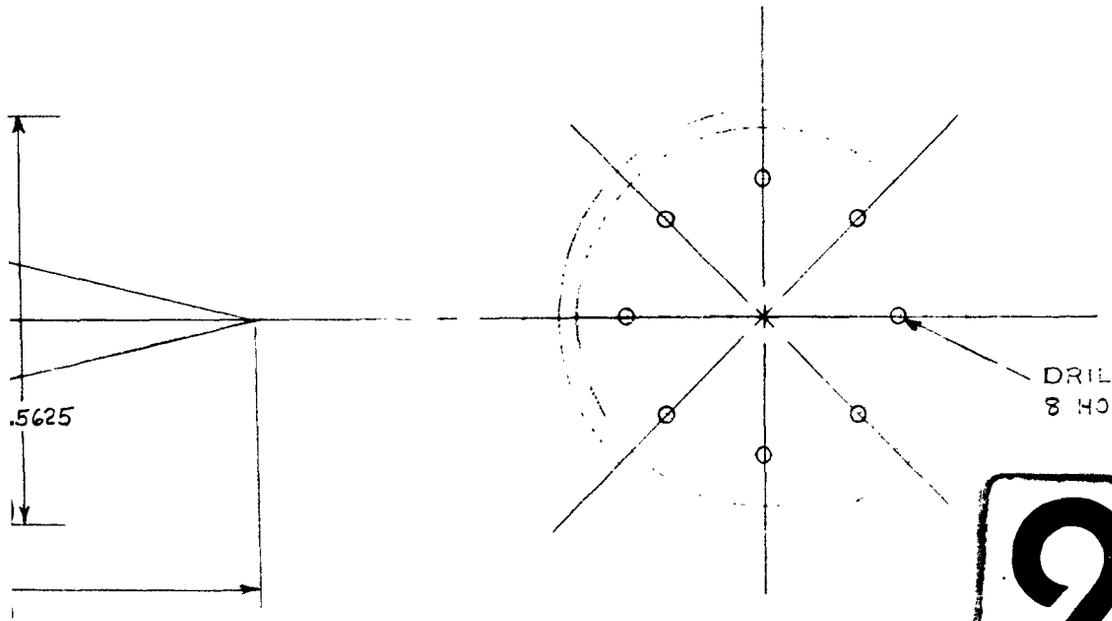

2

TYPE	NEXT ASSY NO.	NEXT ASSY	FINAL ASSY
	USED ON	QUANTITY REQD. 1	

LESS OTHERWISE SPECIFIED DIMENSIONS ARE IN INCHES. TOLERANCES ON FRACTIONS. DECIMALS. ANGLES. 1/64 0.0005 15′	DRAFTSMAN D.J. ALSER	DATE 1/12/62	NAME OXIDIZER INJECTOR A
MATERIAL STAINLESS STEEL 302 OR 303 OR K-MONEL	CHECKER		
HEAT TREATMENT	ENGINEER G. OW		
FINISH ③ ② ALL OVER	EXAMINED		
	PRO. APPRVD.		SCALE FULL WT.

U. S. AIR FORCE
AIR MATERIEL COMMAND

1
DRAWING NO.

This Form replaces AMC Form No. 37-6-28, existing stock of which will be used until exhausted.

WF-L-17 DEC 48 9466

GAE/ME/63-1

NOTICE: WHEN GOVERNMENT DRAWINGS, SPECIFICATIONS, OR OTHER DATA ARE USED FOR ANY PURPOSE OTHER THAN IN CONNECTION WITH A DEFINITELY RELATED GOVERNMENT PROCUREMENT OPERATION, THE UNITED STATES GOVERNMENT THEREBY INCURS NO RESPONSIBILITY, NOR ANY OBLIGATIONS WHATSOEVER; AND THE FACT THAT THE GOVERNMENT MAY HAVE FORMULATED, FURNISHED, OR IN ANY WAY SUPPLIED THE SAID DRAWINGS, SPECIFICATIONS, OR OTHER DATA IS NOT TO BE REGARDED BY IMPLICATION OR OTHERWISE AS IN ANY MANNER LICENSING THE HOLDER OR ANY OTHER PERSON OR CORPORATION, OR CONVEYING ANY RIGHTS OR PERMISSION TO MANUFACTURE, USE, OR SELL ANY PATENTED INVENTION THAT MAY IN ANY WAY BE RELATED THERETO.

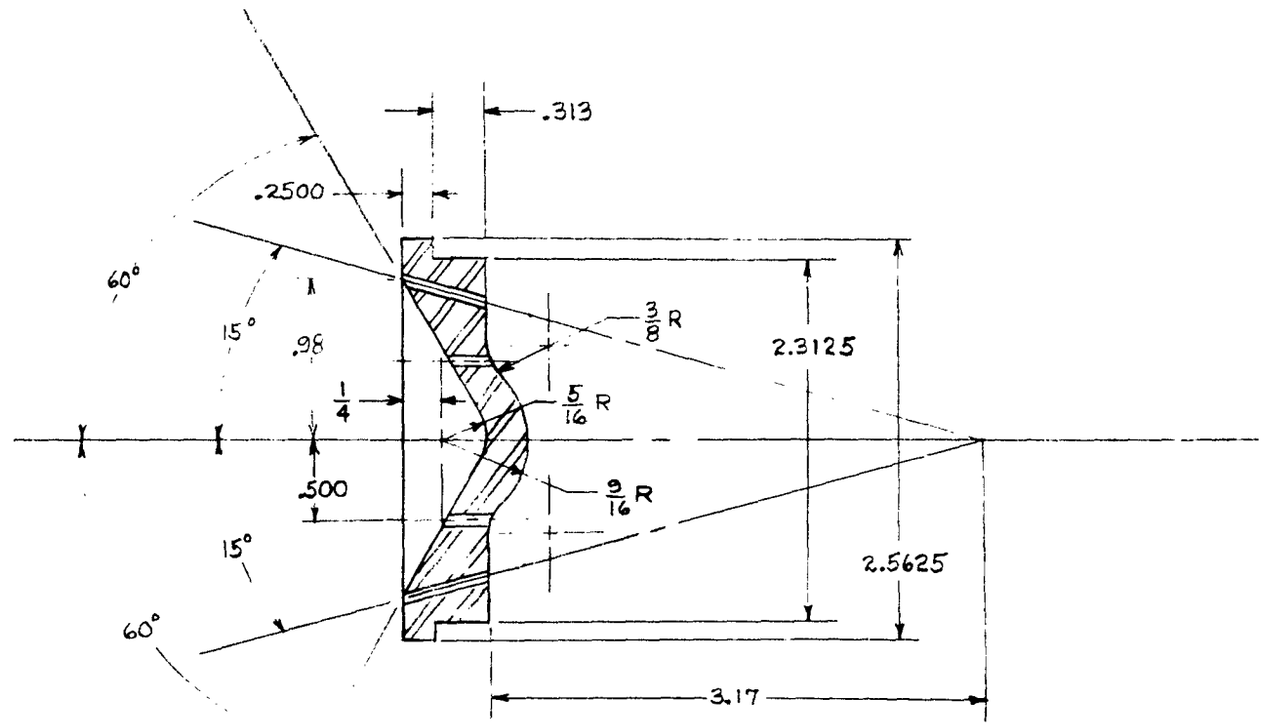

1

① BUFF	④ ROUGH MACH. FINISH
② HAND FINISH	⑤ ROUGH FILE OR GRIND
③ SMOOTH MACH. FINISH	⑥ SAND BLAST
⑦ REMOVE FINS AND SPRUES	
⑧ FINISH ALL SURFACES NOT OTHERWISE SPECIFIED	

UNLESS OTHERWISE SPECIFIED DIMENSIONS ARE IN INCHES. TOLERANCES ON		DRAFTSMAN D. J. A
FRACTIONS. 1/64	DECIMALS. 0.0005	ANGLES. 15'
MATERIAL STAINLESS STEEL 302 OR 303 OR K-MONEL		ENGINEER J. L. P
TREATMENT		EXAMINED
FINISH ③ ② ALL OVER		PRO. APPRVD.

AMC Form No. 1168 (20 Nov 47)

This Form replaces AMC Form No. 57-2-38, existing stock of which will be used until exhausted.

SYMBOL	ALTERATION	DATE	APPROVED

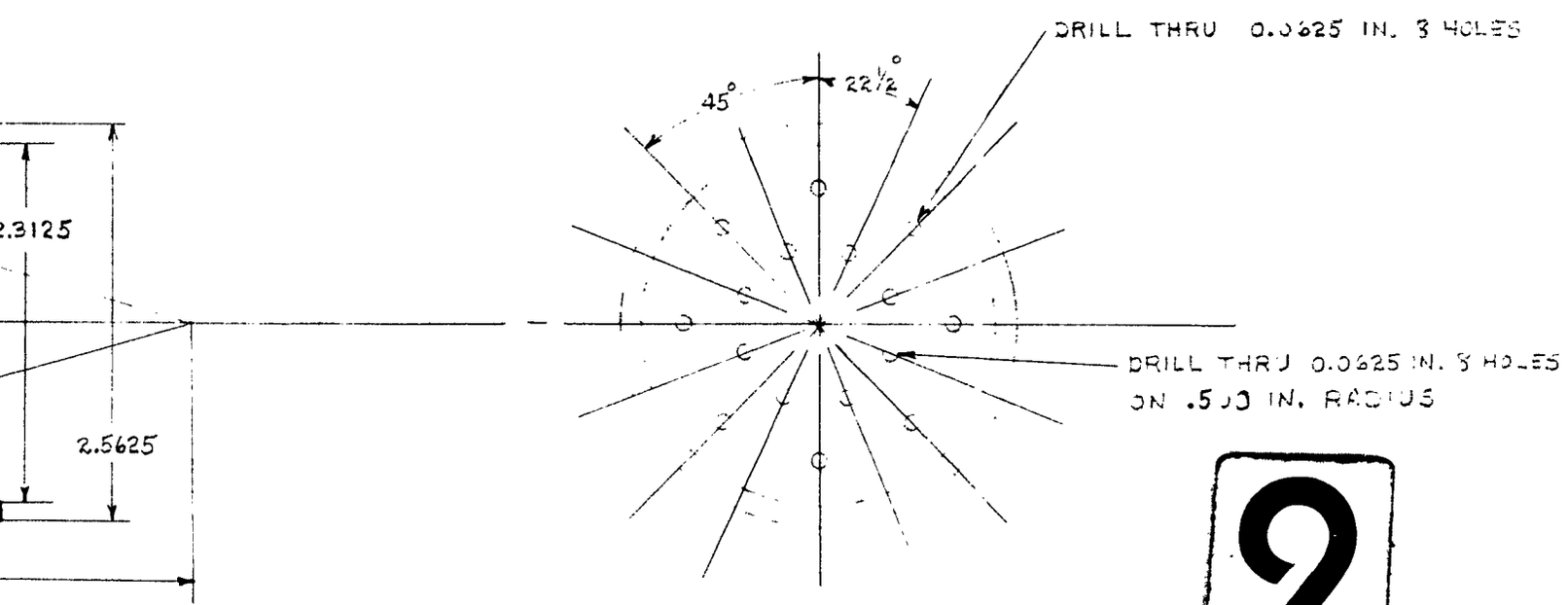

2

TYPE	NEXT ASSY NO.	NEXT ASSY	FINAL ASSY
USED ON		QUANTITY REQD. 1	

UNLESS OTHERWISE SPECIFIED DIMENSIONS ARE IN INCHES. TOLERANCES ON FRACTIONS. 1/64 DECIMALS. 0.0005 ANGLES. 15'

MATERIAL STAINLESS STEEL 302 OR 303 OR K-MONEL

HEAT TREATMENT

FINISH (3) (2) ALL OVER

DRAFTSMAN D. J. ALSER — DATE 1/12/62

CHECKER

ENGINEER J. L. PICKITT

EXAMINED

PRO. APPRVD.

NAME OXIDIZER INJECTOR B

SCALE FULL — WT.

U. S. AIR FORCE
AIR MATERIEL COMMAND

2
DRAWING NO.

This Form replaces AMC Form No. 57-4-58, existing stock of which will be used until exhausted.

WF-C-17 DEC 48 9660

GAE/MB/63-1

NOTICE: WHEN GOVERNMENT DRAWINGS, SPECIFICATIONS, OR OTHER DATA ARE USED FOR ANY PURPOSE OTHER THAN IN CONNECTION WITH A DEFINITELY RELATED GOVERNMENT PROCUREMENT OPERATION, THE UNITED STATES GOVERNMENT THEREBY INCURS NO RESPONSIBILITY, NOR ANY OBLIGATIONS WHATSOEVER; AND THE FACT THAT THE GOVERNMENT MAY HAVE FORMULATED, FURNISHED, OR IN ANY WAY SUPPLIED THE SAID DRAWINGS, SPECIFICATIONS, OR OTHER DATA IS NOT TO BE REGARDED BY IMPLICATION OR OTHERWISE AS IN ANY MANNER LICENSING THE HOLDER OR ANY OTHER PERSON OR CORPORATION, OR CONVEYING ANY RIGHTS OR PERMISSION TO MANUFACTURE, USE, OR SELL ANY PATENTED INVENTION THAT MAY IN ANY WAY BE RELATED THERETO.

STA. 1,2,3,4, 8-HOLES $\frac{1}{16}$" DIA. EQUALLY SPACED

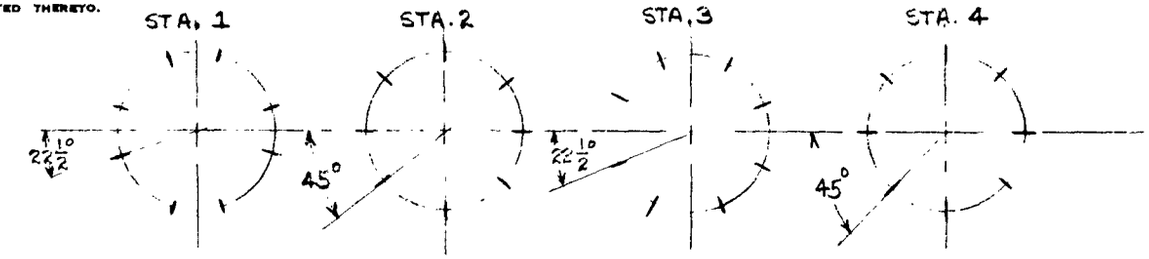

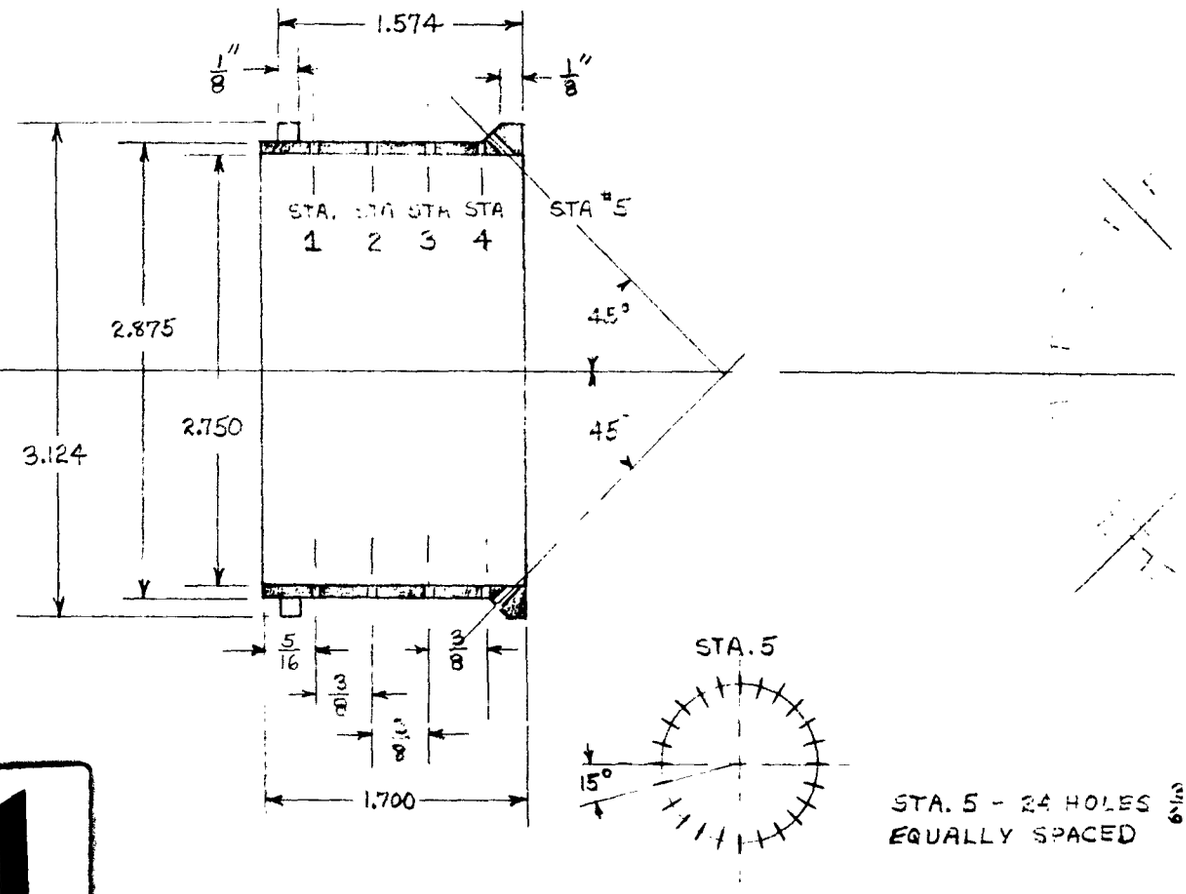

STA. 5 - 24 HOLES EQUALLY SPACED

1

(1) BUFF	(4) ROUGH MACH. FINISH
(2) HAND FINISH	(5) ROUGH FILE OR GRIND
(3) SMOOTH MACH. FINISH	(6) SAND BLAST
(7) REMOVE FINS AND SPRUES	
(8) FINISH ALL SURFACES NOT OTHERWISE SPECIFIED	

UNLESS OTHERWISE SPECIFIED DIMENSIONS ARE IN INCHES.	TOLERANCES ON	
FRACTIONS. 1/64	DECIMALS. .005	ANGLES. 1°
MATERIAL STAINLESS STEEL 302, OR 303 OR K-MONEL		
TREATMENT		
FINISH (3) AND (2)		

DRAFTSMAN D.U. A
CHECKER
ENGINEER D.U.
EXAMINED
PRO. APPRVI

AMC Form No. 1108 (20 Nov 47)

This Form replaces AMC Form No. 57-6-28, existing stock of which will be used until exhausted.

8-HOLES $\frac{1}{16}$" DIA.
ED

SYMBOL	ALTERATION	DATE	APPROVED

STA. 4

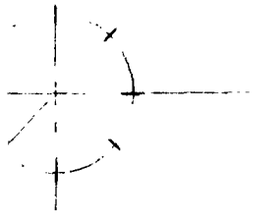

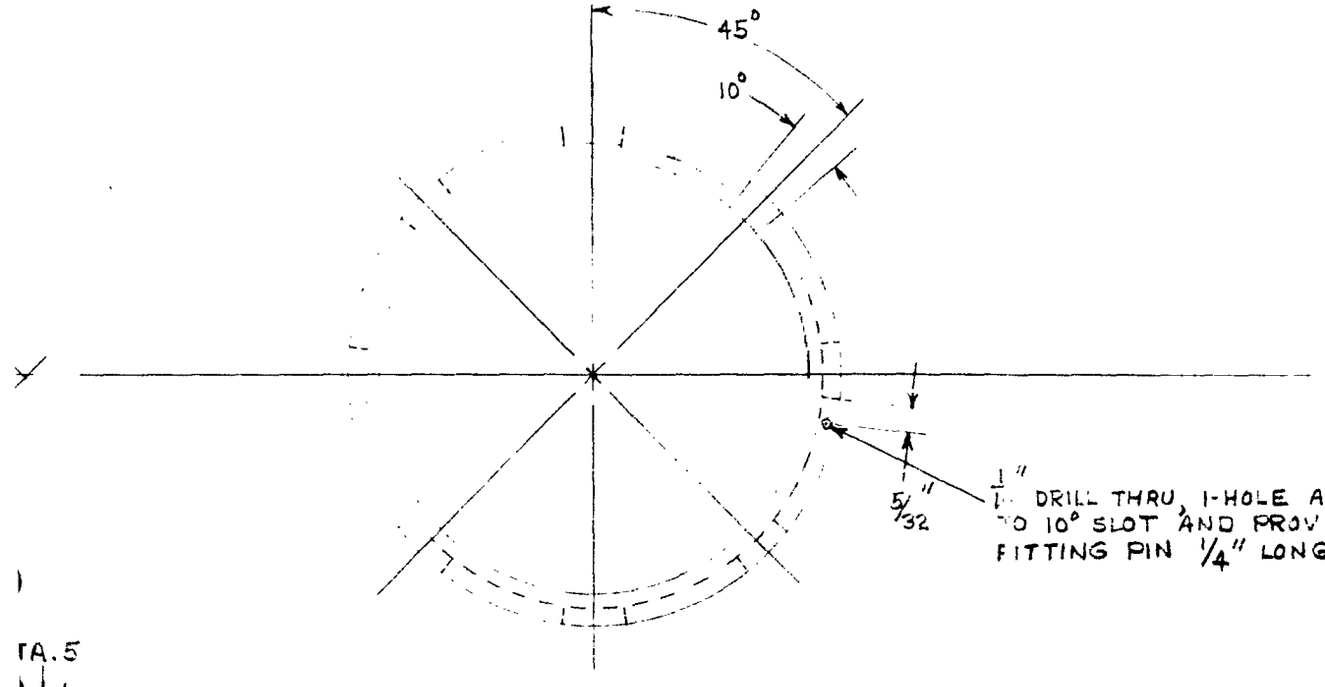

$\frac{1}{4}$" DRILL THRU, 1-HOLE ADJACENT TO 10° SLOT AND PROVIDE FITTING PIN $\frac{1}{4}$" LONG

2

TA. 5

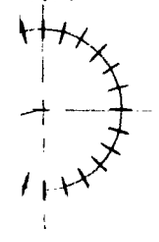

STA. 5 - 24 HOLES $\frac{3}{64}$" DIA. EQUALLY SPACED

TYPE	NEXT ASSY NO.	NEXT ASSY	FINAL ASSY
	USED ON	QUANTITY REQD. 1	

LESS OTHERWISE SPECIFIED DIMENSIONS ARE IN CHES. / ACTIONS.	TOLERANCES ON DECIMALS.	ANGLES.
1/64	.005	1°

TERIAL STAINLESS STEEL 302, 303 OR K-MONEL
EATMENT

ISH (3) AND (2)

DRAFTSMAN	DATE
D.J. ALSER	1/12/62
CHECKER	
ENGINEER: D.J. ALSER	
EXAMINED	
PRO. APPRVD.	

NAME: INNER LINER (AFT)

SCALE FULL | WT.

U. S. AIR FORCE
AIR MATERIEL COMMAND

3
DRAWING NO.

This Form replaces AMC Form No. 57-6-28, existing stock of which will be used until exhausted.

WF-L-17 DEC 48 9488

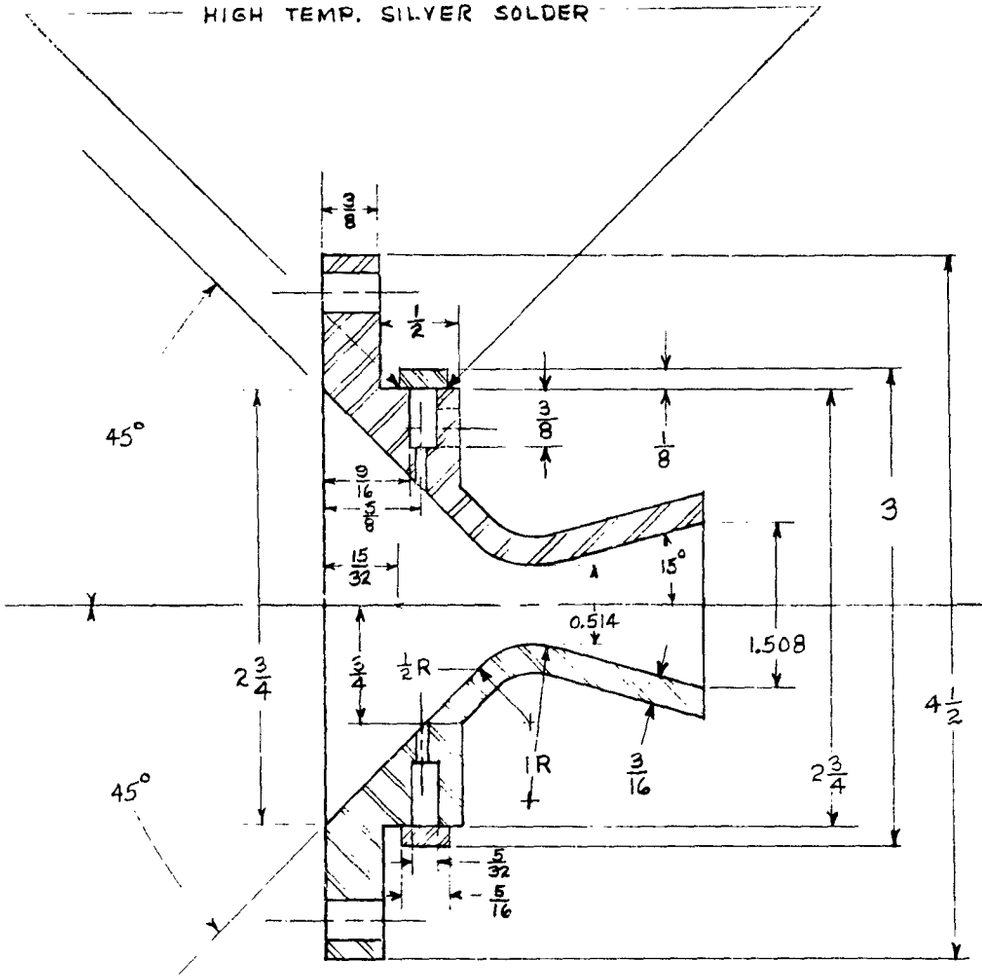

1

WORK ORDE

① BUFF
② HAND FINISH
③ SMOOTH MACH. FINISH
④ ROUGH MACH. FINISH
⑤ ROUGH FILE OR GRIND
⑥ SAND BLAST
⑦ REMOVE FINS AND SPRUES
FINISH ALL SURFACES NOT OTHERWISE SPECIFIED

UNLESS OTHERWISE SPECIFIED DIMENSIONS ARE IN INCHES. TOLERANCES ON FRACTIONS. 1/64 DECIMALS. .005 ANGLES. 30′	DRAFTSMAN D.J.
	CHECKER
MATERIAL COPPER	ENGINEER D.J.
TREATMENT	EXAMINED
FINISH ③ INSIDE SURFACES ③ OUTSIDE SURFACES	PRO. APPRVI

AMC Form No. 1106 (30 Nov 47)

This form replaces AMC Form No. 57-6-28, existing stock of which will be used until exhausted.

SYMBOL	ALTERATION	DATE	APPROVED
A	2ND NOZZLE – 16 HOLES, $\frac{1}{32}$ DRILL 22 $\frac{1}{2}$° SPACING		

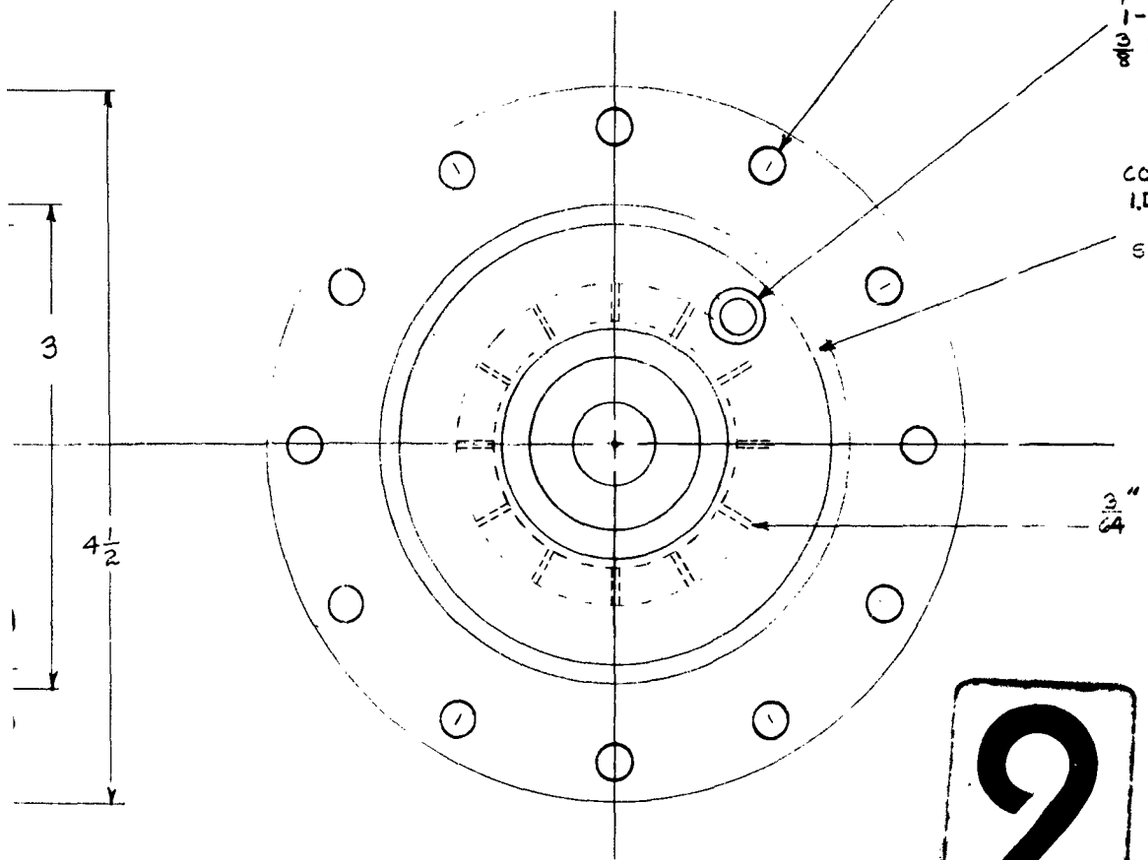

2

WORK ORDER – 62-304

TYPE	NEXT ASSY NO.	NEXT ASSY	FINAL ASSY
USED ON		QUANTITY REQD. 2	

UNLESS OTHERWISE SPECIFIED DIMENSIONS ARE IN INCHES. FRACTIONS. 1/64 DECIMALS. .005 TOLERANCES ON ANGLES. 30'	DRAFTSMAN D.J. ALSER	DATE 2/12/62
	CHECKER	
MATERIAL COPPER	ENGINEER D.J. ALSER	
TREATMENT	EXAMINED	
FINISH (2) INSIDE SURFACES. OUTSIDE SURFACES	PRO. APPRVD.	

NAME: NOZZLE C

SCALE FULL WT.

U. S. AIR FORCE
AIR MATERIEL COMMAND

4
DRAWING NO.

This Form replaces AMC Form No. 57-4-28, existing stock of which will be used until exhausted.

WF—1.17 DEC 48 9466

NOTICE: WHEN GOVERNMENT DRAWINGS, SPECIFICATIONS, OR OTHER DATA ARE USED FOR ANY PURPOSE OTHER THAN IN CONNECTION WITH A DEFINITELY RELATED GOVERNMENT PROCUREMENT OPERATION, THE UNITED STATES GOVERNMENT THEREBY INCURS NO RESPONSIBILITY, NOR ANY OBLIGATIONS WHATSOEVER; AND THE FACT THAT THE GOVERNMENT MAY HAVE FORMULATED, FURNISHED, OR IN ANY WAY SUPPLIED THE SAID DRAWINGS, SPECIFICATIONS, OR OTHER DATA IS NOT TO BE REGARDED BY IMPLICATION OR OTHERWISE AS IN ANY MANNER LICENSING THE HOLDER OR ANY OTHER PERSON OR CORPORATION, OR CONVEYING ANY RIGHTS OR PERMISSION TO MANUFACTURE, USE, OR SELL ANY PATENTED INVENTION THAT MAY IN ANY WAY BE RELATED THERETO.

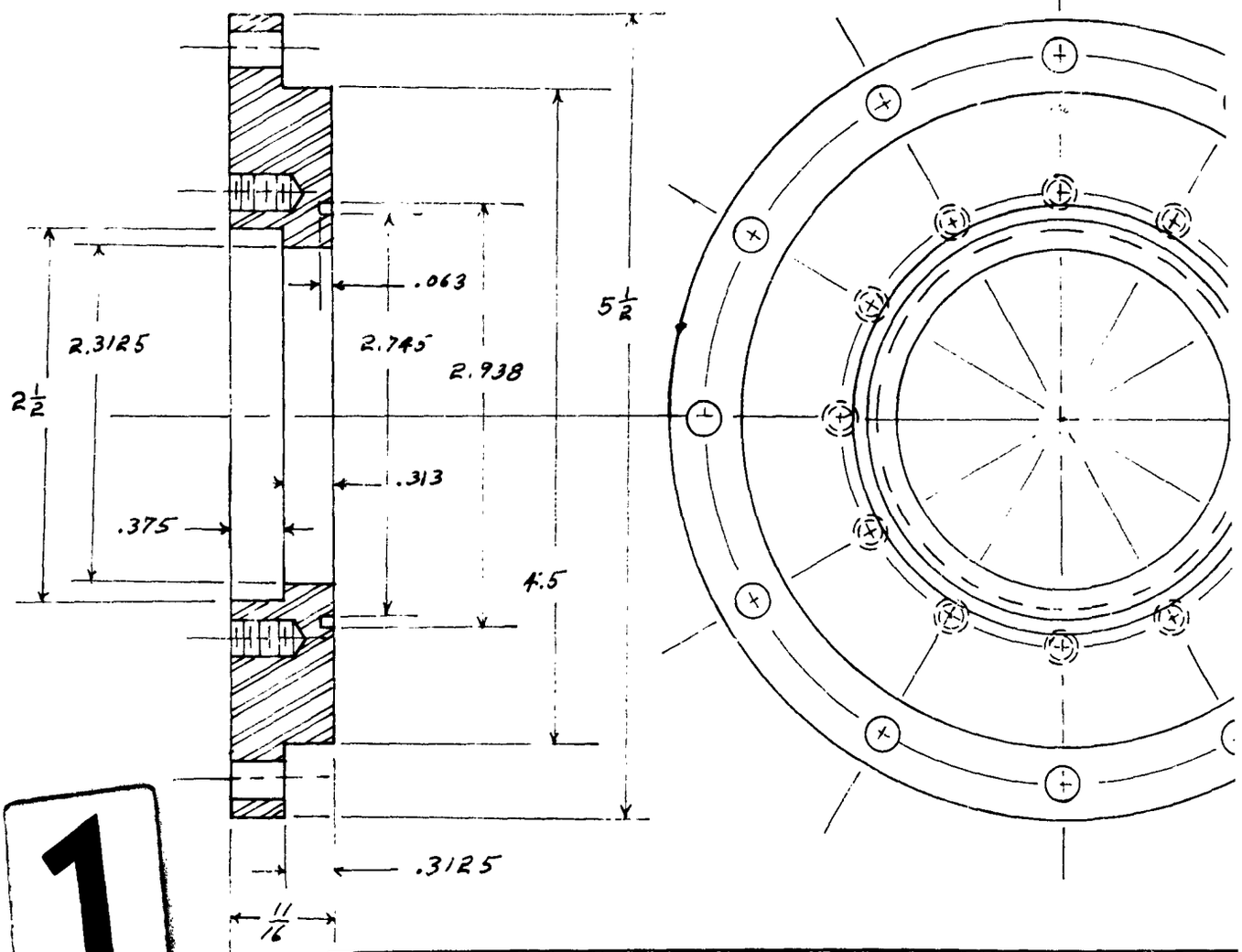

1

(1) BUFF	(4) ROUGH MACH. FINISH
(2) HAND FINISH	(5) ROUGH FILE OR GRIND
(3) SMOOTH MACH. FINISH	(6) SAND BLAST
(7) REMOVE FINS AND SPRUES	
(8) FINISH ALL SURFACES NOT OTHERWISE SPECIFIED	

UNLESS OTHERWISE SPECIFIED DIMENSIONS ARE IN INCHES. TOLERANCES ON FRACTIONS. 1/64 DECIMALS. 0.0005 ANGLES. 30'	DRAFTSMAN J L
	CHECKER
MATERIAL STAINLESS STEEL TYPE 302 OR 303 OR EQUIVALENT	ENGINEER G O
TREATMENT	EXAMINED
FINISH (3) (2) ALL OVER	PRO. APPRVD.

AMC Form No. 1108 (20 Nov 47)

This Form replaces AMC Form No. 57-0-28, existing stock of which will be used until exhausted.

SYMBOL	ALTERATION	DATE	APPROVED

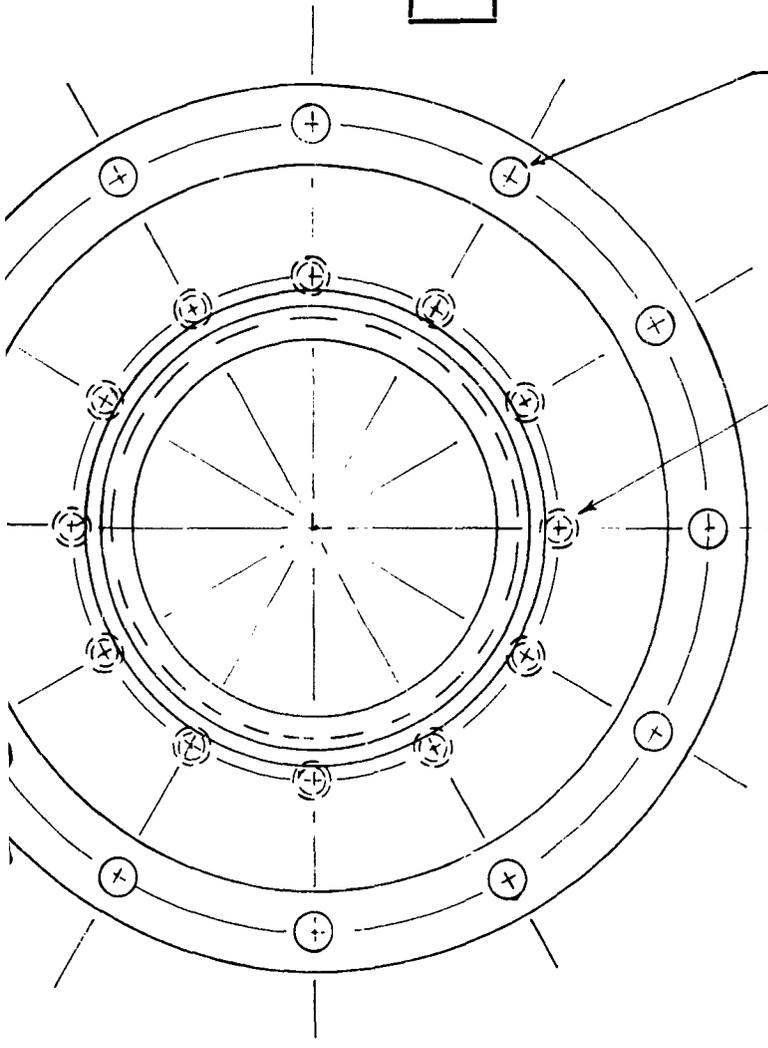

¼ DRILL THRU
12 HOLES EQUALLY SPACED
ON 2 ½ RADIUS

DRILL TAP 7/16 DEEP
FOR ¼ - 28 UNF
12 HOLES EQUALLY
SPACED ON 1½ INCH RADIUS

2

TYPE	NEXT ASSY NO.	NEXT ASSY	FINAL ASSY
USED ON		QUANTITY REQD	

UNLESS OTHERWISE SPECIFIED DIMENSIONS ARE IN INCHES. TOLERANCES ON FRACTIONS. 1/64 DECIMALS. 0.0005 ANGLES. 30'

MATERIAL STAINLESS STEEL TYPE 302 OR 303 OR EQUIVALENT

TREATMENT

FINISH (3) (2) ALL OVER

DRAFTSMAN J L PICKITT — DATE

CHECKER

ENGINEER G O W

EXAMINED

PRO. APPRVD.

NAME INJECTOR PLATE

SCALE FULL — WT.

U. S. AIR FORCE
AIR MATERIEL COMMAND

5
DRAWING NO.

This Form replaces AMC Form No. 57-0-28, existing stock of which will be used until exhausted.

WF-L-17 DEC 48 9600

NOTICE: WHEN GOVERNMENT DRAWINGS, SPECIFICATIONS, OR OTHER DATA ARE USED FOR ANY PURPOSE OTHER THAN IN CONNECTION WITH A DEFINITELY RELATED GOVERNMENT PROCUREMENT OPERATION, THE UNITED STATES GOVERNMENT THEREBY INCURS NO RESPONSIBILITY, NOR ANY OBLIGATIONS WHATSOEVER; AND THE FACT THAT THE GOVERNMENT MAY HAVE FORMULATED, FURNISHED, OR IN ANY WAY SUPPLIED THE SAID DRAWINGS, SPECIFICATIONS, OR OTHER DATA IS NOT TO BE REGARDED BY IMPLICATION OR OTHERWISE AS IN ANY MANNER LICENSING THE HOLDER OR ANY OTHER PERSON OR CORPORATION, OR CONVEYING ANY RIGHTS OR PERMISSION TO MANUFACTURE, USE, OR SELL ANY PATENTED INVENTION THAT MAY IN ANY WAY BE RELATED THERETO.

DRILL TAP $\frac{7}{16}$ DEEP
FOR $\frac{1}{4}$-28 UNF
6 HOLES - 3 HOLES
DIAMETRICALLY OPP.
ON $2\frac{1}{2}$ INCH RADIUS

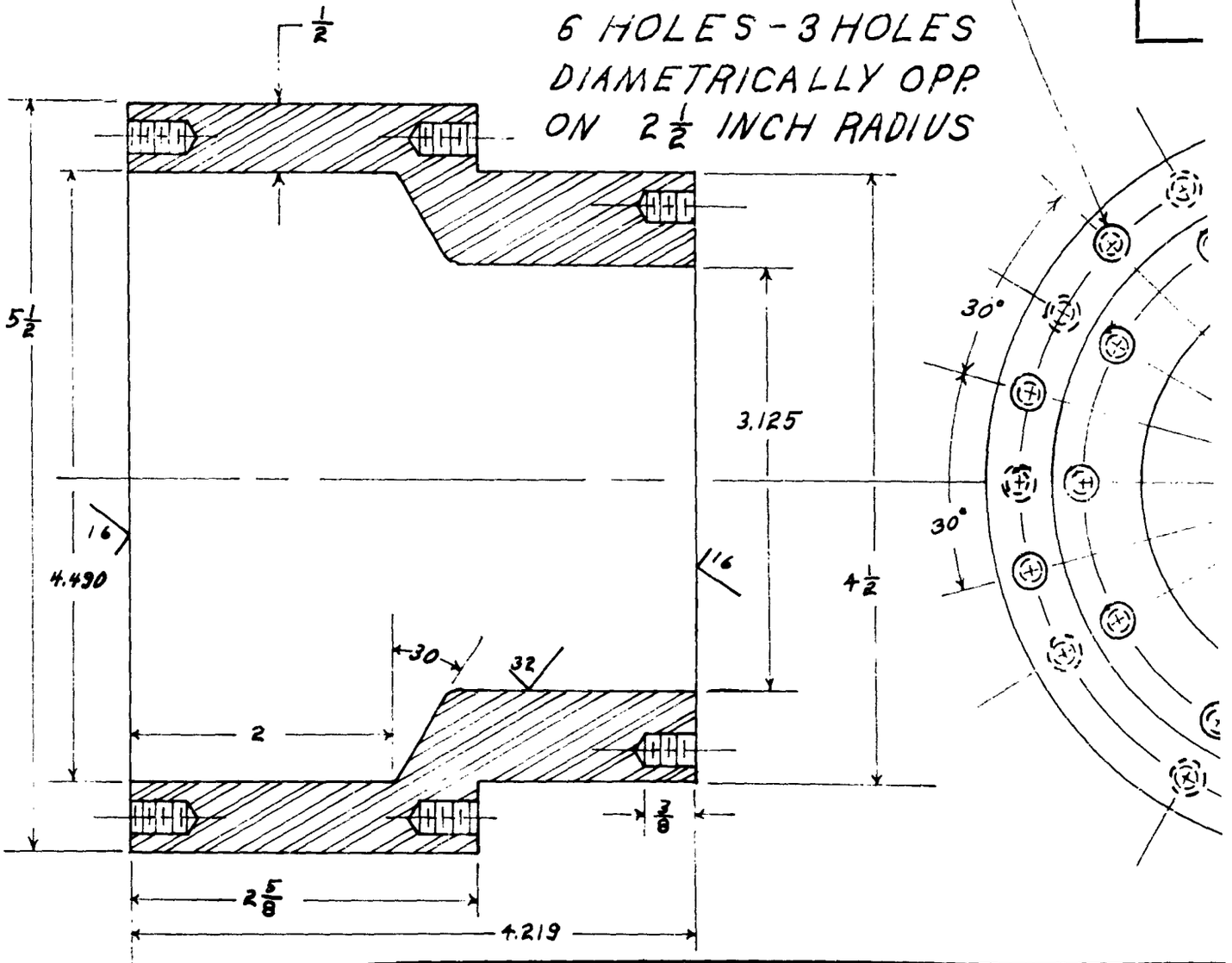

1 BUFF
2 HAND FINISH
3 SMOOTH MACH. FINISH
4 ROUGH MACH. FINISH
5 ROUGH FILE OR GRIND
6 SAND BLAST
7 REMOVE FINS AND SPRUES
8 FINISH ALL SURFACES NOT OTHERWISE SPECIFIED

UNLESS OTHERWISE SPECIFIED DIMENSIONS ARE IN INCHES. TOLERANCES ON FRACTIONS. DECIMALS. ANGLES. /°

MATERIAL STAINLESS STEEL TYPE 302 OR 303 OR MONEL

TREATMENT

FINISH (4) UNLESS SPECIFIED OTHERWISE

DRAFTSMAN J L F

CHECKER

ENGINEER G O

EXAMINED

PRO. APPRVD.

AMC Form No. 1108 (20 Nov 47)

This Form replaces AMC Form No. 37-6-28, existing stock of which will be used until exhausted.

SYMBOL	ALTERATION	DATE	APPROVED

7/16 DEEP
UNF
3 HOLES
ALLY OPP.
H RADIUS

DRILL TAP
3/8 DEEP
FOR 1/4 - 28 UNF
12 HOLES EQUALLY
SPACED ON 2
INCH RADIUS

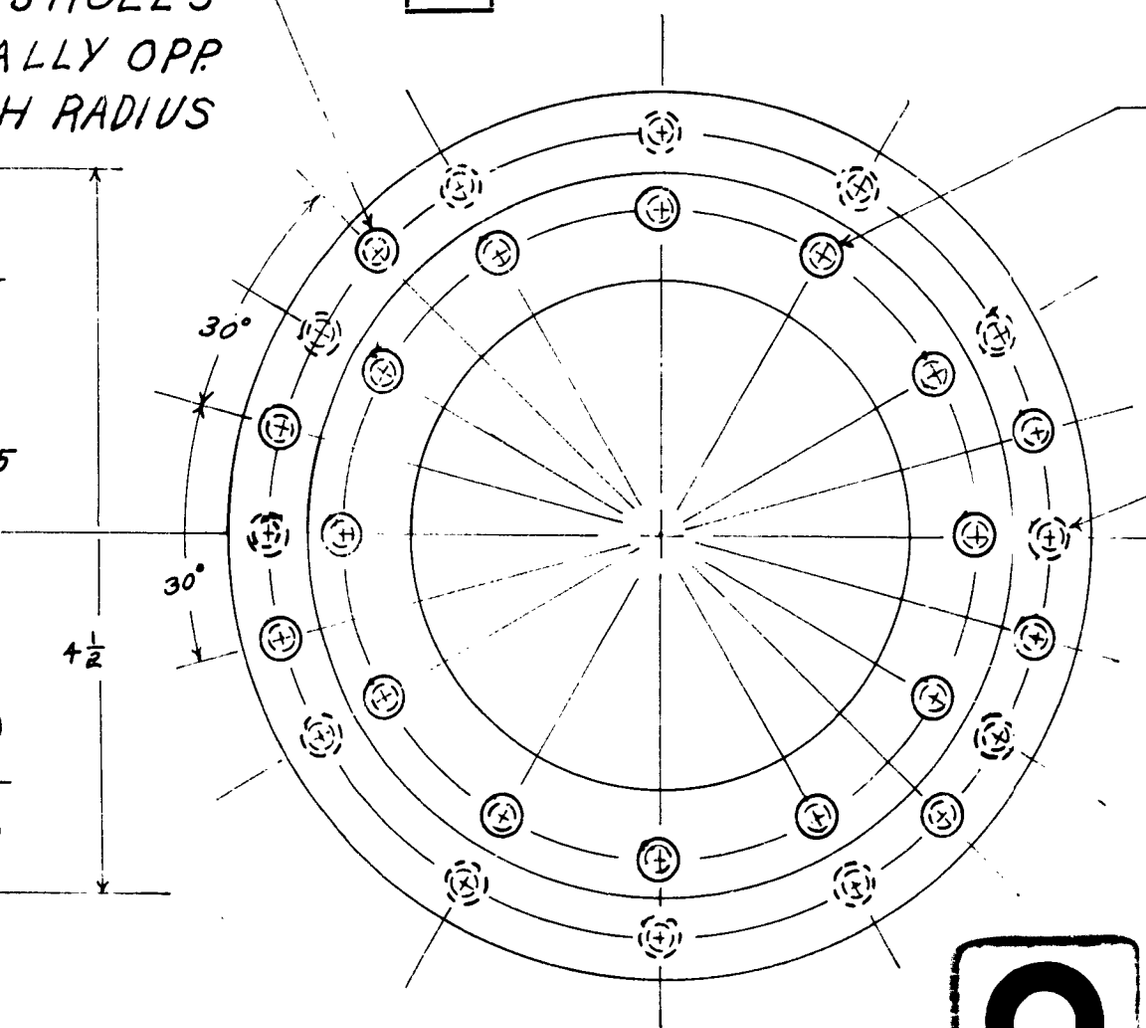

DRILL TAP 7/16 DEEP
FOR 1/4 - 28 UNF
12 HOLES
EQUALLY SPACED
ON 2 1/2 RADIUS

2

TYPE	NEXT ASSY NO	NEXT ASSY	FINAL ASSY
USED ON		QUANTITY REQD	

UNLESS OTHERWISE SPECIFIED DIMENSIONS ARE IN INCHES. TOLERANCES ON FRACTIONS. DECIMALS. ANGLES. 1/64 .0

MATERIAL STAINLESS STEEL TYPE 302 OR 303 OR K MONEL

TREATMENT

FINISH UNLESS SPECIFIED OTHERWISE

	NAME	DATE
DRAFTSMAN J L PICKITT		
CHECKER		
ENGINEER G OW		
EXAMINED		
PRO. APPRVD.		

CHAMBER JACKET

SCALE FULL WT.

U. S. AIR FORCE
AIR MATERIEL COMMAND

6
DRAWING NO.

This Form replaces AMC Form No. 57-0-28, existing stock of which will be used until exhausted.

WF-L-17 DEC 48 9600

THERMOCOUPLES - IRON/CONSTANTAN, SILVER SOLDERED AT $\frac{1}{32}$" FROM INSIDE WALL

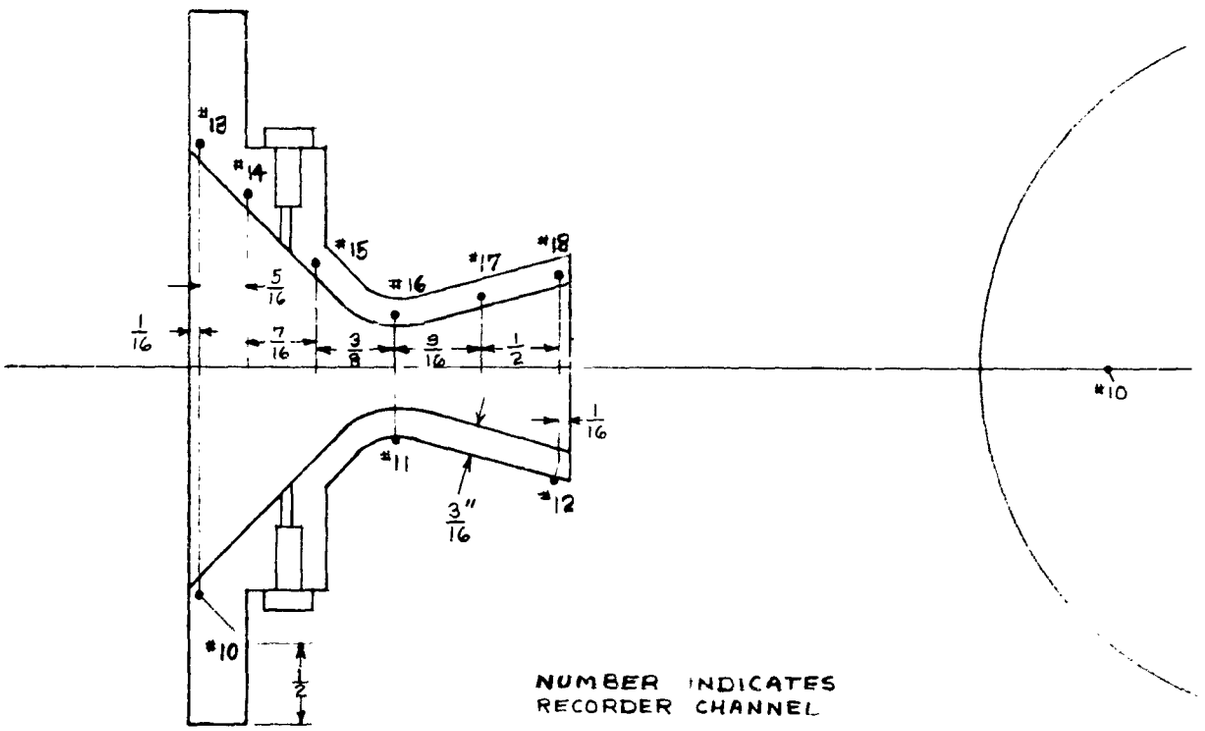

NUMBER INDICATES RECORDER CHANNEL

1

WORK ORDER - 62-3

① BUFF	④ ROUGH MACH. FINISH
② HAND FINISH	⑤ ROUGH FILE OR GRIND
③ SMOOTH MACH. FINISH	⑥ SAND BLAST
⑦ REMOVE FINS AND SPRUES	
⑧ FINISH ALL SURFACES NOT OTHERWISE SPECIFIED	

UNLESS OTHERWISE SPECIFIED DIMENSIONS ARE IN INCHES. TOLERANCES ON FRACTIONS. 1/64 DECIMALS. ANGLES.

MATERIAL

TREATMENT

FINISH

DRAFTSMAN D. J.

CHECKER

ENGINEER D. J.

EXAMINED

PRO. APPR'

AMC Form No. 1108 (30 Nov 49)

This Form replaces AMC Form No. 97-6-58, existing stock of which will be used until exhausted.

SYMBOL	ALTERATION	DATE	APPROVED

IRON/CONSTANTAN,
IT $\frac{1}{32}$" FROM INSIDE

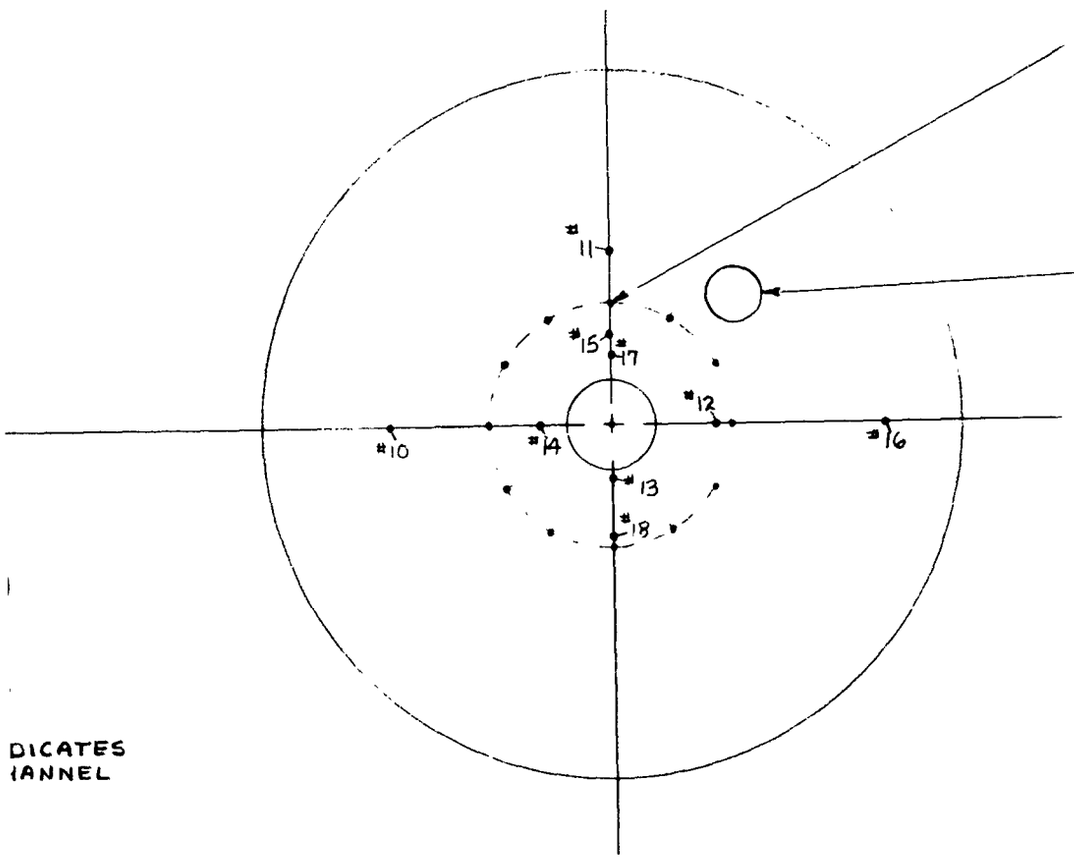

2

DICATES
HANNEL

TYPE	NEXT ASSY NO.	NEXT ASSY	FINAL ASSY
USED ON		QUANTITY REQD. 2	

WORK ORDER - 62-304

UNLESS OTHERWISE SPECIFIED DIMENSIONS ARE IN INCHES. TOLERANCES ON FRACTIONS. $\frac{1}{64}$ DECIMALS. ANGLES.

MATERIAL

TREATMENT

FINISH

DRAFTSMAN D. J. ALSER — DATE 7/1/63

CHECKER

ENGINEER D. J. ALSER

EXAMINED

PRO. APPRVD.

NAME THERMOCOUPLE LOCATION

SCALE FULL — WT.

U. S. AIR FORCE
AIR MATERIEL COMMAND

7
DRAWING NO.

This Form replaces AMC Form No. 57-6-58, existing stock of which will be used until exhausted.

WP-1-17 DEC 48 1000